FUNDAMENTAL STUDY OF JOINING TITANIUM ALLOYS USING ELECTROSLAG TECHNOLOGY

Sin-Jang Chen

B.S. National Tsing Hua University, Taiwan, 1980

M.S. National Cheng Kung University, Taiwan, 1982

A dissertation submitted to the faculty
of the Oregon Graduate Institute of Science and Technology
in partial fulfillment of the requirements
for the degree
Doctor of Philosophy
in
Materials Science and Engineering

January, 1991

The dissertation "FUNDAMENTAL STUDY OF JOINING TITANIUM ALLOYS USING ELECTROSLAG TECHNOLOGY" by Sin-Jang Chen has been examined and approved by the following Examination Committee:

Jack H. Devletian, Thesis Advisor
Professor
Dept. of Materials Science and Engineering

William E. Wood
Professor and Chairman
Dept. of Materials Science and Engineering

David G. Atteridge
Associate Professor
Dept. of Materials Science and Engineering

Thomas M. Loehr
Professor
Dept. of Chemical & Biological Science

ACKNOWLEDGEMENT

I would like to acknowledge the David Taylor Research Center and Office of Naval Research for sponsoring this project under contract #N00014-86-K-0426.

I wish to express my appreciation and sincere thanks to professor Jack H. Devletian for his helpful guidance and encouragement throughout this work. I am grateful to Drs. William E. Wood, David G. Atteridge, and Thomas M. Loehr for examining my thesis.

I like to express my sincere appreciation for the extensive help I received from Robert Turbin, Ken Burns, Andy Villeneuve, Gerhard Boehme, Douglas Davis, and Allan Ryall. I also like to thank Vivek Dikshit, R. Parthasarathy, R Devanathan, John Simmons, Young-Kun Oh for their help and valuable discussions throughout this work. I wish to thank Mr. James Ault of precision Castparts Corporation for providing help for numerous chemical analyses.

I also wish to express my great appreciation to my family in Taiwan for their enormous support and encouragement throughout these years.

TABLE OF CONTENTS

LIST OF TABLES

LIST OF FIGURES

Page

Page

Page

Page

ABSTRACT

FUNDAMENTAL STUDY OF JOINING TITANIUM ALLOYS
USING ELECTROSLAG TECHNOLOGY

Sin-Jang Chen, Ph.D.
Oregon Graduate Institute, 1991

Supervising Professor: Jack H. Devletian

At present, titanium alloys can not be welded in thick sections (>25mm) with commercial welding processes such as submerged arc, gas metal arc and flux cored arc welding because of titanium's excessive high reactivity and resistivity at high temperatures. As a result, the only methods to weld titanium alloys in thick section are electron beam welding which is not practical for large structures and gas tungsten arc welding which is extremely labor intensive. Thus, a substantial need for cost-effective welding of titanium alloys exists.

In adapting the electroslag technique for joining titanium alloys, many fundamental problems had to be overcome. As a result, the mechanisms of ohmic heat generation in both the slag and electrode were studied. Furthermore, the electrochemical effects between the slag and titanium filler metal were analyzed in order the model the heat generation mechanism in electroslag processing for application to both consumable guide and non-consumable guide ESW. Frequent experimental comparisons between ESW of titanium and steel (for reference) were drawn to better verify the models and predictive equations.

An electric path model was developed to explain the overheating of the electrode and guide plate in a consumable guide ESW process. Equations were derived to explain the mechanism of consumable guide ESW process using a low resistivity CaF_2 flux. Also a mathematical model incorporating the effect of ohmic heating on the electrode melting rate was derived to predict the arcing instability occurring in a non-consumable guide ESW of titanium alloys.

As a result of this research and for the first time outside the Soviet Union, the consumable guide electroslag welding (ESW) process has been developed to weld thick-section Ti-6Al-4V and Ti-6211 plates. This joining technique utilized a constant voltage AC power source, pure CaF_2 flux and argon shielding over the slag pool. The resulting weld deposited on 25 mm (1") and 50 mm (2") thick titanium plates were sound and virtually defect-free.

Mechanical properties such as tensile properties, hardness, CVN impact toughness of the welds were investigated. Mechanical properties were correlated to the microstructures and interstitial content of the welds. A model to determine the influence of interstitial elements and grain size on the tensile ductility and toughness of titanium alloys was also developed.

I. INTRODUCTION

Titanium and its alloys are widely used for various structural applications due to their high melting point, specific strength and excellent corrosion resistance particularly in seawater. Though titanium is relatively expensive compared to other structural metals (such as iron, nickel, and aluminum), it is still used for certain critical applications, such as parts in the lower temperature regimes of aircraft gas turbine engines[1] as well as many marine applications. As the applications of titanium and its alloys become increasingly wide spread, there is a demand to develop more productive welding methods to meet the varied needs of different applications. But, titanium is extremely reactive with interstitial elements (O, N, H, C) when exposed to temperatures above 650°C.[2] The basic difficulties in welding titanium and its alloys economically are due to two primary factors: (1) shielding the weld metal and heat affected base metal from the harmful atmosphere and (2) overcoming titanium's extreme resistivity (compared to other common metals) which precludes welding by highly productive processes such as submerged-arc, flux-cored arc and gas-metal arc welding. Therefore, welding must always be performed under vacuum or in a controlled inert gas environment by processes that do not electrically heat (i.e. by ohmic heating) up the titanium filler metal. As a result, the only commercial methods of welding titanium alloys today include: gas-tungsten arc, laser and electron beam welding.

Electroslag welding (ESW), however, has long been recognized as the most cost-effective method to weld thick-section (above 40 mm) steel and stainless steel plates[3,4] over 25 mm (1") thick. Compared to other processes, ESW has many advantages including: one pass operation, high welding speed, no preheating necessity, less welder skill requirement, non-machined joint preparation, and less angular distortion.[5] It also produces very high quality welds, since the slag pool protects the weld metal from the atmosphere.

When applying the ESW process to join thick-section titanium and its alloys in the Soviet Union, several difficulties have arisen as a result of the high chemical reactivity and electric resistivity of titanium (compared to steel). The high reactivity of titanium limits the selection of fluxes to a small number of halides, and requires additional argon shielding over the slag and the heated metal. Titanium's high electrical resistivity causes the electrode to be ohmically heated up to such high temperatures that the occurrence of electrode burnback and arcing must always be considered.

Researchers[6] at the Paton Electric Institute have successfully performed ESW of thick-section titanium and its alloys by using oxide-free CaF_2-base fluxes, special argon shielding techniques and large diameter electrodes. But, the complex relationship between welding variables and the combined effects of the low resistivity CaF_2-based flux and the high resistivity titanium electrode on process stability have not been fully studied.

In order to better understand the fundamental mechanisms involved

in producing a viable welding system for thick section titanium alloys using the ESW process, this research will focus on four main areas of study. These include:

(1) Parametric study of welding variables,

(2) Thermal and electrical characterization of ESW fluxes,

(3) Electrode ohmic heating study, and

(4) Mechanical properties study of Ti-6AL-4V and Ti-6211 alloys.

In part 1, the correlation between the different welding variables (voltage, current, electrode melting rate, resistivity of slag, electrode geometry, and welding gap) and their effects on process stability and base metal dilution are investigated. This is performed to determine experimentally the limits or the "window" of acceptable welding parameters (if any) that can be used to successfully deposit sound weld metal to join thick-section titanium alloy plates. The second part includes slag resistivity measurements to determine the effect of slag electrical properties on ESW process stability and base metal dilution. In this way, the contribution of the slag to the overall performance of the ESW system can be calculated. In the third part, electrode ohmic heating is measured under static conditions and the results are applied to the calculation of the ohmic heating contribution to the electrode melting rate and the production of arcing instability during the ESW process. When combining parts 1, 2 and 3, a mathematical analysis to predict the capabilities of ESW of titanium

alloys is developed and compared to experimental results. In the last part, the mechanical properties of selected welds of Ti-6Al-4V and Ti-6211 alloys are also evaluated to determine the usefulness of this cost-effective welding process. The effects of microstructure and interstitial element contamination are related to the resulting mechanical properties. Furthermore, a model is developed to assess the roles of grain size and interstitial content on the resulting properties of weld metal.

II. BACKGROUND

A. Historical Background of ESW Process

The electroslag process was invented by R.K. Hopkins in the United States, who made his first melt of a consumable electrode under a slag blanket in 1935.[7] This technology later evolved into two of the most important metal processing methods in modern history: electroslag refining (ESR) and electroslag welding (ESW). The present form of the ESW process was developed in the early 1950's at the Paton Electric Welding Institute in the USSR.[3] Later, it was widely used in western Europe and introduced back into the United State in 1959 by Arcos Corporation.[8] However, it was not until the early 1970's that it started to gain more acceptance for welding structural assemblies. This was possible because of the new development of portable light-weight equipment. Since then, the electroslag welding process has been widely used for shipbuilding, heavy equipment manufacturing and bridge construction in the United State.[5]

Beginning in 1956, researchers at Paton Electric Welding Institute successfully applied the electroslag technology to join titanium alloys. Their research activities continued until the mid-1970's, indicated by a summary report of the ESW process given at the 1976 Mezhdunar Conference by Gurevich and associates[6]. In the United States, a comparative literature survey by Bangs[9] for the David Taylor Naval Ship Research and Development Center in 1982 concluded that very limited

work had been done in ESW of thick-sectioned titanium alloys. After that the only research work in ESW titanium alloy was reported at M.I.T.[10,11]

B. Principle of the ESW Process

The ESW process uses the heat generated by resistance heating of the slag pool to melt and fuse the base and filler metals together. The molten metal as well as the molten slag pool are contained in the joint by the parts to be welded and the water cooled retaining shoes. The slag pool floats above the molten metal and provides shielding from the atmosphere. Welding is performed in the vertical or near vertical position. As filler metal is being fed into the weld pool, it sinks to the bottom due to its higher density, and fills up the weld gap. The weld metal solidifies progressively from the bottom upward.

The ESW process is rather different from other fusion welding processes, because there is no arc except at the beginning of the weld. The process is started by striking an arc between the electrode and the base metal. As the arc stabilizes, flux is added to form the slag pool. When the slag pool builds up to a sufficient depth of about 30 mm, it covers the end of the electrode and extinguishes the arc. After about one minute, the process is arcless and can proceed to completion without interruption. While the molten slag continues to be in contact with copper cooling shoes, a small amount of slag solidifies and forms a thin solid layer between the molten slag and copper cooling shoes. As

welding proceeds, the layer of solidified slag acts as protective shield for the solidified weld metal.

The transient period at the beginning of the ESW process is always associated with slag entrapment because there isn't enough heat buildup to melt the solid flux and base metal at the same time. Thus, a run-in tab is used to allow the process to stabilize and insure full penetration in the beginning of the weld. At the end of the weld, porosity occurs at the center of the weld due to solidification shrinkage. Therefore, a run-off tab is also utilized at the end of the weld to allow the molten slag to extend above top of the joint so that a full joint can be completed without porosity. Both run-in and run-off tabs are cut off from the weld by a cutter after welding is completed, leaving the weld free from the starting and ending defects.

There are three main variations of the ESW process, viz, non-consumable guide method, plate electrode method, and consumable guide method. In the first method, a non-consumable guide is used to direct the wire into the slag pool. The guide and welding head are raised upward together along a track as the molten slag rises. The advantage of this method is that it can join very long welds without any interruption. The disadvantages are 1) plates to be joined together need to be lined-up perfectly for the welding head to move along them, and 2) expensive moving-head systems must be used to deposit simple butt welds.

In the second method, a plate electrode is directly fed into the slag pool without any wire electrode. The advantage of this method is a more uniform heating of welding joint and faster welding rate than the

nonconsumable guide method. The disadvantages are 1) a great deal of space on top of the welding head is required to accommodate the length of the plate, 2) a special technique is required to start the ESW process, and 3) a special device is needed to feed the plate electrode to maintain a constant current.

The consumable guide method combines the advantages of the above two methods while eliminating several disadvantages. As the name implies, a guide plate is used not only to direct the filler metal into the slag pool but also itself constantly melts into the slag pool. The guide plate carries a significant amount of welding current, which allows a more uniform heating of the welding joint and faster welding rate than the nonconsumable guide method. In addition, no welding head movement is necessary during the consumable guide ESW process.

C. How Titanium Changes the ESW Process

Research work on the ESW process has mainly focused on steel and stainless steel, and a great deal of information has been generated regarding the effect of welding variables on the process.[3,12-18] But, due to the difference in material characteristics, some modifications of the ESW process are necessary when the ESW process is used to join titanium alloys. These material properties include high chemical activity, higher electrical resistivity, lower density, and lower thermal conductivity of titanium than steel. Each of these are discussed in detail in the following sections.

1. High Chemical Activity of Titanium

Due to the high chemical activity of titanium at elevated temperature (Titanium reacts violently with oxygen in the air when heated above 650 °C), therefore the basic difficulty in welding of titanium and its alloys is shielding the weld metal, heated filler metal, and heated base metal from the air. This is the reason all other welding processes used to join titanium alloys are performed in either a vacuum chamber or a controlled inert gas environment.[2,19] Alhough, the molten metal is protected by the slag pool during welding in the ESW process, the researchers[20] at Paton Electric Institute found that shielding by the slag pool alone was not sufficient to protect the weld metal from interstitial element contamination. Therefore, additional argon shielding above the slag pool was needed to fully protect the titanium alloy from atmospheric contamination. They also concluded that the purest grade of argon should be used for the gas shielding.

The basic argon shielding technology is to flood argon over the slag pool[21] and since argon is heavier than air, it will sink to the bottom of the welding cavity and insulate the slag pool from the air. This technique also provides shielding for the hot filler metal before it is fed into the slag pool. The other technique, used by Shou-Kong Fan[11] for nonconsumable guide ESW of titanium alloy, was to spray argon through a pair of modified copper shoes. As shown in Figure 1, argon spraying from the top of cooper cooling shoes would protect the slag pool and heated portion of filler metal, while the argon spraying from

the bottom of the cooper shoes would protect the solidified weld metal before it cooled to a low enough temperature. The above two methods use argon only as a neutral shielding gas between the heated weld metal and the surrounding air. Kompan et al.[22] had used an additional argon shielding technique to not only protect the weld metal but also reduce its interstitial content. As shown in Figure 2, argon gas was bubbled through the slag pool and molten metal pool during the consumable guide ESW of a titanium alloy. They claimed that bubbling argon through the weld pool could reduce the weld metal oxygen and nitrogen contents, promote uniform penetration of the weld, and reduce the grain size in the weld metal.

Besides the argon shielding protection, the flux used for ESW titanium alloys should not contain any elements (especially O, N, C, and H) harmful to the weld metal. It was shown by researchers[20] at Paton Electric Institute that the principal requirement for the flux in ESW of titanium was the complete absence of oxides. As shown in Figure 3, oxygen content in the molten titanium metal increased even when 5 wt% of the most stable oxides (Al_2O_3, TiO_2, and ZrO) were added into the CaF_2 flux. They concluded that only when the flux contains no oxide, will the molten titanium metal have an oxygen content less than 0.1 wt%. Therefore, the adequate fluxes for ESW of titanium alloys are limited to metal halides only, and among them the CaF_2 flux is the most widely used because it has a high melting point, is cheaply available and is very stable in the molten state.

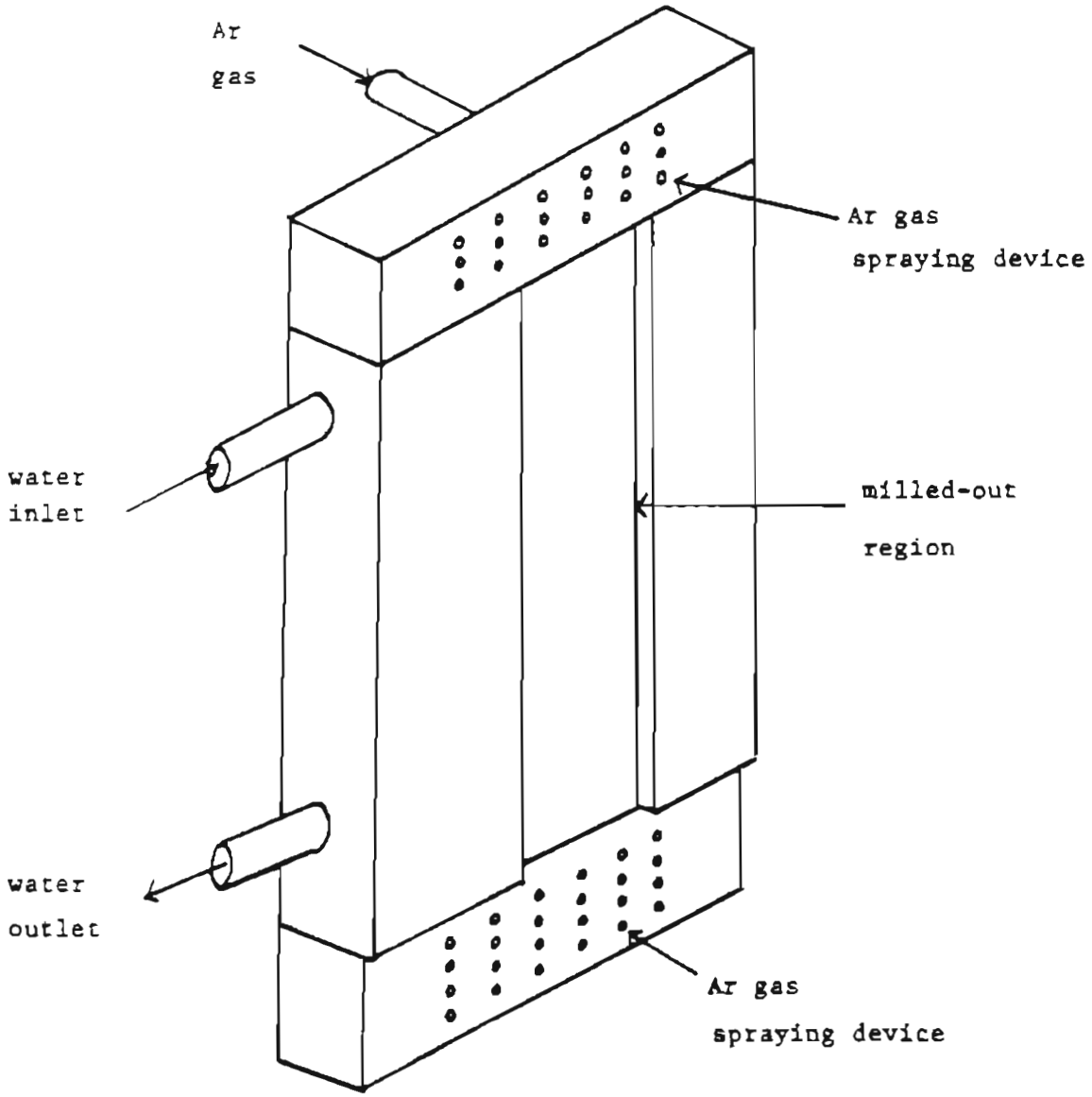

Figure 1. Illustration of a modified copper cooling shoe which shows the argon spraying device[11] for nonconsumable guide ESW of titanium alloys. (After Fan[11])

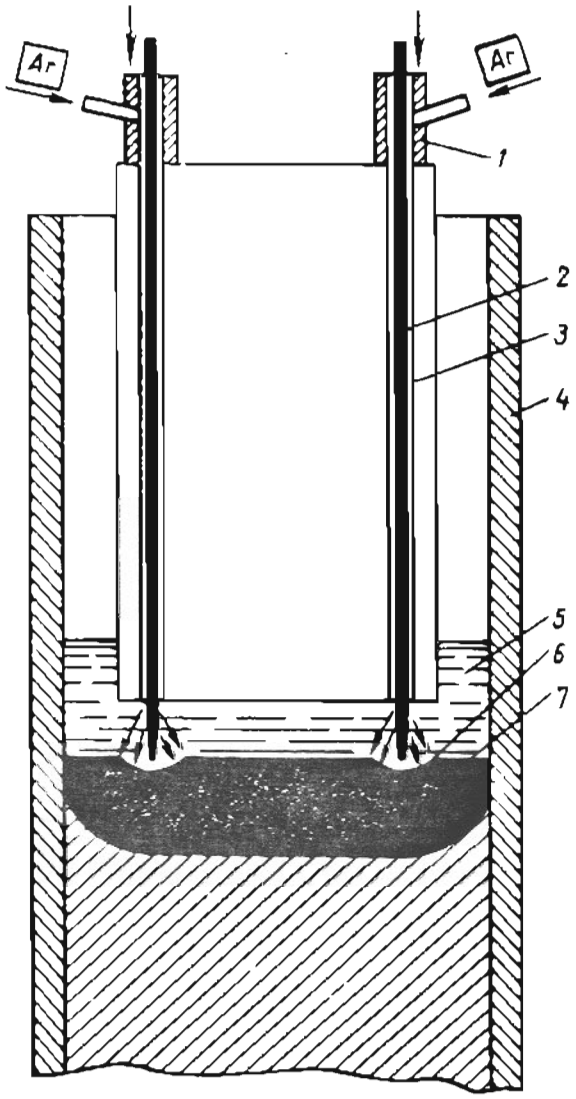

1. gas chamber, 2. electrode, 3. consumable guide,
4. forming plate, 5. slag pool, 6. metal pool, and
7. weld.

Figure 2. Illustration of argon bubbling technique used for consumable guide ESW of titanium alloys.(After Kompan[22])

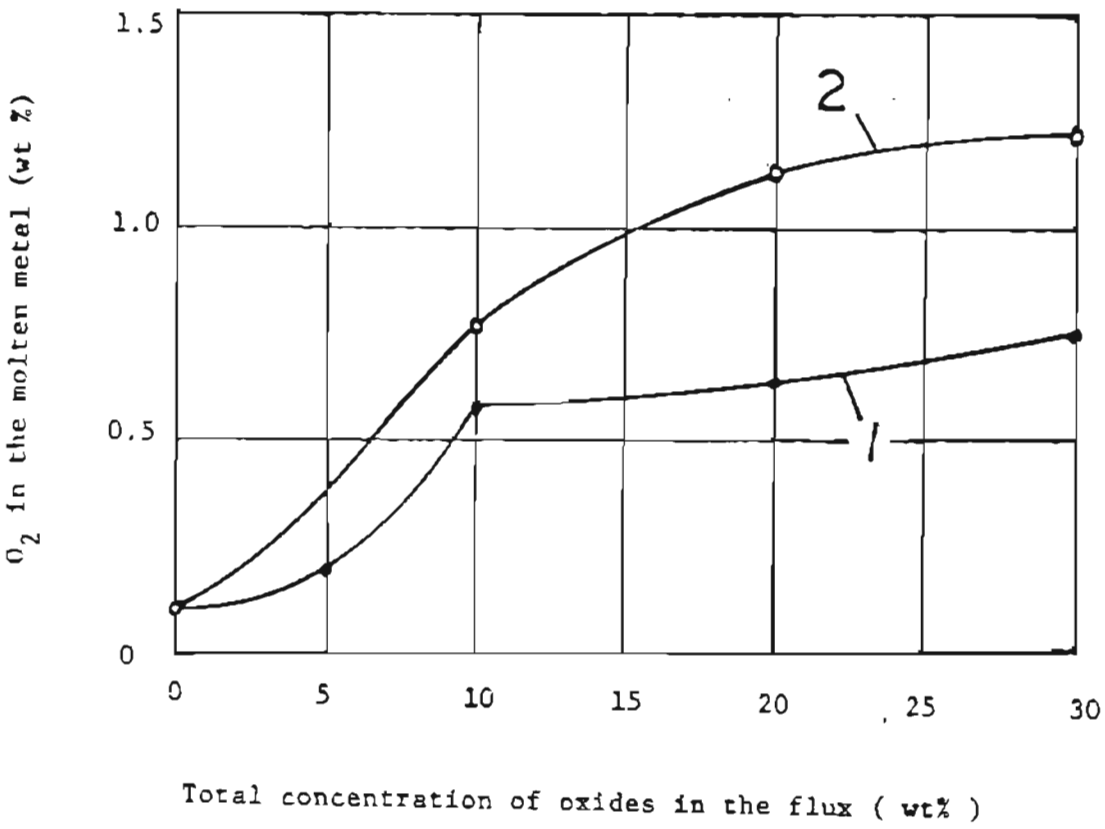

1. Al_2O_3 , ZrO , TiO_2

2. SiO_2 , CaO , MgO

Figure 3. Dependence of oxygen content in molten titanium on the total concentration of oxide in the flux.(After Gurevich[20])

2. High Electric Resistivity of Titanium Alloys

Titanium has an electric resistivity value about 5 times that of steel at room temperature, and Ti-6Al-4V has an even higher value — 17 times that of steel.[23] The higher electric resistivity results in increase of ohmic heating of the filler metal and guide plate in the ESW process. This will contribute to a higher filler metal melting rate and higher welding speed. And in the extreme, the ohmic heating can burn the filler wire out of the slag pool and change the ESW process to an unwanted arc process. When arcing occurs, the weld usually has lack of fusion problems due to inadequate heating of the slag and slag entrapment.

To counteract the filler metal ohmic heating problem caused by higher electric resistivity, the current density passing through the filler metal should be reduced. A reduction of the current density of the filler metal can be achieved by either reducing the welding current or increasing the diameter of the filler electrode. However, the CaF_2 base flux used for ESW titanium alloys has a higher electric conductivity than the oxide base flux used for ESW of steel,[24,25] and uses a higher welding current. Therefore, the only method left, is to increase the filler wire diameter. Researchers at Paton Electric Institute[20] did successfully make the ESW of titanium alloys with large diameter filler metal. Actually, their first success came from ESW of commercially pure titanium using a plate electrode. Then, they performed nonconsumable guide ESW of titanium alloy with 5 mm diameter filler wire[26,27,28] which

had twice the cross-sectional area of the 3.2 mm diameter filler wire used for ESW of steel.

3. Lower Density of Titanium

The density of titanium at its melting point is 4.11 g/cm^3, which is much lower than that of iron (7.02 g/cm^3).[29] Most of the halide, and oxide fluxes used in the electroslag process have densities between 2 and 5 g/cm.[8,24,30,31,32] One of the requirement of fluxes used for the electroslag process is that the flux should have a lower density than the molten metal. This is necessary because, if the density of the flux is close to or exceeds the density of the molten metal, the flux will sink and mix into the molten metal. When that happens, the electroslag process will be interrupted by loss of flux and the resulting metal deposit will be full of slag inclusions.

Based on the above reason, the BaF_2 and LaF_3 fluxes are not suitable for either ESW or electroslag refining (ESR) of titanium alloys, because the density of BaF_2 flux is 3.82 g/cm^3 (measured at melting point of titanium) and the density of LaF_3 flux is 4.46 g/cm^3 (measured at melting point of titanium).[30] Both density values are either close to or larger than the density (4.11 g/cm^3) of molten titanium metal. However, they can be used in small amounts mixed with a CaF_2 base.

4. Lower Thermal Conductivity of Titanium

Titanium has a thermal conductivity value about one-ninth that of

steel.[23,29] In the ESW process, low thermal conductivity of the base metal is beneficial because it reduces the heat input required to make the weld. But, this beneficial effect for ESW of titanium is usually hindered by the lower heating power of the CaF_2 flux and higher melting point of titanium as compared to ESW of steel.

The following is a short summary of the modifications made for ESW titanium alloys to counteract the effects of the previously mentioned physical properties of titanium. Due to the high chemical activity of titanium, it is necessary to use oxygen-free CaF_2 base flux with extra argon shielding for ESW of titanium alloys. The high electric resistivity of the titanium alloys necessitates the use of the largest possible diameter of filler metal or guide plate for both consumable and non-consumable guides to reduce ohmic heating of the filler metal. The effect of titanium having a lower density value than steel on ESW process is that several flux ingredients (BaF_2 and LaF_3) with higher density will not be suitable for ESW of titanium alloys. With lower thermal conductivity, it is possible to perform the ESW of titanium alloys with lower heat input than ESW of steel.

D. Process Variables for ESW of Titanium

Welding variables are factors which affect both the welding operation and quality of the resulting weld. In order to make a good quality weld, it is essential to study all the effects of the welding variables on the welding process. ESW of titanium is characterized by working at

low voltage and high current conditions, due to the high conductivity values of oxide-free CaF_2 base fluxes used in the process. This high current condition combined with the high electric resistivity of titanium leads to the problems of excessive ohmic heating of the filler metal wire and limitations on the usable range of welding variables. Therefore, it is very important to study the effect of welding variables on the ESW process to ensure the soundness and integrity of titanium welds.

There are two types of variables in the ESW process. One type is the fixed or preselected variables which can not be changed during welding. And the other type is the adjustable variables. The fixed variables include flux, power supply, electrode size and number of electrodes, guide plate size and type, electrode extension (dry extension), and welding gap. The adjustable variables which can be adjusted during the welding and usually are used to control the welding process include current, voltage, and electrode feed rate.

The fixed (or preselected) variables only have an indirect effect on the ESW process. They change the ESW process by affecting the adjustable variables. Therefore, in this section, the effect of adjustable variables on the welding parameters will be discussed first and then each of the fixed variables will be discussed. Before starting the discussion, a few welding parameters will be defined first to help the discussion. During ESW, the slag pool acts as a resistor and obeys Ohm's law.

Thus :

$$V_w = I_w R_{slag} \quad \ldots\ldots (1)$$

V_w : Welding voltage
I_w : Welding Current
R_{slag} : Resistance of the slag pool

$$W_s = (n V_e A_e)/(A_g - A_p) \quad \ldots\ldots (2)$$

W_s : Welding speed
n : Number of wires
V_e : Speed of filler wire
A_e : Cross-section area of filler wire
A_g : Cross-section area of welding gap
A_p : Cross-section area of consumable guide plate

$$H_{input} = (V_w I_w)/W_s \quad \ldots\ldots (3)$$

H_{input} : Welding heat input

$$\% \text{ Dilution} = (A_w - A_g) / A_w \ 100 \ \% \quad \ldots\ldots (4)$$

% dilution : Percentage base metal dilution
A_w : Total area of weld metal at transverse section
A_g : Cross-section area of welding gap

1. Adjustable Variables

a. Current, Voltage, and Electrode Feed Rate

ESW of titanium alloys is usually performed with a constant voltage alternating current (CVAC) power source. With a constant voltage power source, the welding current and electrode feed rate are interrelated. This is because when electrode feed rate increases, the immersion depth of the electrode also increases, which in turn decreases the resistance of the slag pool as shown by Birck et al.[33]

Since the voltage is kept constant, the welding current will increase when the resistance decreases, based on Ohm's law as shown in Equation 1. Therefore, increasing electrode feed rate will increase the welding current. Also, based on Equation 2, welding speed will increase when the electrode feed rate increases.

In ESW of steel, several investigators[13,16,34] found a linear relationship between the welding current and electrode feed rate, while, Frost et al.[35,36] and Ann[17] reported that the welding current was proportional to the square root of the electrode feed rate. In non-consumable guide ESW of titanium alloys, Gurevich et al.[28] reported that welding current was proportional to the square root of the electrode feed rate. Despite the difference about the relationship between welding current and electrode feed rate, all researchers did agree that the increase of welding current is slower than the increase of electrode feed rate. Therefore, the heat input of the ESW process will eventually decrease when the electrode feed rate is increased, based on Equations 2 and 3.

b. Effect on Welding Working Range

Frost et al.[35] have suggested a working range of welding voltage and current to make a successful weld, as shown in Figure 4. The lowest voltage boundary (boundary A in Fig 4) is governed by a threshold energy input and voltage for achieving complete penetration. Below this boundary the welding process will operate, but the weld will have incomplete penetration. Boundary B in Figure 4 is established by a

critical energy, below which hot cracking would occur at the weld center. Boundary C in Figure 4 is set by the maximum output of the welding power supply. The last boundary (boundary D in Fig. 4) is based on the minimum electrode feed rate (minimum current) below which the electrode melts by ohmic heating before reaching the slag pool.

When applying this working range concept to ESW of titanium alloys, some modifications are necessary because of the different material characteristics. First of all, due to the low electric resistivity of the CaF_2-base flux used for ESW of titanium alloys, the whole working range will move to a region of lower voltage and higher current. Also, there is a boundary for high voltage, above which the low resistivity CaF_2 flux would not be able to maintain the ohmic condition and arcing would occur on top of the slag pool. This boundary has been reported to be 34 V for nonconsumable guide ESW of titanium alloys[20]. Next, titanium alloys do not have the weld centerline cracking problem, therefore boundary B shown in Figure 4 for ESW of steel doesn't apply to ESW of titanium alloys. Finally, the minimum current boundary will be moved to the higher current side because of severe ohmic heating of titanium electrode caused by its high electric resistivity.

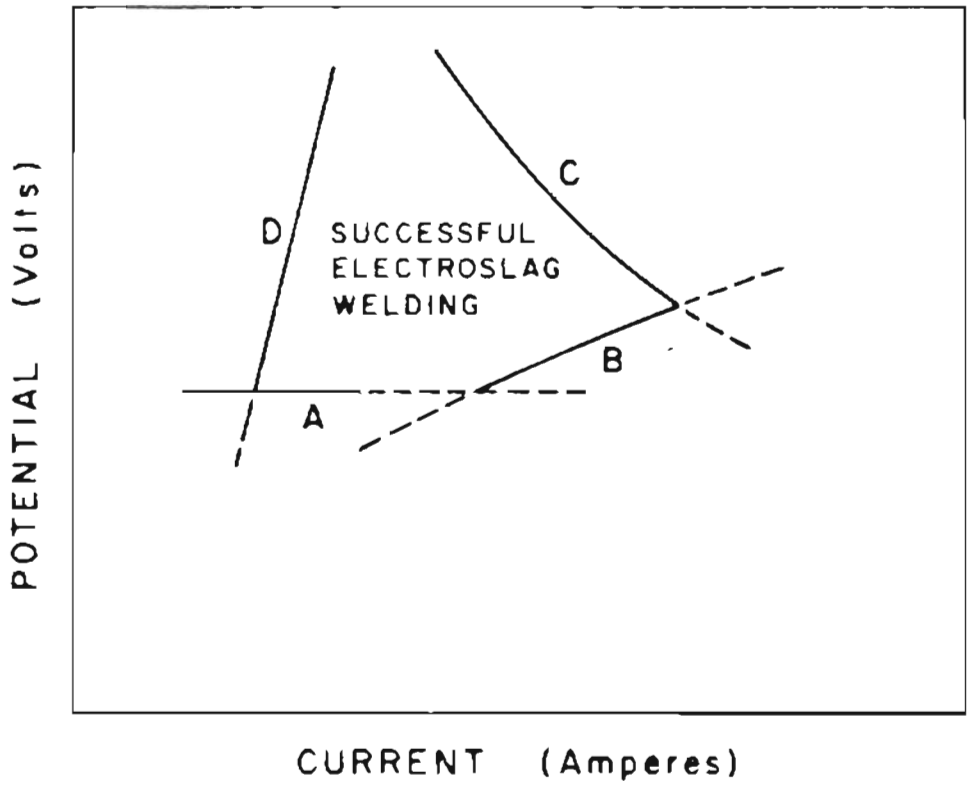

A: Threshold potential, B: critical energy input, C: Maximum power supply output, D: Minimum electrode velocity (current)

Figure 4. Schematic illustration of the electroslag welding process boundaries for successful penetration. (After Frost et al.[35])

c. Effect on the Percentage Base Metal Dilution

A linear (near flat) relationship between the welding current and percentage base metal dilution was reported by Venkataraman[16] and other researchers.[38] It was concluded that increasing the welding current decreased the percentage base metal dilution by a small amount. A similar conclusion was drawn by the researchers at Paton Electric Institute[20] for nonconsumable guide ESW titanium and titanium alloys. However, a parabolic relationship between the welding current and percentage base metal dilution has been reported by other investigators.[3,14,17,37]

Jones et al.[37] have suggested that, at higher welding currents, the percentage base metal dilution is lower because most of the heat is used to melt the filler metal and molten metal pool. Their suggestion is based on the "most direct current path" assumption. At lower welding currents, the electrode remains on top of the molten slag pool. Substantial heat is lost to the air from the surface of the slag pool by radiation and not enough heat is available to melt the base metal. Therefore, there is an optimum current range over which a maximum base metal dilution occurs.

A linear relationship between the welding voltage and percentage base metal dilution was reported by several researchers.[16,38,39] However, Ann[17] and other researchers[40] observed a parabolic relationship between the welding voltage and percentage base metal dilution. At higher voltages, the depth of the electrode immersion is very shallow

due to the relatively large effective resistance. This causes heat to concentrate on top of the slag pool only, and less amount of heat is available for melting the base metal. Also, stability of the ESW process may be disrupted by an arc flashing between the electrode and surface of slag pool.

On the other hand, at a relatively low voltage the heat input is lower as shown in Equation 3. In this case, the electrode will penetrate deep into the slag pool, and welding current will flow directly from the tip of the electrode to the molten metal pool. This leads to a lower percentage base metal dilution because most of the heat is used to melt the electrode. Researchers[20] at the Paton Electric Institute reported that, when nonconsumable guide ESW of titanium alloy was made with voltage values lower than 22 V, the welds had no base metal penetration at all because not enough heat was generated in the slag pool. Therefore, to make an electroslag weld with a high percentage base metal dilution, welding voltage levels should be kept as high as possible without any arcing.

2. Effect of Electric Resistivity of Slag

The electrical resistivity of the slag has been reported to be the most important variable in the electroslag process.[41-45] In ESW process, a high resistivity slag draws too little current from the power supply and doesn't have enough heat to maintain the electroslag process. On the other hand, a low resistivity slag (like CaF_2 flux) will draw excessive current from the power supply and increase the arcing

instability of the process.[46-47] Therefore, a slag with optimum electric resistivity should be used to maintain a stable electroslag process.

The fluxes used for ESW of titanium alloys are limited to CaF_2 or SrF_2 base fluorides as reported by the researchers at the Paton Electric Institute.[48-51] As compared to the oxide-base fluxes used for ESW of steels, the CaF_2 or SrF_2 base fluxes have much lower electric resistivity.[24,25,52,53] The consequence of having a lower resistivity flux is that the ESW of titanium alloy has a lower allowable working voltage (35 V maximum) as compared to 50 V in ESW of steel with oxide-base flux. This is because an arc could break out at high voltage levels in ESW of titanium alloys with low resistivity CaF_2-base flux.[3,20] Because of the lower allowable working voltage, the ESW process of titanium alloys has lower heating power.

In the ESR process, Hara et al.[25] and other researchers[30,41,54] also reported that the lower resistivity CaF_2-base flux generated less heat than the higher resistivity oxide-base flux. But, Ann[17] reported that in ESW of steel at same welding voltage, welds made by a flux with higher percentage of CaF_2 flux (lower resistivity) had higher base metal penetration (higher heating power) than welds made by a flux with less percentage of CaF_2 flux. The reason for this controversy between Hara et al. and Ann lies mainly on the power supply characteristics. A constant current power supply is used by Hara et al. for ESR process and a constant voltage power supply is used by Ann for ESW process. The power output (voltage times current) decreases as the load (resistance

of slag pool) is decreased in a constant current type of power supply. This is because when the load is decreased, the voltage decreases while the current remains constant. The opposite is true for the constant voltage power supply; that is, the power output increases as the load (resistance of slag pool) is decreased.[55,56] In summary, the ESW of titanium alloys using the low resistivity CaF_2-base flux can produce an explosive arcing problem at high welding voltage levels and low heating power because of the lower allowable working voltage.

3. Effect of Slag Pool Depth and Welding Gap

The slag pool consists of three variables: depth, length (welding gap), and width (plate thickness). The primary concern about these three variables is that their dimensions should be kept within the optimum ranges for a stable ohmic heating process. The minimum values are required to provide enough clearance for the electrode (including guide plate) from short circuiting or arcing to the copper cooling shoes and base metal. While the maximum values are required to prevent excessive heat losses to the copper cooling shoes. For 50 mm thick base metal plates of both steel and titanium alloys, the optimum range for slag pool depth is 30 to 50 mm[3,16,20] and for the welding gap the range is 25 to 38 mm.[14,17,21,57]

According to the "most direct current path" assumption, Jones et al.[37] have reported that in the slag pool, welding current will pass either from the electrode to the base metal or from the electrode to the molten metal pool depending on whichever path has a lower resistance.

Among these two paths, the former is proportional to half of the welding gap and the latter is proportional to the slag pool depth. The most likely path in ESW of titanium alloys is from the electrode to the base metal, because of the shallow immersion depth of the electrode resulting from the low resistivity of CaF_2-base flux.

If the current did pass from the electrode to the base metal, then the maximum allowable distance between them would be directly related to the maximum allowable voltage based on the Ohm's law. When the voltage is set above this limit, the electrode will lift out of the slag pool and an exposed arc would occur on top of the slag pool.

4. Electrode and Guide Tube Geometry

Non-consumable guide ESW of titanium alloys with a wire electrode has been shown to be more difficult to make[20,26-28] compared to ESW with a plate electrode or a consumable guide method. The main reasons are burn-back problem of small diameter wire electrodes caused by rapid ohmic heating and intense heat concentration near the electrode tip in the slag pool.[44-45,58-59]

To reduce the ohmic heating problem in non-consumable guide ESW of titanium alloys, a 5 mm diameter titanium electrode was used by the researchers[20] at Paton Electric Institute as compared to 2.4 and 3.2 mm diameter steel electrodes commonly used in ESW of steel. They also used an automatic slag pool level control device to maintain a constant low value of electrode dry stickout to reduce the ohmic heating problem. Without the slag pool level control, the electrode dry sickout would

vary greatly causing not only varying welding heat input but also a chance of electrode burn-out from the slag pool.

5. Power Supply

It is interesting to note that only a constant voltage alternating current (CVAC) type power supply was used for ESW of titanium alloys at the Paton Electric Institute[3,20]. But, both AC and DC power supplies are used for ESW of steel. The specific reason wasn't given in the Soviet literature.

In the United States, a CVDC power supply was used by Fan et al. at M.I.T.[11] to make non-consumable guide ESW of titanium alloys, which they claimed to have been made under stable ohmic heating conditions. But, the fact that their welds contained abnormal amounts of copper (2.4 to 13.6 wt%) melted from the non-consumable guide tube, and their suggestions to use a plate electrode and to use a slag pool depth-sensing device to control the electrode dry stickout tend to suggest that they encountered the problem of overheating the electrode caused by ohmic heating. Possibly, some arcing might have occurred between the guide tube and the surface of the slag pool.

Two possible reasons for the preferred choice of AC over DC power supply for ESW of titanium alloys are economics and polarization characteristics of the slag. At high welding current conditions, as seen in ESW of titanium alloys with CaF_2-base flux, an AC power supply was more economical than a DC power supply in term of initial cost and maintenance of the machine.[55,56] The second reason is that using an AC

power supply could reduce or totally eliminate the electrode polarization effect in the electroslag process as reported by Mitchell et al.[60-61] They also reported that at a high current density, the electrode polarization effect may convert the electroslag process to an arc process. Therefore, the electroslag process using an AC power supply can tolerate significantly higher current density values without arcing than the electroslag process using DC power supply. Both reasons suggest that, at high welding current conditions, the AC power supply is a better choice for ESW of titanium alloys.

The reason for using a constant voltage type power supply for ESW of titanium alloys is more obvious. The constant voltage type of power supply is widely used for different welding processes that use a continuously fed wire electrode. Constant voltage power sources have the self-regulating capability to adjust welding current in order to maintain a fixed voltage level. This provides the ESW process with not only an easy way of controlling welding voltage and current, but also a means of ensuring a uniform base metal penetration.

E. Weld Evaluation

As compared to commercially pure titanium, the alpha + beta titanium alloys, such as Ti-6Al-4V and Ti-6Al-2Nb-1Ta-0.8Mo (Ti-6211), have a better combination of strength and toughness. These alpha + beta titanium alloys have wider applications as structural materials. But, the researchers[62-64] at the Paton Electric Institute have reported that ESW of high strength alpha + beta titanium alloys had low Charpy V-notch

(CVN) impact toughness and tensile ductility in both weld metal and coarse grain heat affected zone (HAZ) base metal. They also reported that low toughness and ductility were due to the coarse grain structure produced by the high heat input and slow cooling rate of the ESW process. Similar results in ESW of steel, have been reported by Culp[65,66] and other researchers.[16-18] These low CVN impact toughness and tensile ductility have generally been attributed to the coarse prior beta grain size produced by the ESW process. But the actual mechanism is not well understand.

Terlinde et al.[67] have proposed that tensile ductility decreases when the prior beta grain size is increased in a Ti-Al alloy due to the dislocation pile-ups at the grain boundary. Other researchers[68-70] have reported that in Ti-6211, poor hot ductility was associated with the presence of a grain boundary alpha film. However, Damkroger et al.[71] have concluded that poor hot ductility was associated with large amounts of a lamellar widmanstatten alpha + beta microconstituent in Ti-6Al-4V and Ti-6Al-6V welds. A similar conclusion was given by Yashwant[72] in a heat-treated Ti-6Al-6V-2Sn weld. Besides the microstructure effect, it has been reported[73-75] that increasing interstitial elements content, especially oxygen content, will lower the CVN impact toughness and tensile ductility of alpha + beta titanium alloys. In summary, the low CVN impact toughness and tensile ductility of ESW alpha + beta titanium alloys could be due to microconstituents (such as: large prior beta grain size, grain boundary alpha film, and lamellar widmanstatten alpha + beta structure) and/or increasing interstitial elements content.

III. EXPERIMENTAL PROCEDURE

A. Consumable Guide ESW

1. Materials and Equipment

Materials used in this project included: (a) 50 mm thick plates of Ti-6Al-4V and Ti-6Al-2Nb-1Ta-0.8Mo (Ti-6211) which were received in the beta forged air cooled condition and (b) filler metals matching the compositions of the plates as shown in Table 1.

Table 1. Chemical compositions (wt %) of titanium alloy plates and matching filler metals.

Materials	Al	V	Nb	Ta	Mo	O	N	H
Base Metal :								
Ti-6Al-4V 50 mm Thick Plate	6.32	4.15	-	-	-	.215	.021	.004
Ti-6211 50 mm Thick Plate	5.52	-	2.05	.95	.56	.077	.006	.001
Ti-6Al-4V 25 mm Thick Plate	6.0	4.0	-	-	-	-	-	-
Filler metal :								
Ti-6Al-4V 3.2 mm Diameter	5.95	4.15	-	-	-	.143	.008	.001
Ti-6Al-4V 2.4 mm Diameter	6.10	4.03	-	-	-	.147	.003	.009
Ti-6211 2.4 mm Diameter	5.9	-	2.0	.90	.60	.056	.008	.001

The plates were cut into smaller sections measuring 5 cm x 20 cm x 30 cm with the 20 cm side parallel to the rolling direction. Other materials used include 50 mm thick A36 steel plates and their matching filler metals. These materials were used to study the effect of different welding variables on the electroslag welding process, therefore, their chemical compositions were not analyzed.

Due to the high reactivity of titanium, interstitial contamination was always a concern. In this study, the molten weld metal was protected by pure CaF_2 flux and argon gas shielding over the molten slag pool. Reagent grade pure CaF_2 flux, with the impurity contents shown in Table 2, were used as basic flux throughout this investigation.

Table 2. Impurity contents of reagent grade pure CaF_2 fluxes (Typically 99 % pure),(Source: CERAC,Incorporated)

Element	wt %
Al	0.005
Fe	0.005
Mg	0.1
Si	0.05
Zn	0.02
Cr	< 0.001
Cu	< 0.001
	< 0.2

For the comparitive study of the welding variables, Hobart PF 201 running flux was used to make the ESW of the steel alloy. The chemical composition of Hobart PF 201 running flux is shown in table 3.

Table 3 Chemical composition of Hobart PF 201 running flux. (Source: Hobart Brothers company)

Compound	wt %
CaO	12.20
MgO	2.34
MnO	22.46
CaF_2	8.62
SiO_2	32.95
Al_2O_3	8.32
TiO_2	8.02
K_2O	0.88
Na_2O	0.57
FeO	1.81
P_2O	<0.05
	98.22

To study the effect of conductivity on welding parameters, LaF_3 and YF_3 fluxes, both having lower electric conductivities than the CaF_2 flux, were added to the pure CaF_2 flux. The CaF_2 fluxes with 12.5 wt% or 25 wt% of either LaF_3 or YF_3 additions were mixed and melted in a vacuum induction furnace before actual welding.

Because of the ionic nature of pure CaF_2 flux, an alternating current constant voltage (AC CV) machine with 100% duty cycle at 44 V, 1000 A was used to join the titanium alloys (Figure 5). The welding voltage was directly controlled in the power supply, but the welding current was indirectly adjusted by changing the electrode feed rate. For comparison, some welds were made by a direct current constant voltage power supply system (which consist of two DC machines being connected together in parallel) with 100% duty cycle at 1500 A.

The wire feeding system, shown in Figure 6, was used to feed a single wire or dual wires into the molten slag pool with feed rates ranging from 20 mm/s to 150 mm/s. This system could feed both 2.4 mm and 3.2 mm diameter wires into the welds successfully.

Two water cooled copper shoes were used to dam the slag pool. These cooling shoes were clamped on either side of the welding plates by a pair of 30 cm size C clamps. These cooling shoes had 1.6 mm deep 44.5 mm wide grooves for weld reinforcement.

2. Plate Fixture

Two plates with 50 mm x 200 mm x 300 mm were placed between run-in and run-off tabs with the 200 mm edge vertically up and 25 mm to 32 mm apart. The plates were welded to the run-in block and run-off block by TIG welding as shown in Figure 7. After the ESW was made, both the run-in and run-off were removed from the welds, leaving the welds essentially free of defects associated with starting and ending of the ESW process.

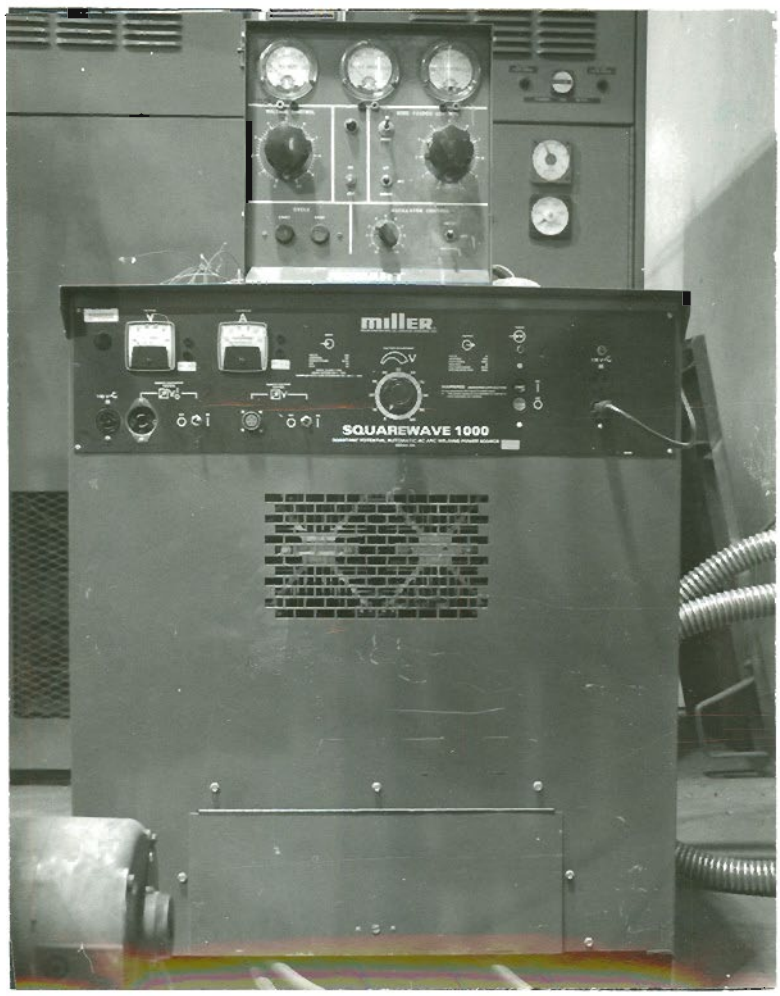

Figure 5. Square wave constant voltage alternating current power supply for ESW, rated 100% duty cycle at 44 V and 1000 A.

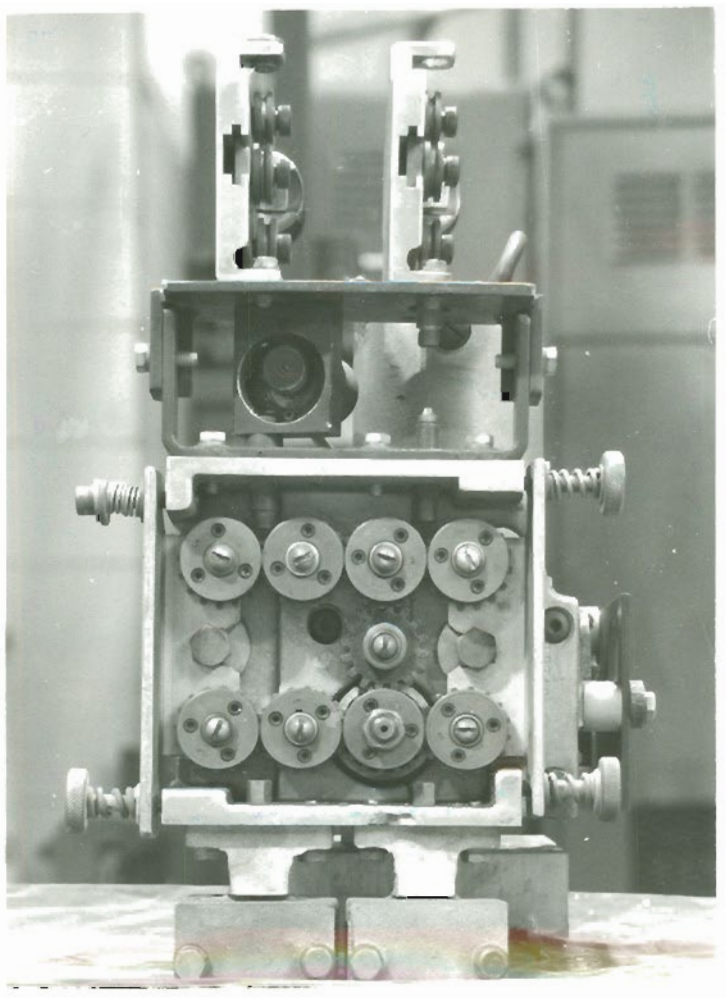

Figure 6. Wire feeding device for ESW.

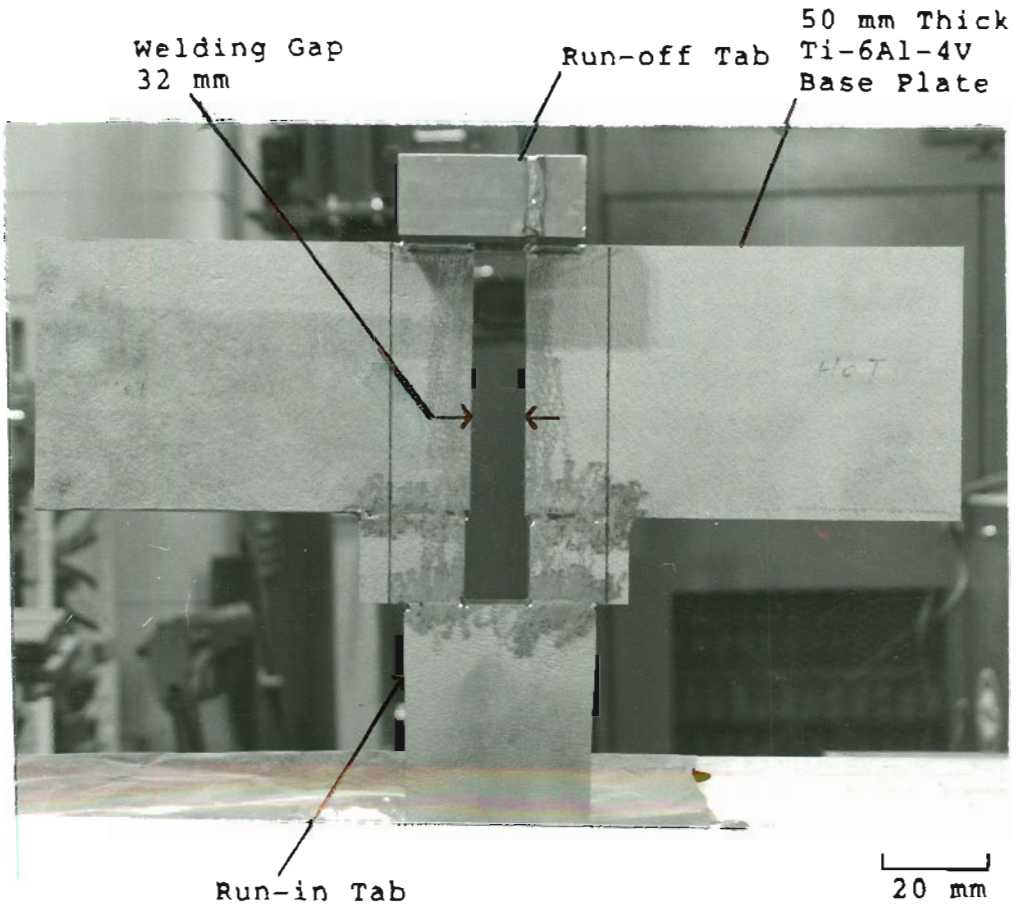

Figure 7. Photo of electroslag weld plate fixture.

3. Consumable Guide Plate Preparation.

Guide plates with outside dimensions 12.7 mm x 38 mm were used for all 50 mm thick welds and guide plates with outside dimensions 12.7 mm x 19 mm were used for 25 mm thick welds. All guide plates were machined from a 12.7 mm thick plate to the final shape, then joined together by the TIG welding process as shown in Figure 8. The length of the consumable guide was around 61 cm. The end section of the guide plates were reduced as shown in Figure 8(A) for dual filler metals and was tapered off as shown in Figure 8(B) for single filler metal to prevent the starting arc from spreading to the edge of the guide plate and freezing the wire feed hole. If the hole was frozen, the wire would be stuck to the inside of the guide hole and the arc diminished before the electroslag process got started. Also a round groove was chosen to ensure good electric contact between the filler wire and consumable guide plate

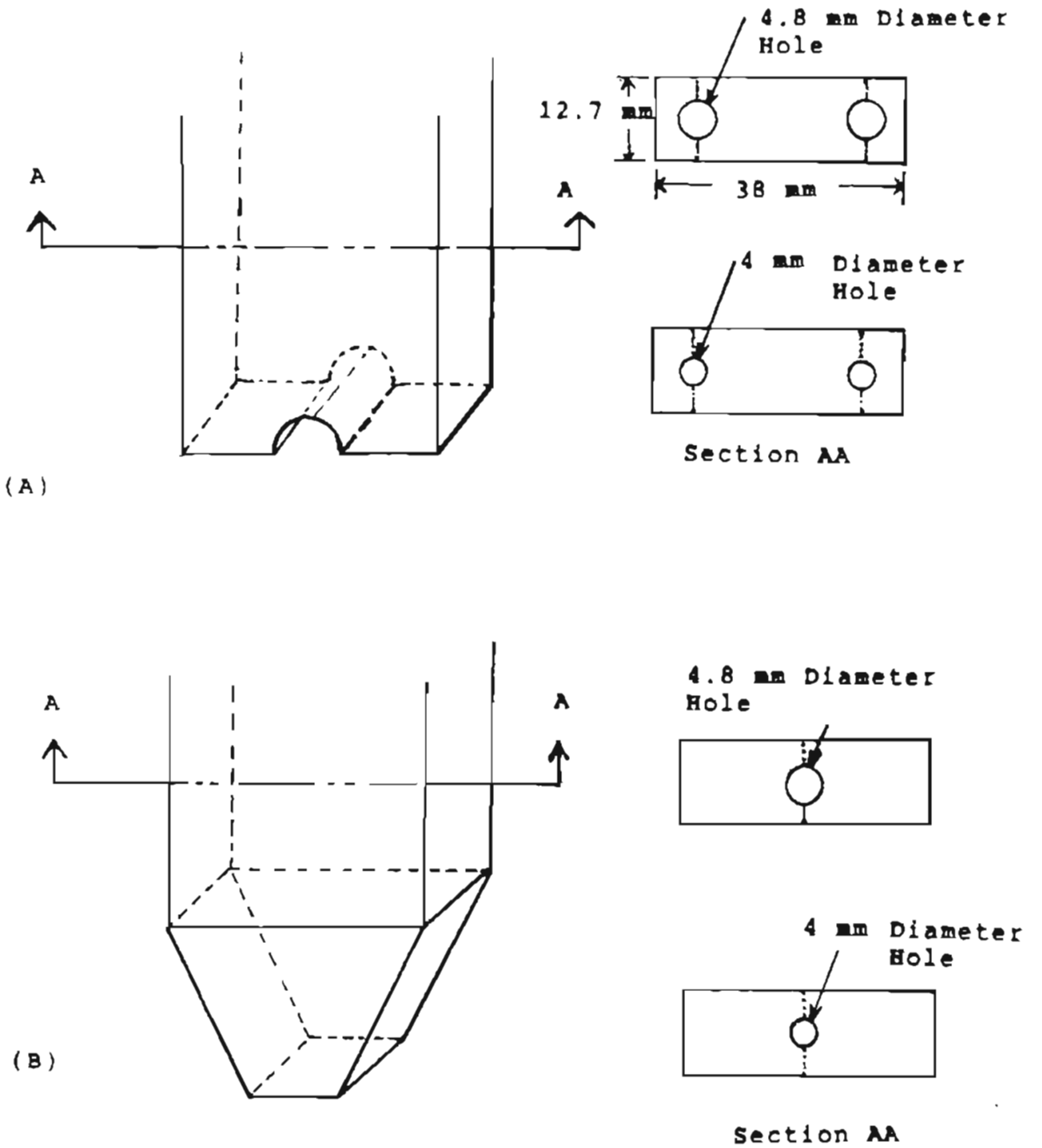

.... Joined Together by GTAW Process

Figure 8. Guide plate configurations for (A) 3.2 mm and 2.4 mm diameter dual filler metals and (B) 3.2 mm and 2.4 mm diameter single filler metals.

4. Flux Preparation

The as received reagent grade CaF_2 flux was in a loose powder form (smaller than 325 mesh size). The fine powder flux was not suitable for ESW directly, because of its light weight the powder was easily blown out of the weld by the hot argon shielding gas. Therefore, the flux was melted in a induction furnace using a graphite crucible and an Ar gas protective atmosphere. The fused fluxes were then crushed to smaller than a 5 mesh size.

The weighted flux was kept inside the furnace at 200 °C overnight before welding to remove all the moisture. The weighted flux was manually added into the welding cavity, after the welding arc was initiated. For the 50 mm welds, 150 g of flux was added first to establish the stable molten slag pool, and then flux was added around 10 g per minute to accommodate the loss of the slag to the cooling shoes. For the 25 mm welds, 100 g of flux was added first to establish the stable molten slag pool, and then flux was added around 10 g per minute to accommodate the loss of the slag to the cooling shoes.

5. Weld Set-Up and Procedure

The welding head consisting of the wire feeding mechanism and a guide plate holder was mounted on a stationary welding fixture. The consumable guide was centered with respect to the welding gap. Most of the welds were made with a Miller AC CV machine. A schematic of the weld setup is shown in Figure 9.

Prior to starting the weld, the power supply, the wire feed motor, the Ar shielding gas, the recording devices and the water circulation in

the cooling shoes were turned on. Welding was started by striking an arc on the starting block and a measured amount of the flux (150 g for 50 mm thick weld and 100 g for 25 mm thick welds) was slowly added. After the molten slag pool build up to a depth of 25 mm to 38 mm, the electroslag process stabilized and the arc was extinguished. Then, the welding current and voltage levels were adjusted to the desired values and were kept constant throughout the rest of the weld.

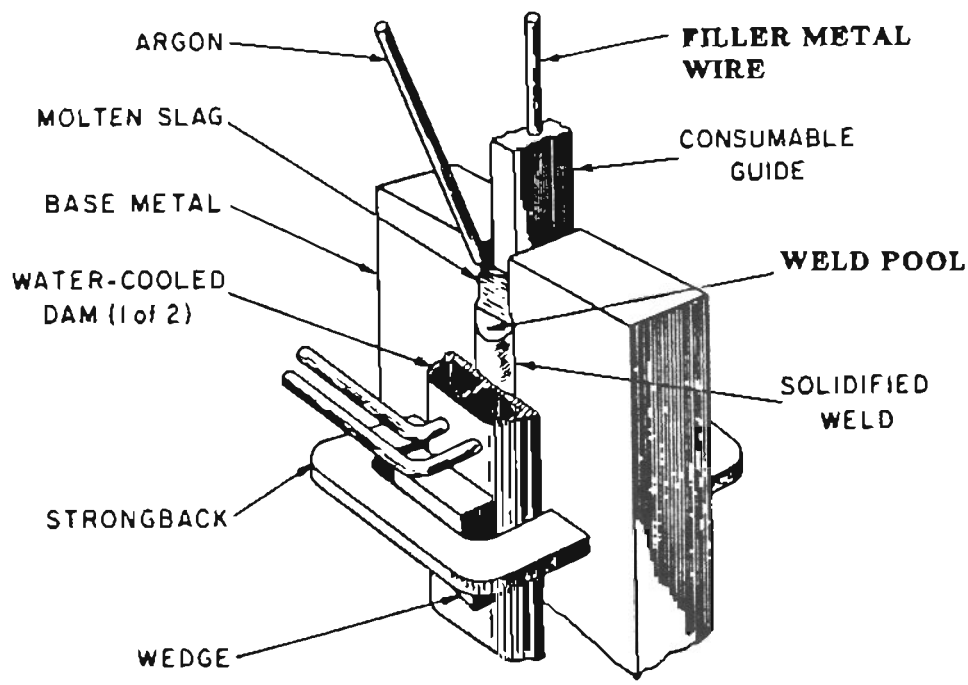

Figure 9. Schematic view of the consumable guide ESW process for 50 mm thick titanium plates using a single filler wire fed through a plate guide.

6. Process analysis

Welding current and voltage fluctuations were monitored and recorded by a GULTON strip chart recorder. The wire feed rate was measured using a JET-LINE wire feed measuring device. Average welding speed was calculated by using the total length of the welds divided by the total welding time. Transverse sections from the bottom, middle and top of the welds were machined and macroetched in a solution containing 200 ml H_2O, 30 g oxalic acid, 2ml HF, and 5g of $Fe(NO_3)\ 9H_2O$. The sections were studied with respect to base metal dilution, weld metal grain size and weld defects.

The base metal dilution was calculated from the following equation as illustrated in figure 10. The area of both melted base metal and weld deposit were measured by a planimeter. Also, selected welds were chosen for chemical analysis to study the interstitial effect.

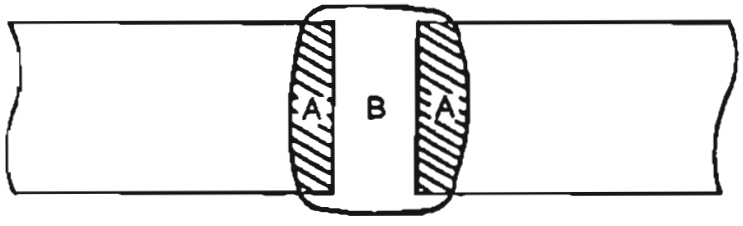

$$\% \text{ Dilution} = \frac{\text{Areas A}}{\text{Areas A + Area B}} \times 100$$

A: Area of melted base metal
B: Area of deposited weld metal

Figure 10. Illustration of the percentage base metal dilution calculation.

B. Electrical Resistivity Measurements

1. Slag Resistivity

After reviewing several possible methods to measure slag resistivity,[25,76-80] a four-electrode probe with a thermocouple was chosen to measure the resistivity of molten slags. The schematic illustration of the electrical circuit diagram of the measuring system is shown in Figure 11. From an AC power source, the alternating current with 1 kHz frequency was applied through the two outer electrodes to the molten slag. The potential difference (V_{slag}) between the two inner electrodes and the potential difference (V_s) across a standard resistor connected in series to the circuit were converted to DC signals and recorded by a 2-channel recorder. After the measurement, the resistivity values were calculated using equation 7. Simultaneously, the temperatures of the molten slag were measured by a W/W-26%Re thermocouple and recorded.

Based on Ohm's law:

$$V_{slag} = I\ \rho_{slag}\ C \quad \text{..... (5)}$$

$$I = V_s/R_s \quad \text{..... (6)}$$

From Equation 5 and 6:

$$\rho_{slag} = (1/C) \times (V_{slag}\ R_s/V_s) \quad \text{..... (7)}$$

V_{slag}: potential difference in the molten slag
I_{slag}: applied current to the molten slag
ρ_{slag} : resistivity of molten slag
C : Cell constant of the four-electrode probe
V_s : Potential difference across a standard resistor
R_s : Resistance of a standard resistor

Before measuring the resistivity values of the molten slag, the cell constant of the probe was determined first. The cell constant determinations were carried out at room temperature with a standard solution (1 N KCl aqueous solution) which resistivity value was known. The resistance values were measured at different electrode immersion depths at room temperature. The cell constant values at corresponding immersion depths were calculated using equation 7. The cell constant values were checked both before and after the resistivity measurements that were experimentally determined at the elevated temperature of interest.

Approximately 500 g of flux was melted in a graphite crucible using a high frequency induction furnace and the molten slag was protected by argon circulated on top of the crucible. When the flux was melted and its temperature was several hundred degrees above its liquidus temperature, the induction furnace was shut off and the four-electrode probe was immersed into the molten slag. The resistance values of molten slag at different temperatures were measured. Also, the immersion depth of electrodes was measured in order to determine the appropriate cell constant value.

Resistivity values of KCl and LiF fluxes which melt at much lower temperatures than CaF_2 flux were measured first to verify the accuracy of this method of measurement. A k type thermocouple was used instead of the W-5%Re / W-26%Re thermocouple due to the lower melting point of KCl and LiF fluxes. After verification, resistivity values of reagent grade CaF_2 flux at different temperatures were measured.

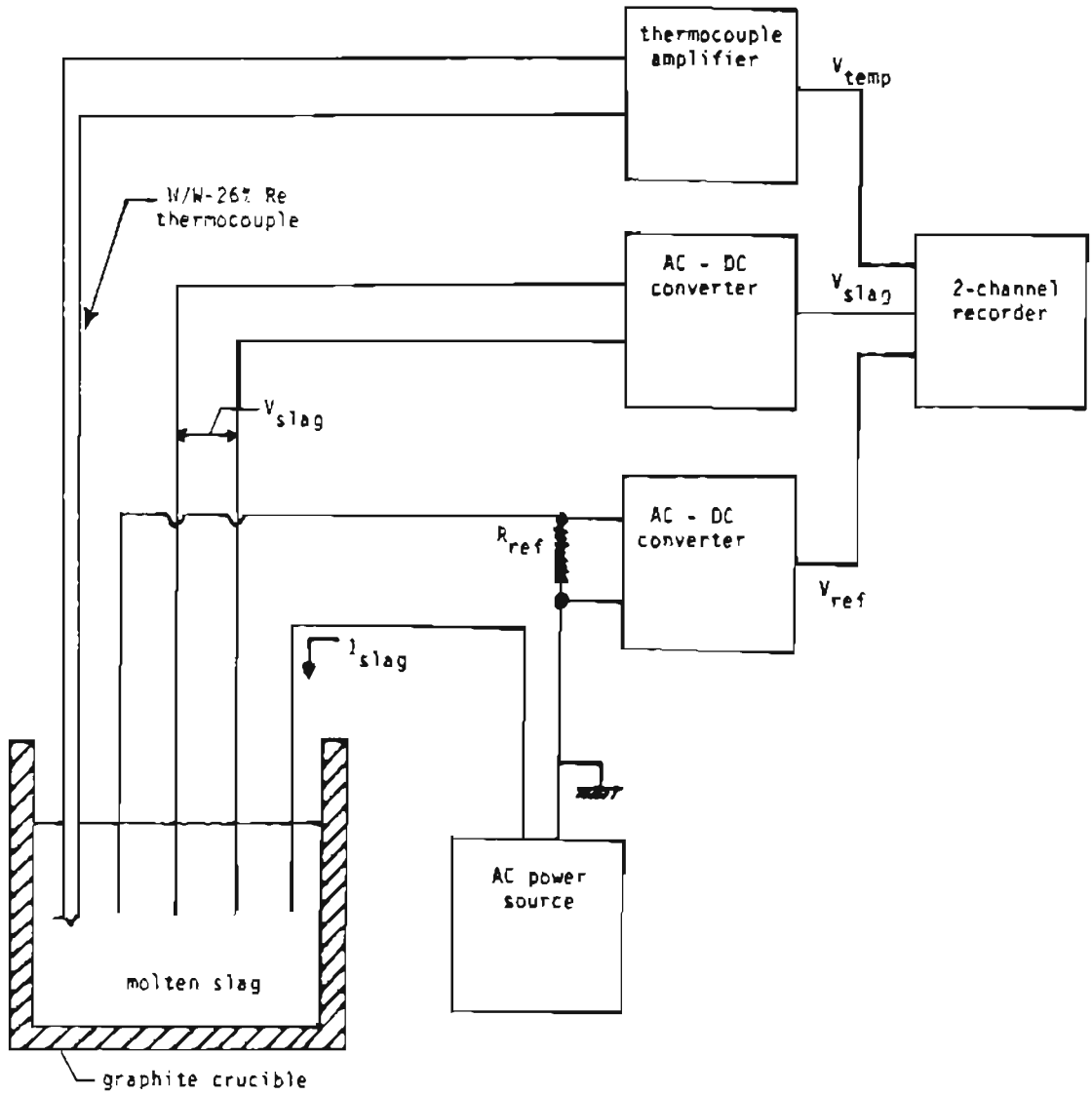

Figure 11. Schematic view of the resistivity measurement circuit diagram.

2. Electrode Resistivity and Ohmic Heating Measurements

The same four-electrode measuring technique describe above was adapted to measure the resistivity and ohmic heating of filler metal electrodes. The electric circuit diagram is shown in Figure 12. A 250 mm long electrode was placed between two copper holders which were connected to a DC CC (direct current constant current) power source. When current flows through the electrode, it heats up due to it's own electrical resistance.

The potential drop across a 50 mm gage length in the middle of the electrode and the potential drop across a standard resistor were measured. At the same time, the temperature rise of the electrode was measured by a k-type thermocouple which was spot welded in middle of the electrode. All measurements were recorded by strip chart recorders as shown in Figure 12. After the measurement, the resistivity values at different temperatures were calculated using equation 7 by substituting the electrode length over cross-section area value for the cell constant value. The initial ohmic heating rate of the electrode was obtained by measuring the slope at the beginning of the recorded temperature rise curve.

All measurements were repeated twice and the average values were used throughout this study. Titanium, steel, and stainless steel alloys were used to study the effect of resistivity on ohmic heating. Also, using different diameter electrodes (2.4 mm, 3.2 mm, and 12.5 mm diameter electrodes) and different applied currents (30 A and 135 A), the current density was varied from 0.24 A/mm^2 to 30 A/mm^2 and its

effect on electrode ohmic heating was evaluated. The resistivity values from room temperature to 1000 C of commercially pure Ti, Ti-6Al-4V, Ti-6211, 309 stainless steel, and low carbon steel were compiled from measurements made with different current density values. Some copper coated titanium and steel electrodes were tested before and after removal of copper coating to study the effect of copper coating on electrode ohmic heating.

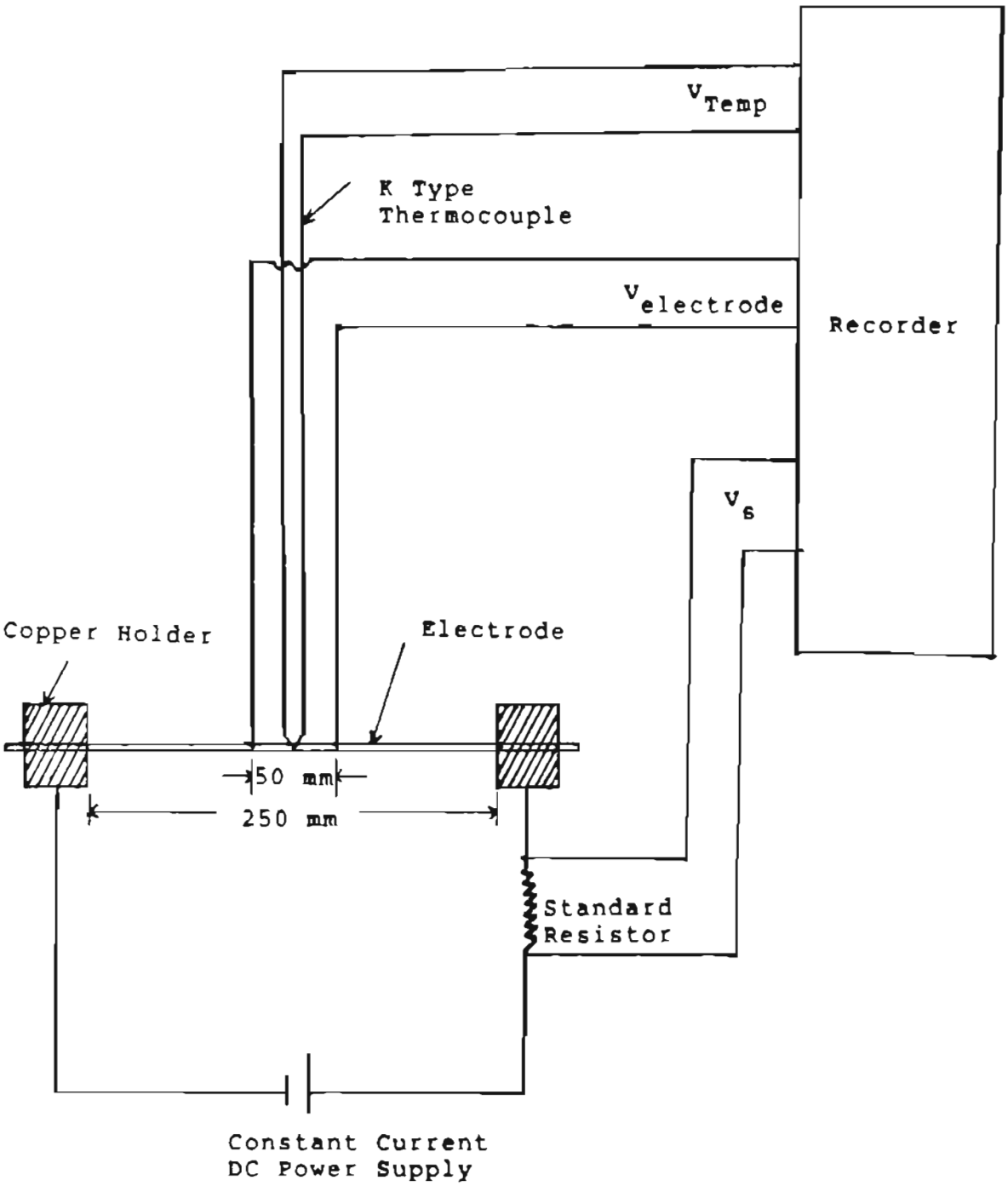

Figure 12. Schematic view of the resistivity and ohmic heating measurement circuit diagram.

C. Nonconsumable Guide ESW Process

1. ESW Steel for Reference

A short nonconsumable guide ESW system was set up to deposit stainless steel filler metal into a thick-wall steel tube as shown in figure 13. The welding head was manually withdrawn from the slag pool while the wire electrode was still being fed into the slag pool. Welding was initiated by striking an arc between the wire electrode and bottom plate. After the arc had been initiated, a fixed amount of flux was slowly added into the weld to form the slag pool. The depth of the slag pool was kept at around 25 mm to 32 mm.

Both AC and DC power supplies with constant voltage control were used along with pure CaF_2 flux and Hobart 201 flux (oxide base) to make the welds. Welding variables including voltage, current and wire feed rate were recorded. After the welds were made, they were sectioned down the middle and macroetched using a 10% nital solution to reveal the side wall penetration of the welds. Average penetration values were calculated by dividing the penetration area by the total welding length.

2. ESW Titanium Alloys

Since a thick-wall titanium alloy tube was not available, a 38 mm diameter hole was machined in the middle of a 10 cm x 10 cm square and 50 mm thick Ti-6Al-4V alloy plate. Two of the plates were lined-up and set on a base plate to form a 38 mm diameter 10 cm deep well. Similar to the steel welds, the nonconsumable guide ESW using pure CaF_2 flux was made by depositing a 3.2 mm diameter Ti-6Al-4V alloy wire into the well.

Both AC and DC power supplies with constant voltage control were used to make the weld.

In another attempt to make nonconsumable guide ESW of titanium alloy, the consumable guide plate and the welding head were attached to a vertical moving mechanism. As welding proceeded, the welding head as well as the guide plate were withdrawn upward from the molten slag pool. If the guide plate withdrawal speed was adjusted to be equal to the welding speed, the nonconsumable guide process could proceed smoothly until the end of the weld.

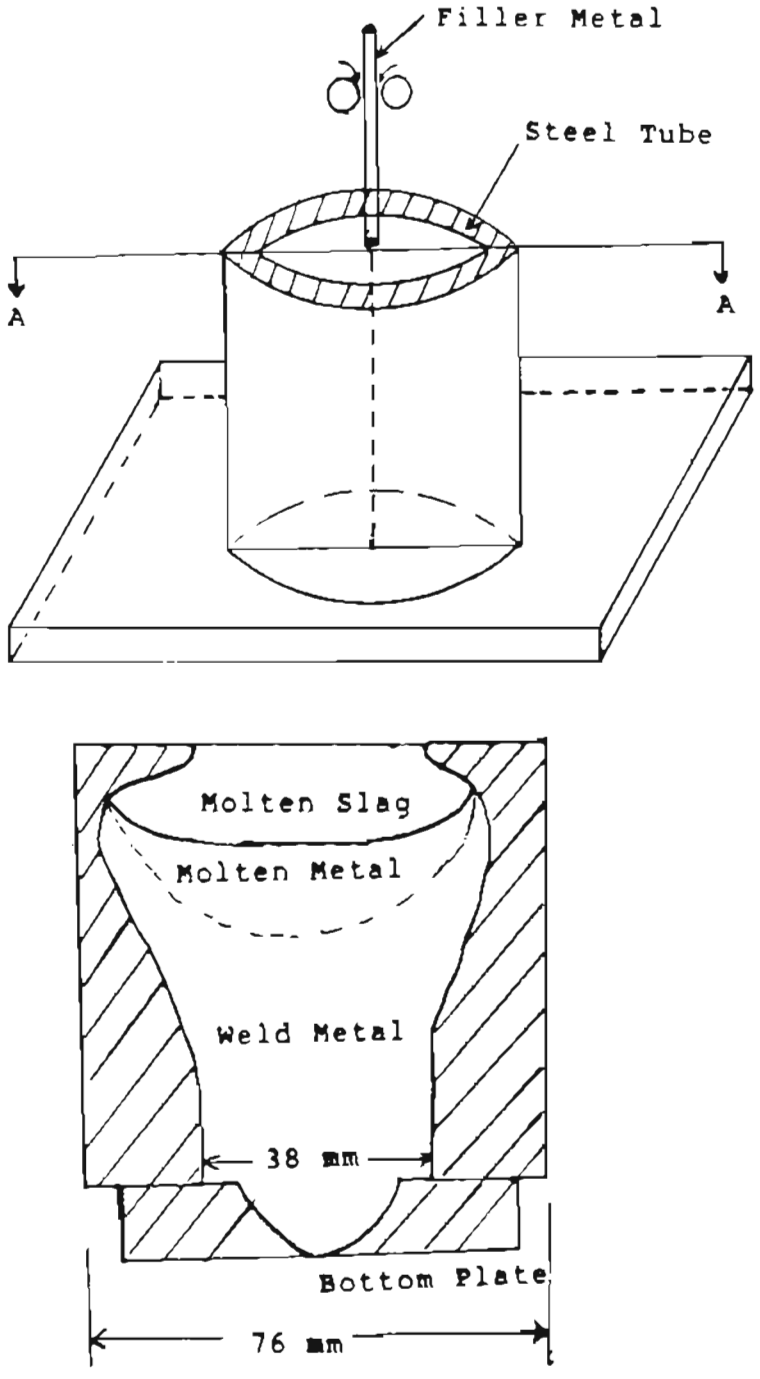

Figure 13. Nonconsumable guide ESW set-up for depositing stainless filler metal on a short steel tube.

D. Weld Evaluation

Three sets of experimental conditions were used to evaluate the structure and mechanical properties of 50 mm thick electroslag welds made with the optimum welding conditions developed in the previous section. These three sets were:

(1) ESW Ti-6Al-4V plates using high purity flux,

(2) ESW Ti-6Al-4V plates with reagent grade flux and

(3) ESW Ti-6211 plates using high purity flux.

After these welds were made, they were sectioned and machined for the following tests and observations.

1. Metallographic Observation

Transverse-to-weld sections were removed from each weld for macro-structure observation. Both transverse and longitudinal specimens from the weld center, heat affected zone (HAZ), and base metal were cut from each weld for microstructural assessment. All specimens were ground through different grit grinding papers, and were polished through 5, 0.3, and 0.05 micron alumina polishing wheels. A solution containing 200 ml H_2O, 30 g oxalic acid, 2 ml HF, and 5 g $Fe(NO_3)_3 \cdot 9H_2O$ was used to reveal the grain structure of the welds. The Kroll's reagent etchant containing 1-3 mL HF, 2-6 mL HNO_3, H_2O to 1000 mL was used to reveal the general microstructure.

tely 0.5 mm thick slices were cut by an abrasive silicon carbide wheel. These thin slices were ground to 100 micron thickness with pure methanol cooling. Discs with 3mm diameter were punched from these slices and were further thinned by electro-polishing. Electro-polishing was carried out in a jet polishing unit at -45 °C by using $CaCl_2$ in pure methanol solution. Then, these discs were examined under a Hitachi-800 scanning transmission electron microscope operating at 200 KV.

2. Chemical Analysis

Complete chemical analyses of selected welds and slags were performed, since the amount of the interstitial element content (especially oxygen, and nitrogen) has a great effect on the mechanical properties of the titanium alloys. Approximately 0.5 mm thick specimens were extracted from locations within the weld, heat-affected zone (HAZ) and base metal from mid-sections of each weld for oxygen and nitrogen analyses as well as selected carbon and hydrogen analyses.

3. Mechanical Testing

Transverse-to-weld tensile specimens having a 12.7 mm diameter were machined as per ANSI/ASTM E8 - 79a standard in order to assess the weld joint properties. To ensure the specimens were tested in the weld metal, all weld metal longitudinal specimens and smaller size 6.4 mm diameter specimens which had a gage length (25mm) smaller than the weld width (around 40 mm), were also tested. Tension tests were carried out in an Instron machine at a cross head speed of 0.041 mm/s.

Both Rockwell C hardness and Knoop microhardness tests were per-

formed on the metallographic sections of electroslag welds. Specimens for the microhardness test were taken from the same specimens for the transverse-to-weld microstructural studies. Microhardness readings were taken with a knoop indenter using a 500 gram load. Measurements were made 1 mm apart starting from the weld center to the base plate. Five measurements were taken at each location across the weld along the mid-thickness plane, and the average values were reported.

After the welded specimens were macroetched to reveal grain structure, the exact location of each notched CVN toughness specimen could then be accurately machined out of the welds as shown in Figure 14. Macroetching also permitted precise placement of the notch (using a broaching technique) in the CVN specimens. The specimens were then machined to final dimensions according to ASTM specification E23. The CVN toughness specimens were tested at three different temperatures: 0°C, 25°C, and 100°C (32°F, 77°F, and 212°F) respectively.

4. Fractography and Fracture Path Study

The fracture surfaces of both tensile and CVN toughness specimens were examined in a JEOL scanning electron microscopy. To study the relationship between the microstructure and the fracture path, some selected fractured specimens were nickel-plated and sectioned perpendicularly to the fractured surface. The schematic illustration of the sections made on a fractured CVN specimen is shown in Figure 15. The new sections were then ground, polished, and examined under the optical microscope.

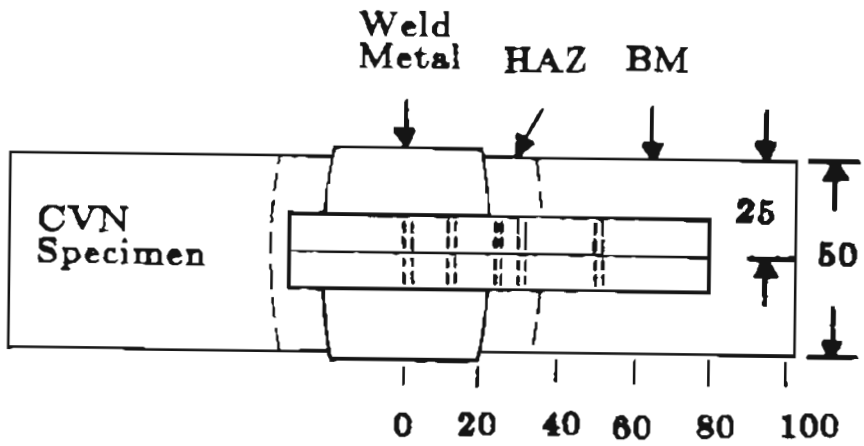

Figure 14. Specimen location for CVN toughness blanks taken from electroslag welds. The blanks were etched and notched in the appropriate location (dotted lines), and then machined to final dimensions. (All unit in mm).

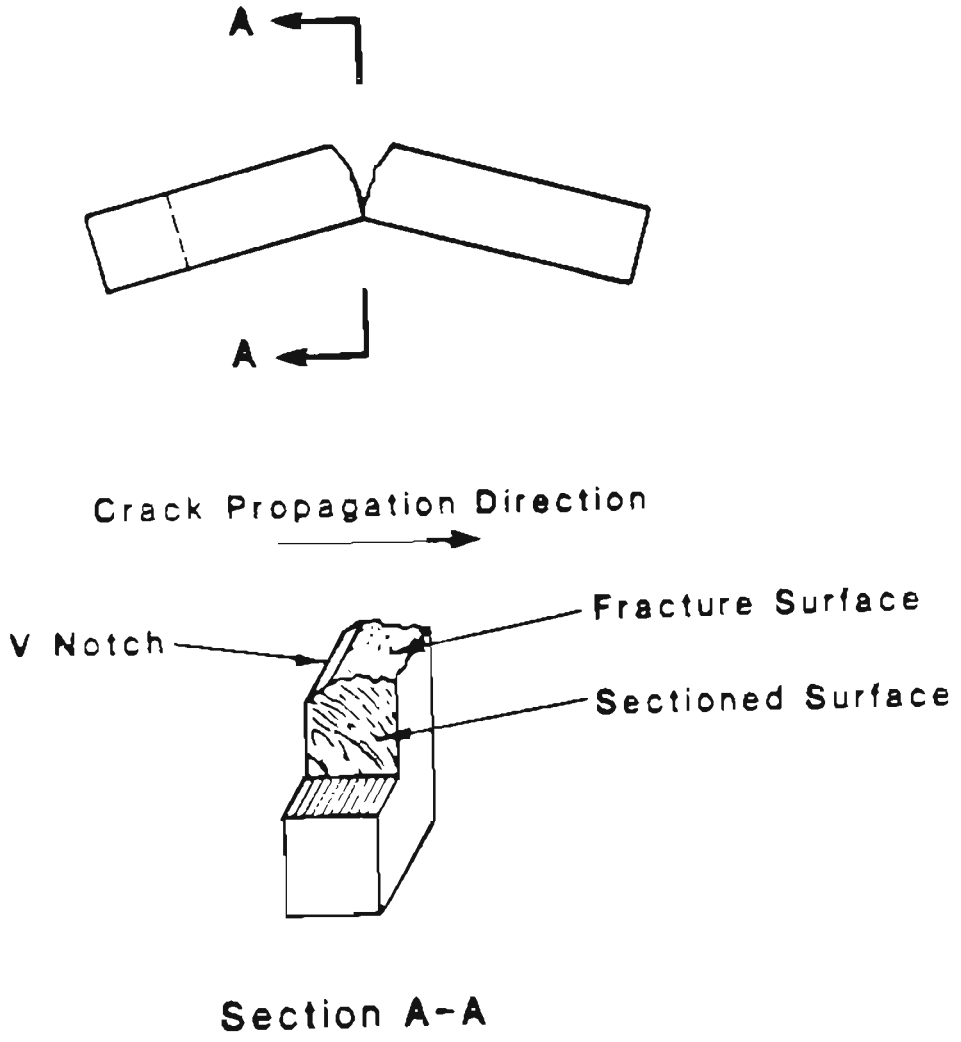

Figure 15. Schematic illustration showing sections made on fractured CVN specimen for crack propagation analysis.

IV. RESULTS

A. Consumable Guide ESW Ti Process Development

Sixty welds were made by the consumable guide ESW process with different welding variables, as shown in Table 4, in order to study the effect of different welding variables on the process stability and quality of the welds. The welding variables were divided into two groups. The first group of variables were those that had been fixed or preselected before welding. These variables included : electrode diameter, number of electrodes, welding gap, flux, power type and plate thickness. The second group of variables were those that were adjusted during the welding. These variables were welding voltage and welding current (or wire feed rate). In all welds, the currents and wire feed rates were not independent variables, because they were interrelated to each other. This was a characteristic of the constant voltage power supplies used for ESW of titanium alloy.

The adjustable variables (voltage and current) had a direct effect yon process stability as well as quality of the welds as shown in Table 4. If these variables were not properly adjusted during the welding, the ESW process would be interrupted by short circuiting or arcing. The resulting welds were unsatisfactory because of lack of fusion caused by slag entrapment. The preselected variables had only an indirect effect on the welding process. They affected the response of adjustable variables which controlled stability of the ESW process. If these variables were not selected properly, the working range of the adjustable

variables would be severely limited or non-existent.

Table 4 Consumable guide ESW of Ti-6Al-4V and Ti-6211 plates.

Weld No.	wire Dia. (mm)	No.of Wires	Gap (mm)	Flux	Ave. Current (A)	Ave. Voltage (V)	Power Type	Wire Feed Rate (mm/s)	Remarks
Ti-6Al-4V 50 mm thick plate :									
1	2.4	2	25	CaF_2	1000	30	AC	80	
2					900	30		55	
3					1100	30		70	
4					1200	25		80	
5					750	25		30	
6					950	25		45	
7					900	35		-	Arcing
8					600	35		-	Arcing
9					1200	30		75	
10					1600	30	DC(r)	72	Arcing
11					1600	25		80	Arcing
12			32	*	975	30	AC	65	
13				*	-	35		-	Arcing
14				*	975	30		62	
15	3.2	1		CaF_2	1000	30		60	
16					750	30		35	Arcing
17					900	30		50	
18					900	25		55	
19					750	25		25	Arcing
20					1000	25		60	
21				SrF2	950	30		60	
22				CaF_2	1100	25		65	
23					1500	25	DC(s)	50	Arcing
24					1500	30		65	Arcing
25	2.4				930	25	AC	110	
26					1130	25		130	
27					850	25		66	Arcing
28		2			950	25		47	
29					1150	25		68	
30					1100	25		61	

Table 4 (continued)

Weld No.	wire Dia. (mm)	No.of Wires	Gap (mm)	Flux	Ave. Current (A)	Ave. Voltage (V)	Power Type	Wire Feed Rate (mm/s)	Remarks
31					800	25		31	Arcing
32					1120	30		66	
33					950	30		47	
34					1150	35		66	Arcing
35					800	30		40	
36					1200	35		102	Arcing
37				**	1000	30		66	
38				**	1050	30		70	
39				**	1200	30		82	
40				**	1100	25		48	
41				**	1200	25		70	
42				***	1150	30		75	
43				***	900	30		48	
44				***	800	30		40	Arcing
45	2.4	2	32	****	1100	30		57	
46				****	800	30		40	Arcing
47				****	1200	30		80	
48				*****	1200	30		75	
49	3.2	1		CaF_2	1000	30		62	
50				(CaF_2)	1000	30		60	
51				(CaF_2)	1000	30		60	
52		2		CaF_2	1200	30		40	
53				CaF_2	1000	30		30	
54				(CaF_2)	1000	30		30	
Ti-6Al-4V 25 mm thick plates :									
55	3.2	1	25	CaF_2	600	30		36	(1"plate)
56					700	30		45	
57					450	30		22	
58					400	30		20	Arcing
Ti-6211 50 mm thick plates :									
59	3.2	1	32	(CaF_2)	1000	30		60	
60					1000	30		60	

* CaF_2-40% SrF2-10% LaF_3
** CaF_2-25% LaF_3
*** CaF_2-12.5% LaF_3
**** CaF_2-12.5% YF_3
***** CaF_2-25% YF_3

1. Working Range of ESW Variables

For consumable guide ESW of 50mm Ti-6Al-4V plates using an AC square wave power supply and pure CaF_2 flux, the optimum range for voltage was 25-30 volts and current was 850-1200 amps as shown in Figure 16. When the voltage was kept below 25 volts, the weld exhibited lack of fusion resulting from insufficient heat input. When the voltage was adjusted above 30 volts, the welds again had lack of fusion problems resulting from unstable arcing above the slag pool. That is, above 30 volts, the welding process changed from a stable ohmic electroslag mode to unstable arcing. The unstable arcing produced virtually no side-wall fusion because most of the arc heat was expended as radiation and vaporizing a surface layer of the slag pool.

Although not as critical as voltage, the current had to be maintained within 850 A - 1200 A as shown in Figure 16. The minimum current value below which arcing occurred on top of the slag pool was approximately 850 A. This value corresponds to a current density of 1.8 A/mm^2 (including the cross sectional area of the filler metal and consumable guide plates). The maximum current value above which severe guide plate oxidation occurred was approximately 1200 A corresponding to a current density value of 2.5 A/mm^2. However, the argon shielding gas provided protection for all of the heated titanium parts during the ESW process. The maximum current value was also bounded by the limitation of power supply. The machine was rated 100% duty cycle at 1000 A, therefore it could only be used continuously at 1200 A for 6 to 7 minutes.

Compared to the working range reported for steel for a similar

thickness with CV-DC, and the highly resistive Hobart 201 flux,[16] the working range for ESW the titanium alloys was smaller and shifted to lower voltages and higher current values. The difference was mainly caused by electrical resistivities of the different fluxes used for ESW of titanium verse steel. Molten CaF_2 slag used for ESW titanium alloys had lower resistivity than the molten oxide-base slag (Hobart 201 flux) used for ESW steels, and it favored operation at low voltage and high current conditions.

But welds made in this low-voltage and high-current welding regime had lower base metal dilution due to its lower heat input values. For example, a 50 mm thick plate of steel could be welded by using Hobart 201 flux with 600 A, 45 V and 0.21 mm/s travel speed (129 kJ/mm), while a similar weld of Ti-6Al-4V could be deposited by using pure CaF_2 flux with 1000 A, 30 V, and 0.47 mm/s travel speed (64 kJ/mm). Clearly, the high resistivity slag is capable of substantially increased heat input by virtue of its ability to sustain high voltages without any arcing instability.

2. Dilution of the Welds

The average percentage base metal dilution values of the consumable guide ESW of 50 mm thick Ti-6Al-4V plates using AC power supply and pure CaF_2 flux were plotted with respect to welding voltages and currents as in Figure 17. The average base metal dilution values were measured from the macroetched transverse sections at the bottom, middle and top of the welds. It is clearly shown in Figure 17 that base metal

dilution increased with increasing voltage and was independent of current level.

The effect of current on the base metal dilution was counter-balanced by the filler metal feed rate. When current was increased, by increasing the filler metal feed rate, the welding speed was also increased and the time allowed for conducting heat to the base metal decreased. In the ESW process, the base metal dilution was directly proportional to the welding voltage and the filler metal melting rate was directly proportional to welding current.

The average base metal dilution values were also plotted as a function of the welding heat input in Figure 18. The welding heat input was calculated from equation 3. However, the welding heat input alone is not a good indication of the base metal dilution in the consumable guide ESW Ti-6Al-4V alloy as shown in Figure 18. For example, when the heat input was 60 kJ/mm, the average base metal dilution value varied from 0% to 35%. This is a direct result of neglecting heat distribution and heat loss in the molten slag pool. Especially, When low filler metal melting rate was used, equation 3 gave very high heat input prediction because of low welding speed. But the weld had low base metal dilution because heat produced by the slag was concentrated on top of the slag pool and a large portion of heat was lost to the air which was unavailable for melting the base metal.

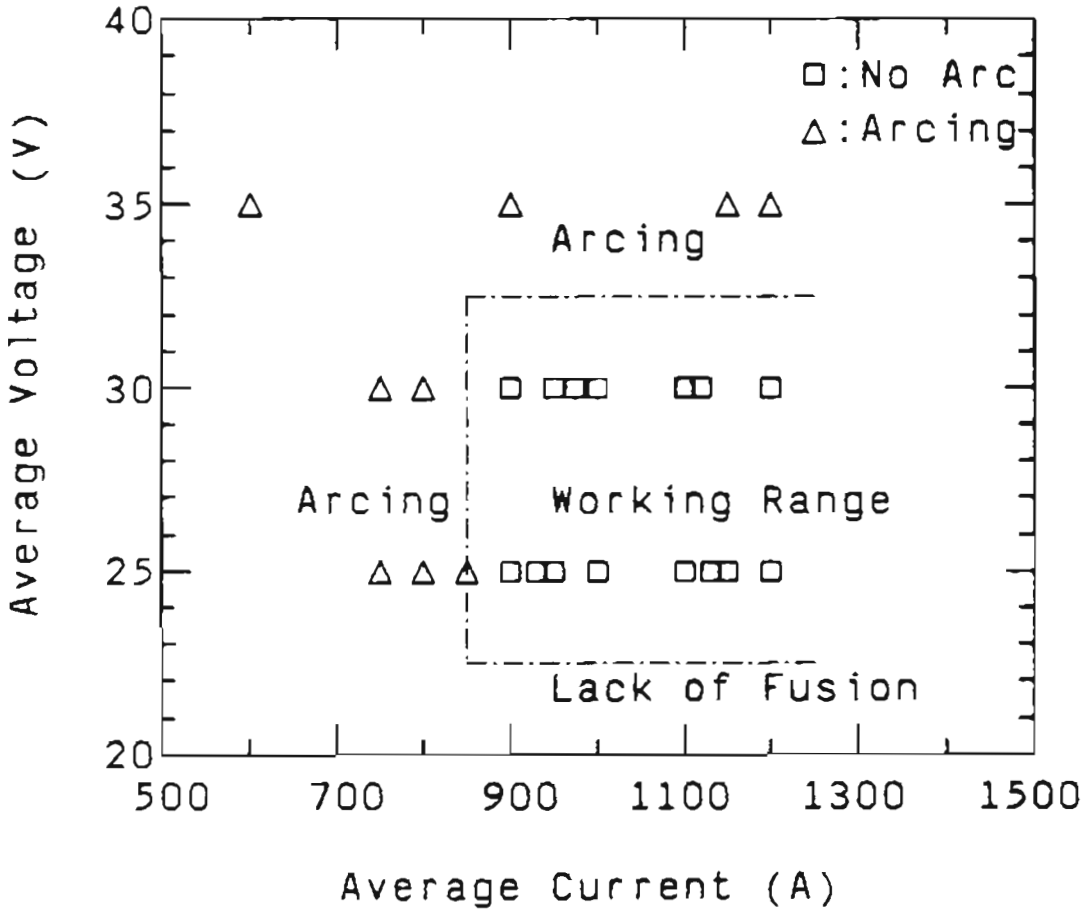

Figure 16. Welding voltage and current working range for consumable guide ESW of 50 mm (2") thick Ti-6Al-4V plates using AC power supply, pure CaF_2 flux.

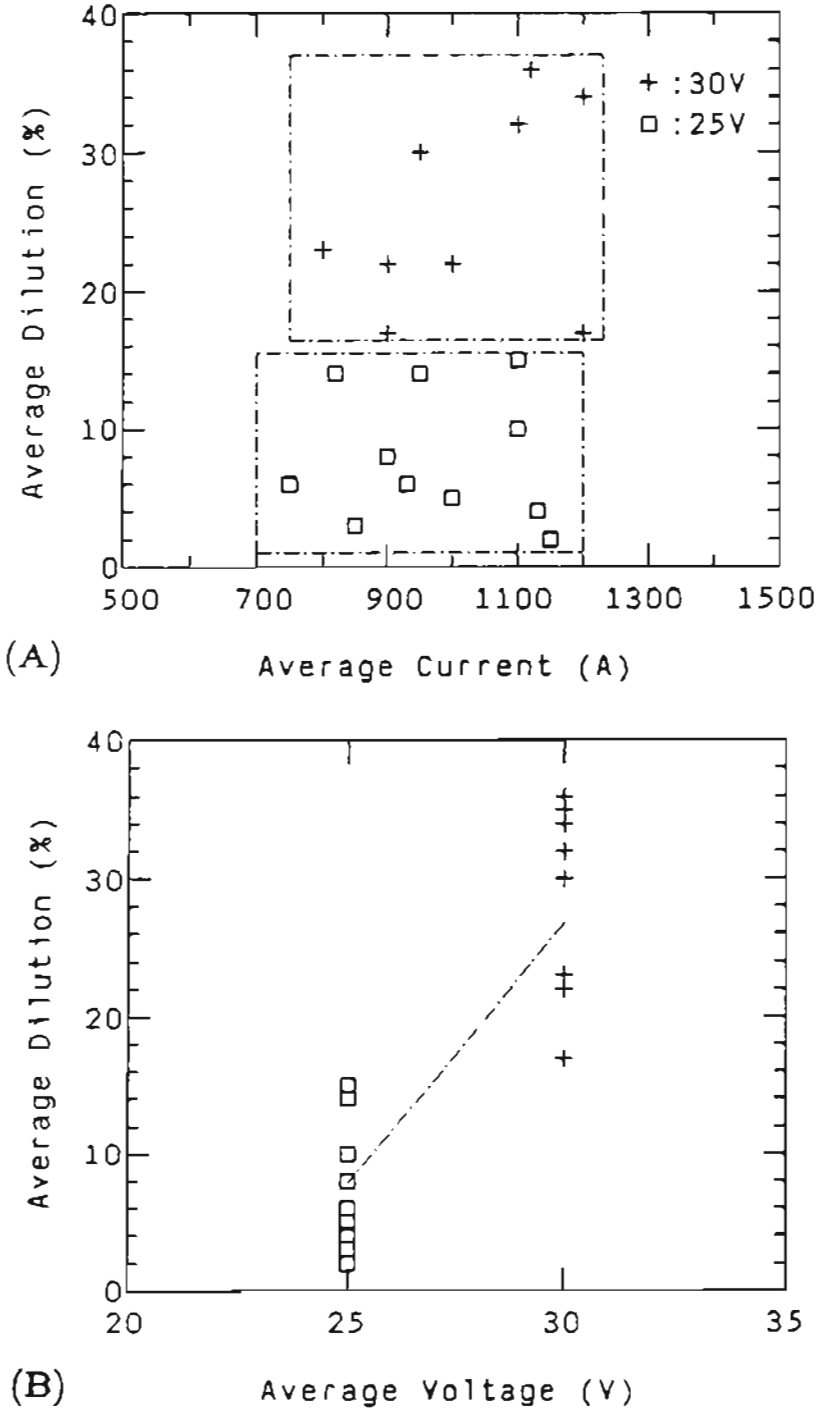

Figure 17. Effect of welding variables on average base metal dilution of 50 mm thick Ti-6Al-4V electroslag welds made with reagent grade CaF_2 flux (A) Current and (B) Voltage.

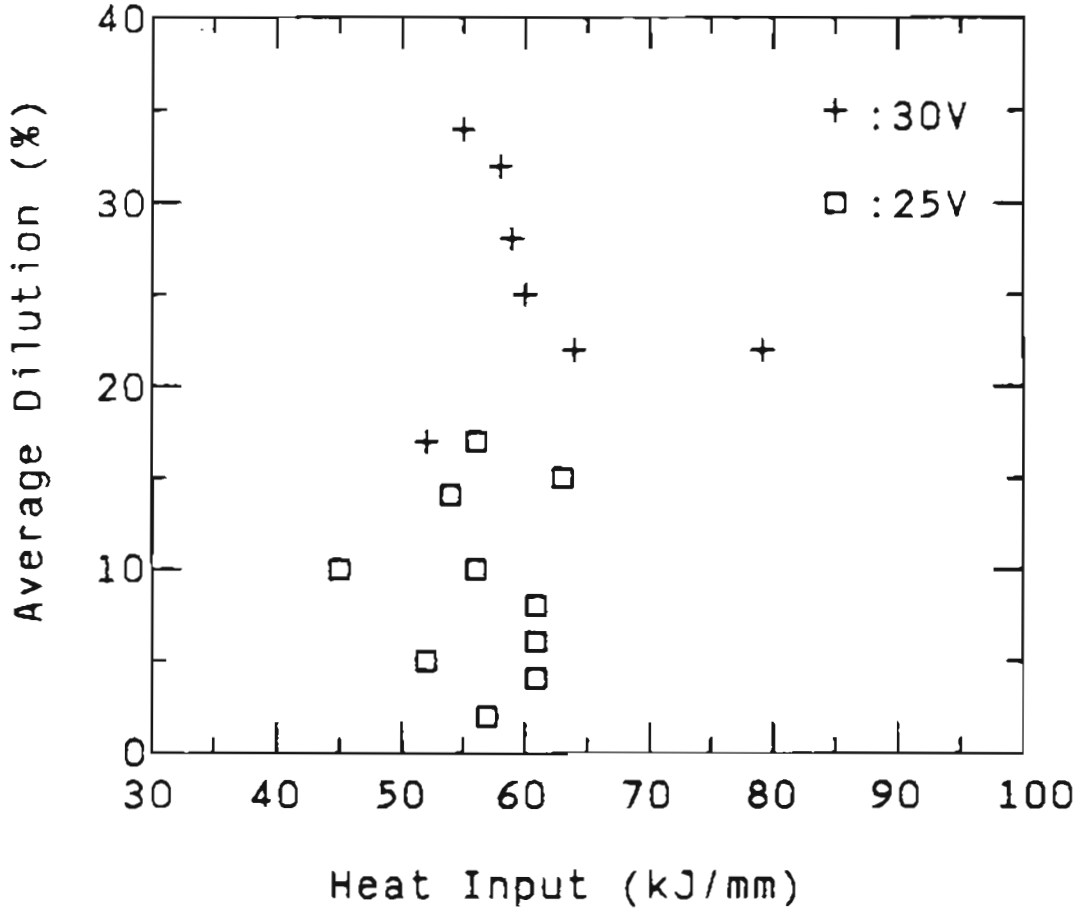

Figure 18. Correlation between the welding heat input and average base metal dilution of 50 mm thick Ti-6Al-4V electroslag welds made by AC power supply and pure CaF_2 flux.

3. Filler Metal Diameter

In consumable guide ESW of 50 mm thick Ti-6Al-4V alloys, four different combinations of filler metals were used to study the effect of filler metal diameter on the welding process. These four combinations are as follows:

A. single 2.4 mm diameter filler metal
B. dual 2.4 mm diameter filler metals
C. single 3.2 mm diameter filler metal
D. dual 3.2 mm diameter filler metals.

These filler metal combinations were successful used to join 50 mm thick Ti-6Al-4V plates together. The working range of voltage and current shown in Figure 19 was the same for all four combinations of filler metals. Because the guide plates had same cross-section area as shown in Figure 8. Comparing with the non-consumable guide ESW of titanium alloy in later section, the consumable guide plate made it possible to use smaller diameter filler metal for ESW of titanium alloy without arcing.

When current was plotted against filler metal melting rate (filler metal feed rate times filler metal cross-section area times number of filler metals) as in Figure 20, a single linear correlation was obtained in spite of different combination of filler metals were used. The linear relationship between current and filler metal melting rate showed that in the consumable guide ESW process, filler metal melting rate was not controlled by the ohmic heating (proportional to I^2R) of the filler

metal. The filler metal melting rate was controlled by the heat conducting from the surrounding molten slag pool which was directly proportional to the welding current.

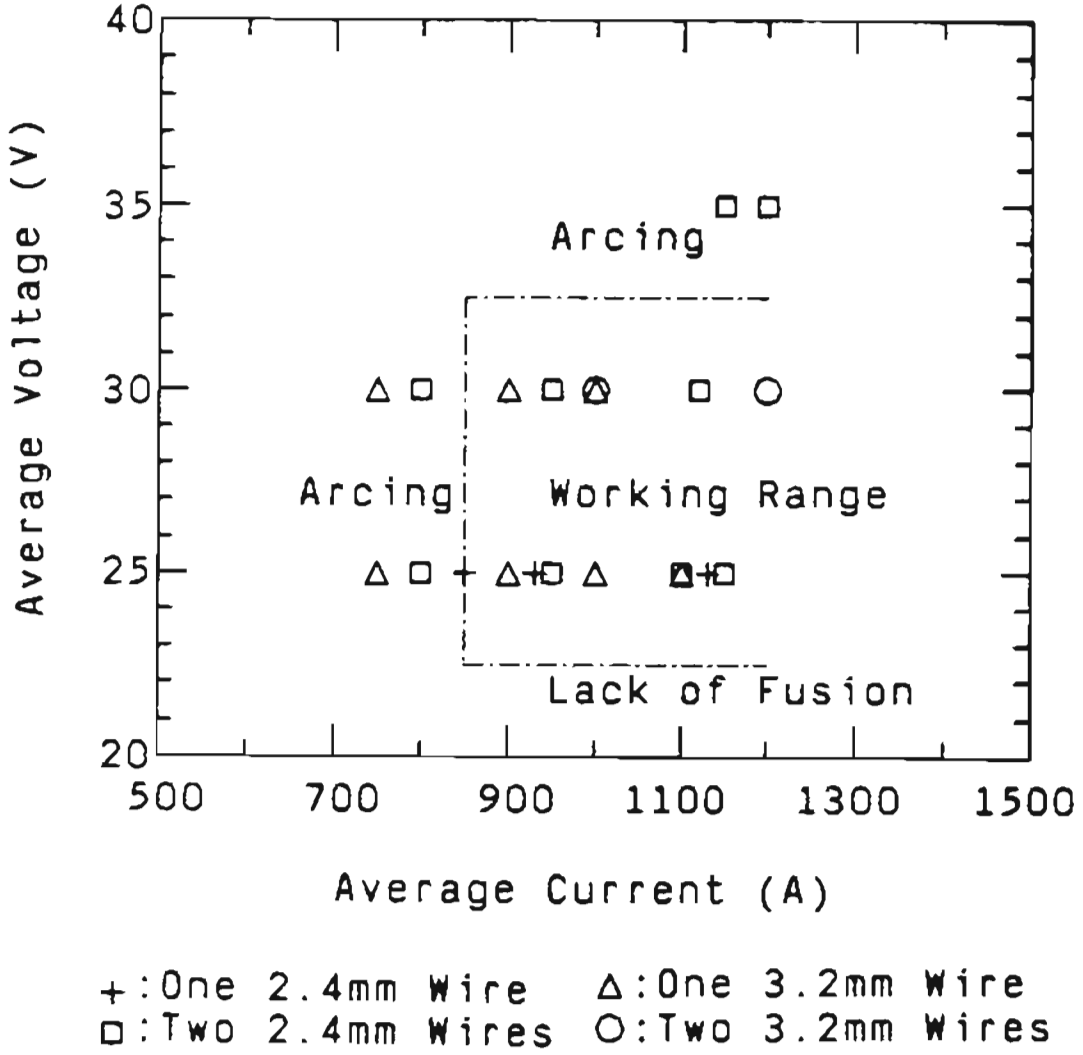

Figure 19. Effect of filler metal diameter on the working range of consumable guide ESW of 50 mm thick Ti-6Al-4V plates jointed by AC power supply and pure CaF_2 flux.

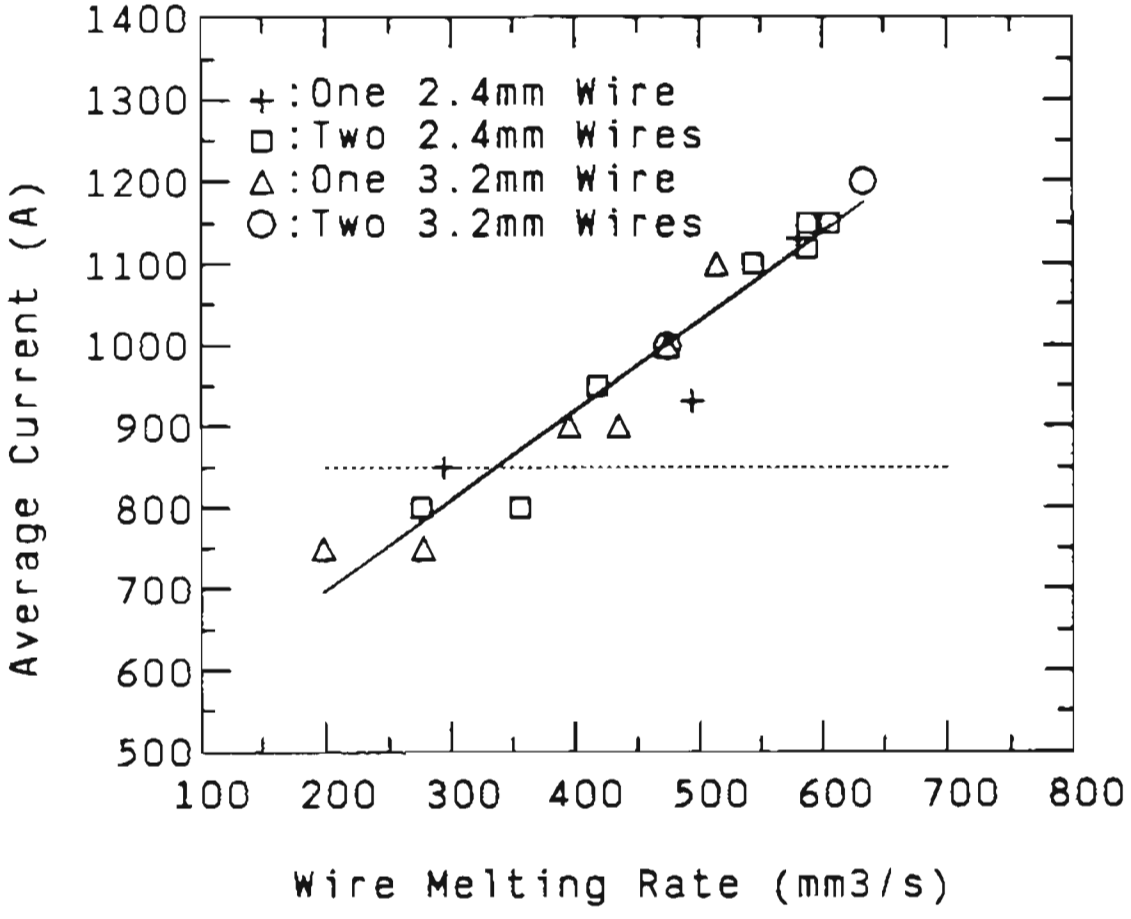

Figure 20. Correlation between current and filler metal melting rate of 50 mm thick Ti-6Al-4V electroslag welds using AC power supply, pure CaF_2 flux and different diameters of filler metal.

4. Plate Thickness Effect

The welding conditions used to join 50 mm (2") Ti-6Al-4V plates were modified and applied to join 25 mm (1") Ti-6Al-4V plates. These modifications included reducing the cross-section of guide tube to half, decreasing welding gap from 32 mm to 25 mm and reducing the initial flux addition from 150 g to 100 g but maintaining a slag pool of the same depth. The working range of current obtained at 30 V was 450 A - 600 A shown in Figure 21. When the current was kept above 700 A, the guide plate turned red hot, and when the current was kept below 450 A, the process became unstable and arcing occurred on top of the slag pool.

This current working range corresponded to current density values between 1.8 A/mm^2 and 2.5 A/mm^2, similar to the results obtained from consumable guide ESW of 50 mm thickness welds. This shows that. if the slag pool depth and voltage were unchanged, the current had to be increased with increasing plate thickness to maintain the same current density in both guide plate and slag pool. Then, the working current density range could be used to predict the required working current range for consumable guide ESW of different thicknesses of titanium plates. For example, the current working range for consumable guide ESW of 100 mm (4") thick titanium plates would be 2000 A to 2800 A.

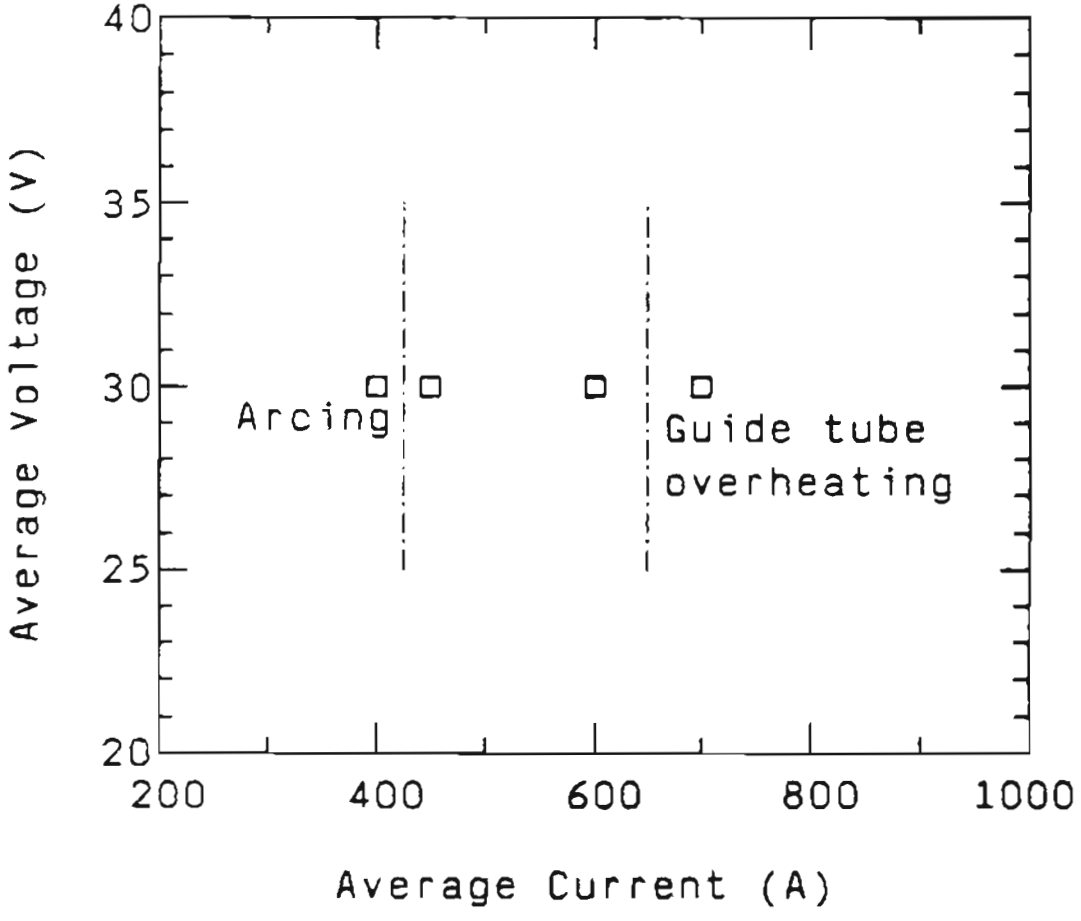

Figure 21. Current working range for consumable guide ESW of 25 mm (1") thick Ti-6Al-4V plates using AC power supply and pure CaF_2 flux.

5. Flux Alloying

Another attempt to widen the working window for ESW titanium was the addition of different fluorides to increase the resistivity of the pure CaF_2 flux. These fluxes included LiF, NaF, MgF_2, SrF_2, AlF_3, LaF_3, and YF_3. After preliminary study, LiF, NaF, MgF_2, and AlF_3 flux additions were disregarded because of their volatility at the ESW temperature range. Both LaF_3 and YF_3 flux additions study were carried on because these two flux were very stable at ESW working temperature range, and showed signs of increasing the resistivity of CaF_2 flux.

Up to 25 % of either LaF_3 or YF_3 flux were added to the pure CaF_2 flux for ESW titamnium alloys. The effect of LaF_3 and YF_3 flux additions on welding current and filler metal melting rate of ESW process were shown in Figure 22. Compared with the welds made by the pure CaF_2 flux at the same filler metal feed rate, the welding current decreased with increasing amount of either LaF_3 or YF_3 flux addition. Though this showed signs of reducing the welding current, the effect was still insufficient to widen the working range as shown in Figure 23. The welding working range for LaF_3 or YF_3 flux additions to the pure CaF_2 flux remained the same as the welding working range by using the pure CaF_2 flux alone.

Fluxes with LaF_3 and YF_3 additions greater than 25 % were not used because their densities are higher than that of molten titanium alloy. This resulted in slag entrapment in some welds made with 25 % LaF_3 or YF_3 additions to the CaF_2 flux. The effect of LaF_3 or YF_3 flux addition on the base metal dilution is shown in Figure 24. At the same welding

current, welds made by CaF_2 flux with either LaF_3 or YF_3 flux addition had lower base metal dilution than welds made by pure CaF_2 flux. This result could be explained by the higher heat input of the welds made by pure CaF_2 which had the highest welding current at the same filler metal melting rate (same welding speed), and same welding voltage as shown in Figure 22.

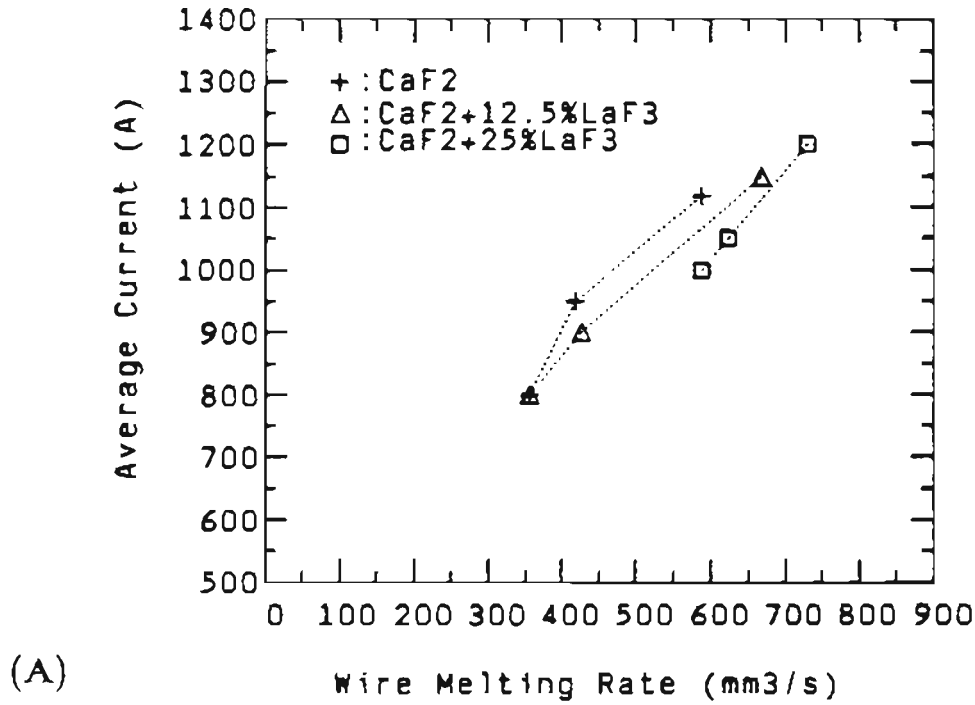

(A)

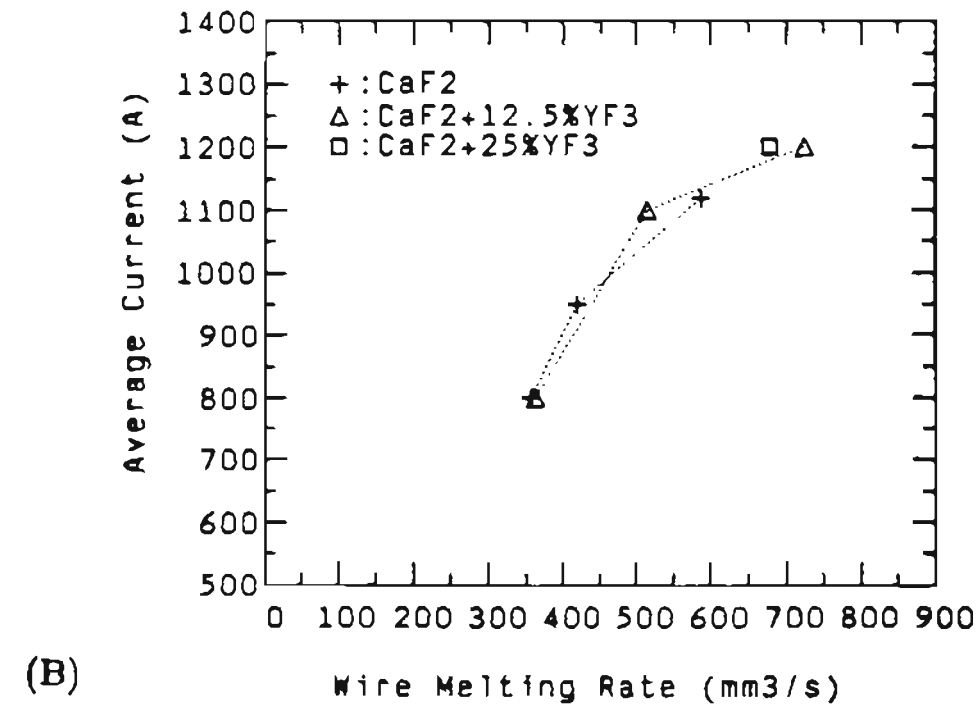

(B)

Figure 22. flux additions effect on current and filler metal melting rate of 50 mm thick Ti-6Al-4V electroslag welds made with two 2.4 mm filler metals, 30 volts and AC power supply: (A) LaF_3 flux addition, and (B) YF_3 flux addition.

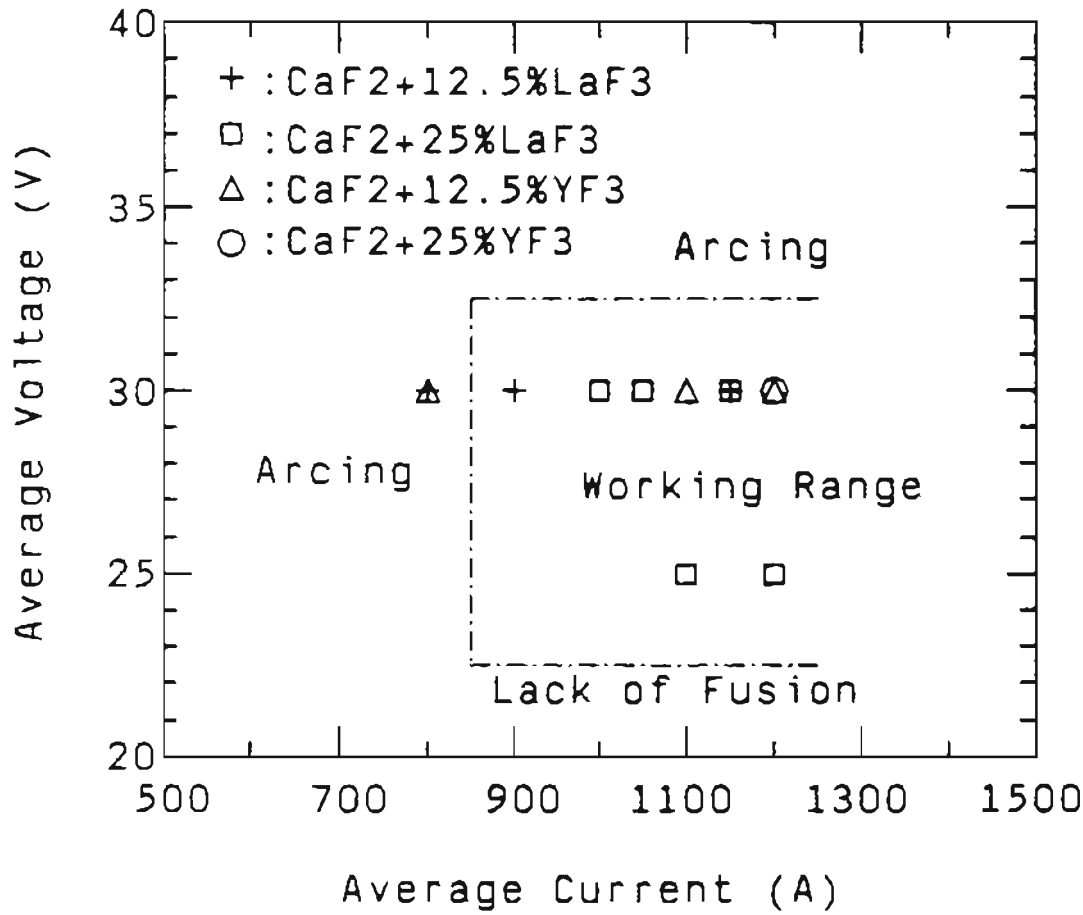

Figure 23. Welding voltage and current working range for electroslag welds made with different fluxes.

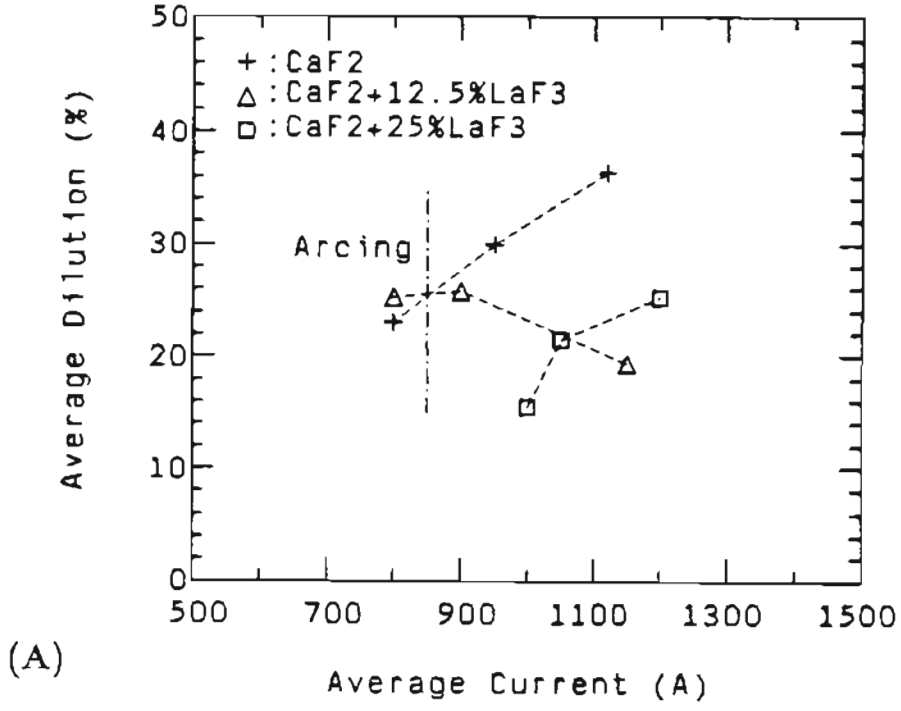

(A)

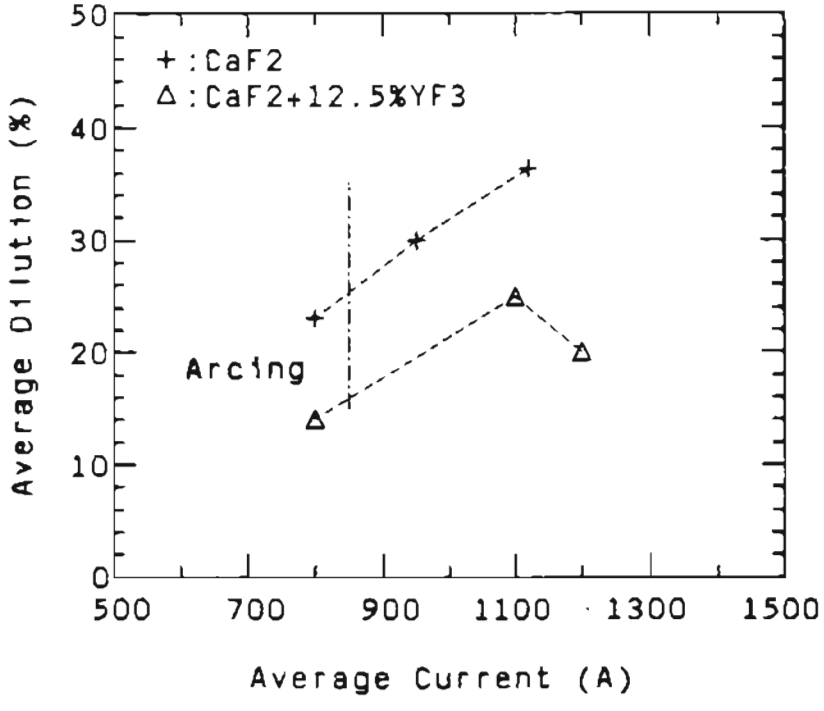

(B)

Figure 24. Flux additions effect on the percentage base metal dilution of 50 mm thick Ti-6Al-4V electroslag welds (A) LaF_3 flux addition, and (B) YF_3 flux addition.

6. ESW With DC Power Supply

Unlike AC welding, attempts at ESW of Ti-6Al-4V with a CV DC power source proved unsuccessful. Regardless of the combination of current, voltage, polarity, welding speed and filler metal diameter, consumable guide ESW with DC power could not develop enough ohmic heat to produce a fully fused weld joint. In all cases, an unstable arc developed above the slag and no window of acceptable welding parameters could be established. The welding current fluctuated between 900 A and 2100 A as shown in Figure 25 (B), compared with a smaller current fluctuation between 750 A and 1050 A in a stable AC ESW process (Figure 25 (A)).

The only technique to successfully utilize DC CV power was to drive the guide plate (while the filler wire was still feeding through the guide plate) into the slag pool at a speed approximately equal to half the welding speed. For example, the guide plate of a weld deposited on 50 mm thick plate at a welding speed of 50 mm/min had to be driven into the slag pool at a speed of approximately 25 mm/min to reduce current density and sustain ohmic slag heating. Thus, by this method, the guide plate length (consumed during welding) was at least 1.5 times the length of weld.

Although this method produced sound welds, the action of driving the guide plate represented unnecessary procedural requirements. In addition, often there was inadequate space available above the welding head to accommodate the long guide plate. Compared to the simplicity of the AC CV welding system, the DC moving guide plate method would not be considered practical.

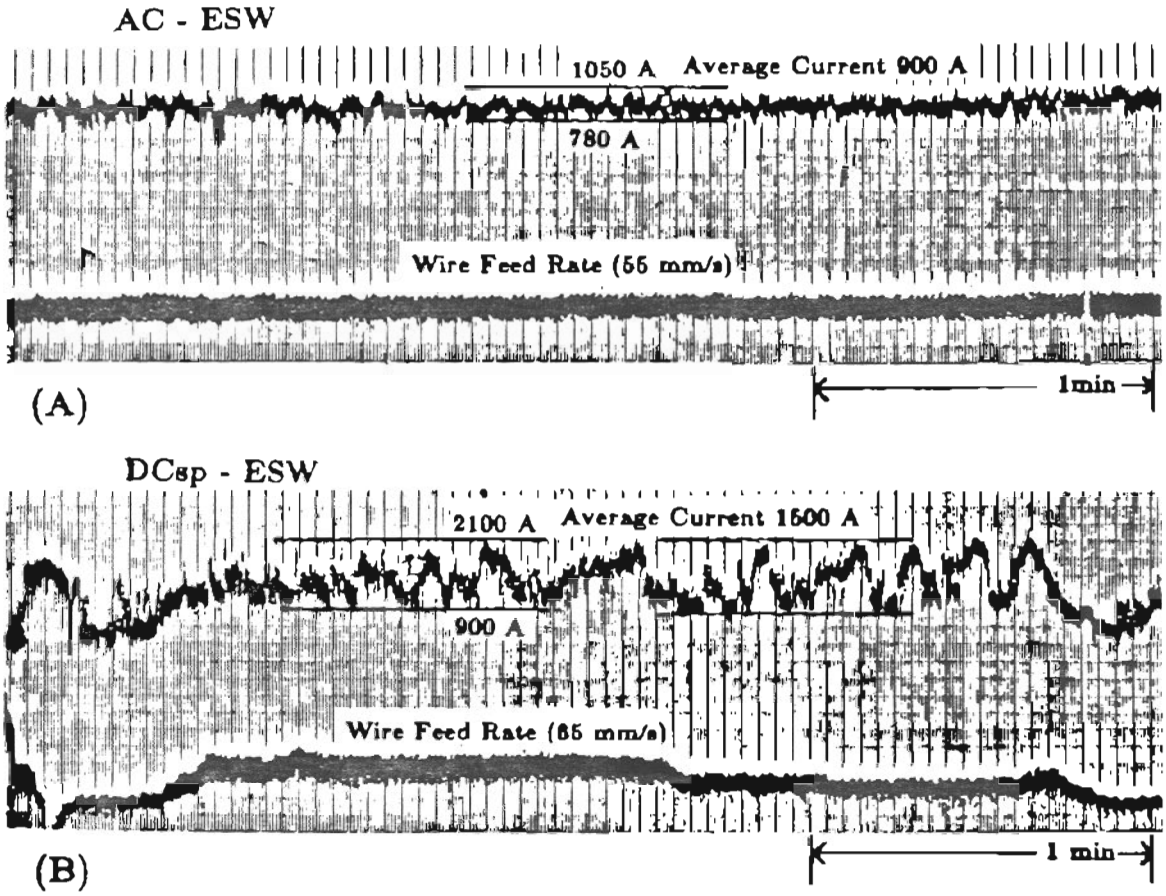

Figure 25. Chart recording of the welding current and filler metal feed rate during consumable guide ESW of 50 mm thick Ti-6Al-4V plates:(A) stable process using AC power supply, and (B) unstable process using DC power supply.

7. Interstitial Element Contamination

Interstitial elements content of the titanium welds, specifically the oxygen and nitrogen levels, are shown in Table 5. Results of Ti-6AL-4V welds showed that welds made by high purity CaF_2 flux (# 51) had lower interstitial element contents than welds made by reagent grade CaF_2 flux (#49, #52), in both longitudinal and transverse sections. The results also indicated that contamination came from air because the welds that had a high oxygen content also had a high nitrogen content and the top of the weld (end) had higher oxygen and nitrogen contents than the bottom of the welds (beginning). Air could get into the ESW process through the gap between cooling shoes and base plates, or it could be fed into the molten slag pool as a stagnant layer on the filler metal. Another source of contamination is the guide plate which could pick up interstitial elements during fabrication and welding.

Despite all the possible sources for contamination, the results of Ti-6211 weld showed that it was free of interstitial elements contamination. The Ti-6211 weld was deposited with high purity CaF_2 flux and special cooling shoes which contained an argon spraying device similar to the one shown in Figure 1.

Table 5. Interstitial elements content (wt%) of titanium electroslag weld and base metals.

Identification	O	N	H	C
Ti-6Al-4V :				
Base Metal	.22	.021	.001	.033
Weld # 38	.22	.014	-	-
Weld # 54	.21	.019	.004	-
Weld # 51 Longitutional Section :				
Bottom	.19	.015	.005	-
Middle (10 cm from bottom)	.28	.022	.004	-
Top (20 cm from bottom)	.23	.015	.005	-
Weld # 52 Longitutional Section :				
Bottom	.19	.007	-	-
Middle (10 cm from bottom)	.28	.034	-	.021
Top (20 cm from bottom)	.32	.034	-	-
Weld # 49 Transverse Section :				
Weld center	.35	.027	-	-
Weld (10 mm from WC)	.35	.029	-	-
HAZ (24 mm from WC)	.25	.018	-	-
HAZ (30 mm from WC)	.20	.012	-	-
BM (40 mm from WC)	.19	.011	-	-
Weld # 51 Transverse Section :				
Weld Center	.22	.011	-	-
Weld (10 mm from WC)	.22	.014	-	-
HAZ (24 mm from WC)	.19	.009	-	-
HAZ (30 mm from WC)	.18	.007	-	-
BM (40 mm from WC)	.19	.009	-	-
Ti-6211 :				
Base Metal	.077	.006	.004	-
Weld # 59 Transverse Section :				
Weld Center	.085	.005	-	-
Weld (10 mm from WC)	.091	.008	-	-
HAZ (24 mm from WC)	.083	.006	-	-
HAZ (30 mm from WC)	.084	.007	-	-
BM (40 mm from WC)	.077	.006	-	-

WC: Weld center
HAZ: Heat affected zone of base metal
BM: Base metal

8. Steel Welds for Reference

Fifty-mm thick steel plates with the same welding gap and guide tube geometry as Ti-6AL-4V electroslag weld joints were welded by ESW with either pure CaF_2 or Hobart 201 (oxide base) fluxes. Results in Table 6 indicate that ESW of steel alloy has a larger working range than ESW of Ti-6Al-4V alloy. By using pure CaF_2 flux, the current working range for ESW of the steel plate was 500 A to 1200 A, which was wider than the current working range (850 A to 1200 A) for ESW of Ti-6Al-4V alloy. But the voltage working range for ESW of steel alloy was 25 V to 30 V, which was the same as the voltage working range for ESW of Ti-6Al-4V alloy.

When Hobart 201 flux was used, the working range of ESW of steel was further widened beyond that of ESW of steel using pure CaF_2 flux. The current working range was 500 A to 1200 A and the voltage working range was 30 V to 55 V.

It is important to know that the voltage working range for ESW is controlled by the flux resistivity and welding geometry. With the same welding geometry, the electroslag welds made by the higher resistivity Hobart 201 flux had a larger working range than did the electroslag welds made by lower resistivity CaF_2 flux. For the same plate thickness, the current working range for ESW was controlled by the resistivity of filler metal and guide plate. The welds made by lower resistivity steel filler metal and guide plate had a wider current working range than the welds made with the higher resistivity titanium filler metal and guide plate.

For 50 mm thick welds, the filler metal melting rates were plotted against average welding currents at 30 V in Figure 26. Comparing all steel electroslag welds, welds made by Hobart 201 flux had higher filler metal melting rates than welds made by pure CaF_2 flux at the same average welding current. Also, at the same average welding current, Ti-6Al-4V welds made by pure CaF_2 flux had higher filler metal melting rates than steel welds made by both pure CaF_2 flux and Hobart 201 flux.

Hobart 201 flux could not be used in ESW of Ti-6Al-4V alloy, because titanium reacted severely with oxygen contained in Hobart 201 flux. The ESW process changed totally to an arcing process. The weld metal was saturated with oxygen and became so brittle, it could simply be chipped away.

Table 6 Comparison study of titanium vs steel consumable guide ESW with one matching filler metal (3.2 mm diameter), 32 mm welding gap, and AC power supply.

Weld No.	Material	Flux	Ave. Current (A)	Ave. Voltage (V)	Wire Feed Rate (mm/s)	Remarks
61	Ti	*	-	40	-	arcing
62	steel	*	600	45	27	
63	steel	*	700	38	30	
64	steel	CaF_2	1000	30	25	
			700	30	20	
65	steel	CaF_2	-	35	26	arcing
			-	35	15	arcing
			600	30	18	
66	steel	*	600	30	27	
			750	30	32	
			1000	30	37	

* : Hobart 201 flux

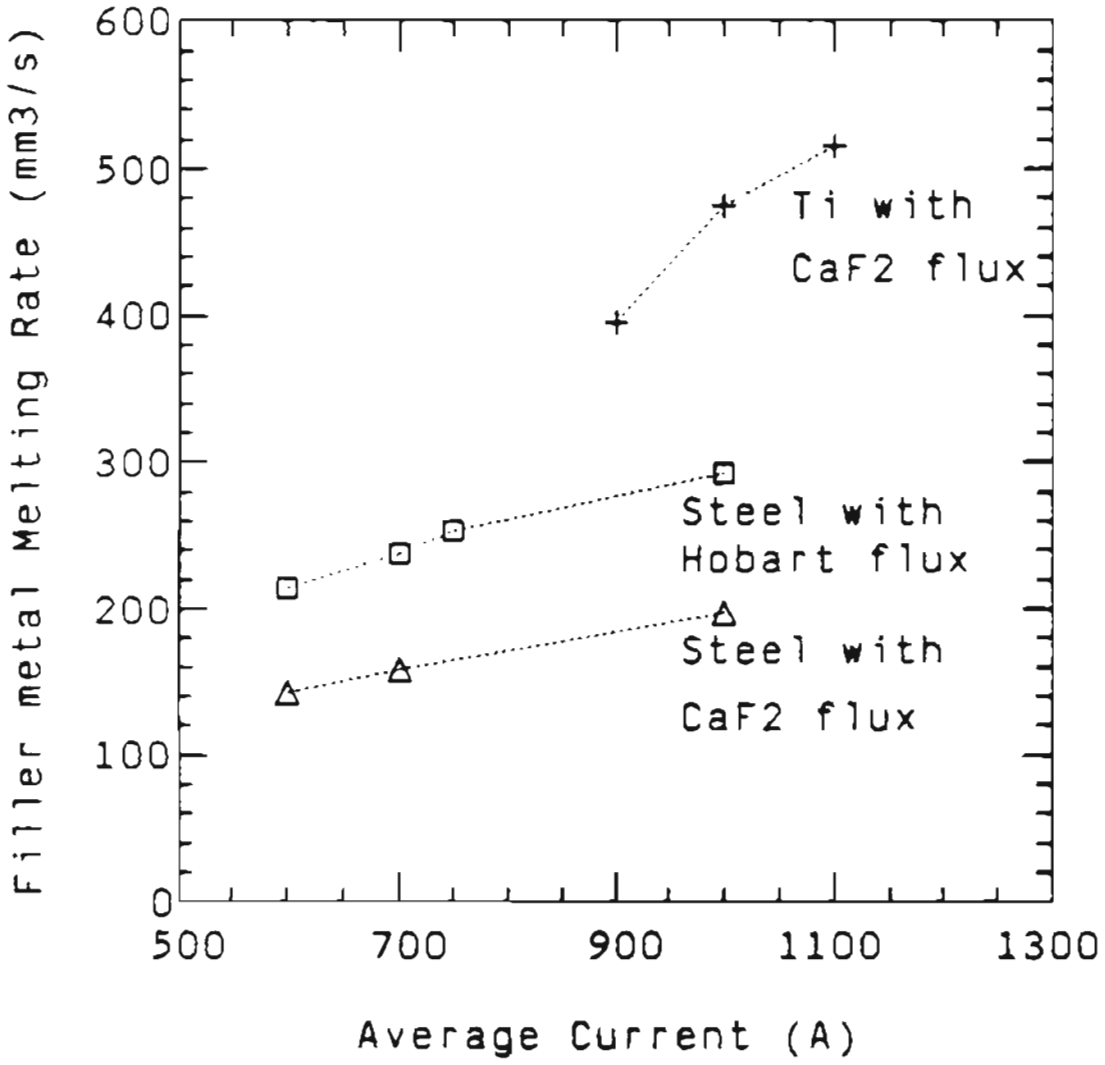

Figure 26. Filler metal melting rate and average welding current relationship at 30 V for ESW of 50 mm thick Ti-6Al-4V plates with pure CaF_2 flux, steel plates with Hobart 201 flux, and steel plates with pure CaF_2 flux.

B. Resistivity Measurements

1. Slag Resistivity

Since slag resistivity values and slag conductivity values are reciprocals of each other, and it is convention to use the conductivity term for the molten slag, only conductivity values will be used in this section. The cell constant at different immersion depths was measured before and after the conductivity measurement of the molten KCl slag. From Figure 27 (A), it was found that the cell constant values remained almost unchanged after exposing to molten KCl slag. The measured conductivity values at different temperatures of the molten KCl and LiF slags were in good agreement with the values reported by Paul Clack et al[81] as shown in Figure 27 (B). This showed that the four electrode probe method was reliable to measure the slag conductivity.

The cell constant values after the conductivity measurement of pure CaF_2 slag were lower than the cell constant values before the conductivity measurement as shown in Figure 28 (A). The difference was due to tungsten electrodes used for the conductivity probe deteriorated during the conductivity measurement of pure CaF_2 slag. Therefore, the average cell constant data were used for the calculation of slag conductivity values.

Measured conductivity values of pure CaF_2 slag at different temperatures are shown in Figure 28 (B) along with other researcher's data reported by Hara et al[25]. Conductivity values of pure CaF_2 slag measured in this study are consistently lower than conductivity

values reported by Hare et al. There are several possible explanations for the difference. The most likely explanation is the deterioration of tungsten electrodes due to oxidation at high temperatures, which lowers the cell constant values of the probe as shown in Figure 28 (A) and consequently lowers the measured slag conductivity values.

The other explanation is due to the effect of thermal expansion and surface tension of the molten slag making it difficult to measure the exact immersion depth of the probe into the molten slag pool, which is essential to relate the measured resistivity value to the predetermined cell constant value.

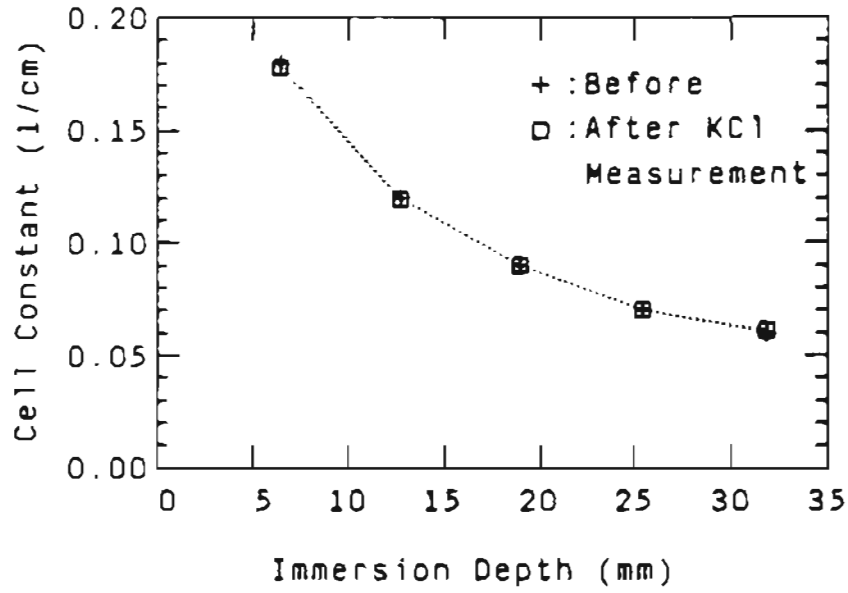

(A)

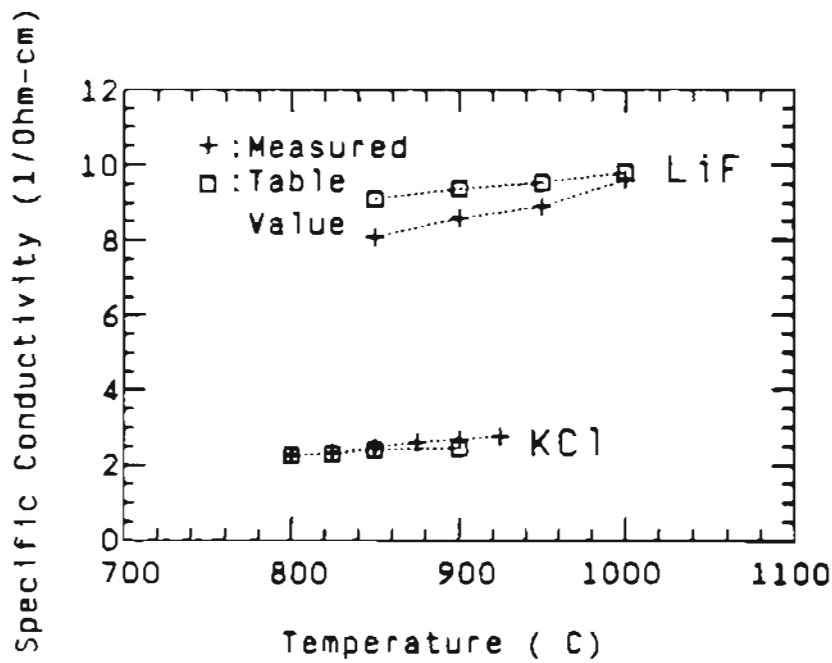

(B)

Figure 27. (A) Cell constant values determined at varying immersion depth before and after the conductivity measurement of KCl slag. (B) Measured conductivity values of KCl and LiF slags at different temperatures.

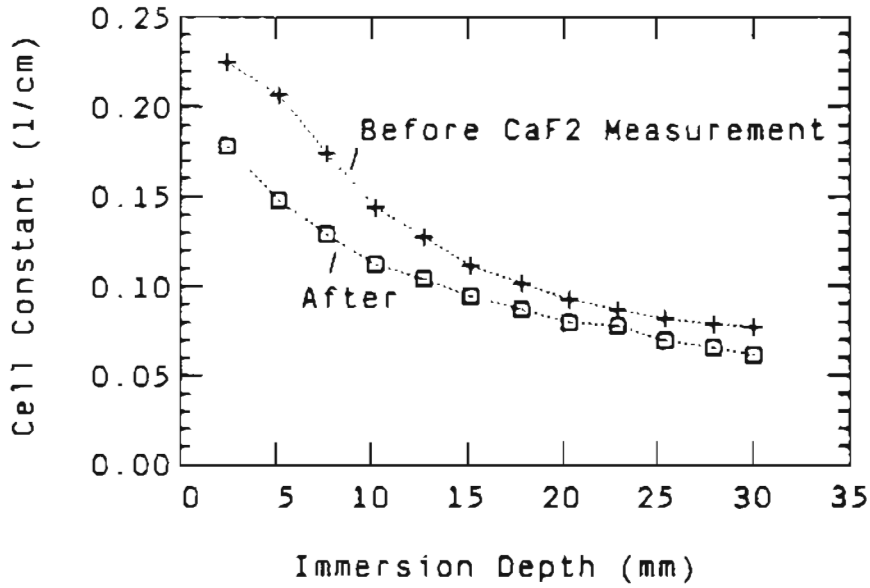

(A)

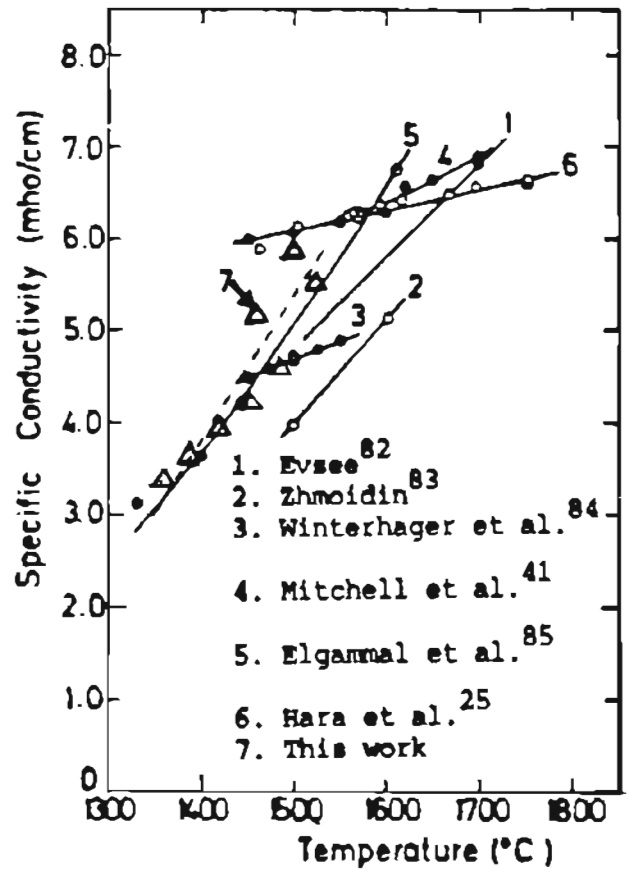

(B)

Figure 28. (A) Cell constant values determined at varying immersion depths before and after the conductivity measurement of pure CaF_2 slag. (B) Measured conductivity values of pure CaF_2 slags at different temperatures along with other researcher's data.

2. Filler Metal Resistivity

Heating rate experiments were performed in order to establish the correlation between the electric resistivity and ohmic heating of the filler metal in the ESW process. The temperature rise of different metal electrodes having a 3.2 mm diameter, caused by the ohmic heating of the applied current, was shown in Figure 29. The temperature rise of the Ti-6Al-4V electrode was the fastest, followed by the stainless steel electrode and the low carbon steel electrode. Also, the temperature rise was faster when the applied current was 135 A than when the applied current is 30 A. Another factor affecting the ohmic heating was the diameter of the electrode. When same current was applied to different diameter titanium alloy electrodes, the temperature rise was faster when smaller diameter electrode was used as shown in Figure 30.

The electric resistivity at different temperatures for different alloy electrodes was presented in Figure 31. It confirmed results from the ohmic heating measurements. By comparing the stainless steel, low carbon steel, and the Ti-6Al-4V electrodes, the Ti-6Al-4V electrode had the highest ohmic heating rate because it had the highest electric resistivity values. The electric resistivity values of Ti-6Al-4V and Ti-6211 electrodes are almost the same, but the electric resistivity values of commercially pure titanium are much lower than both Ti-6Al-4V and Ti-6211 electrodes.

Using copper coated electrodes is a common practice in the welding industry. The main purposes of copper coating are oxidation protection and lubrication during welding. Also, it is believed that copper coat-

ing would reduce the resistivity of the electrode. But, as shown in Figure 32, both copper coated low carbon steel and commercially pure titanium electrodes had the same resistivity values as those electrodes with their copper coating removed.

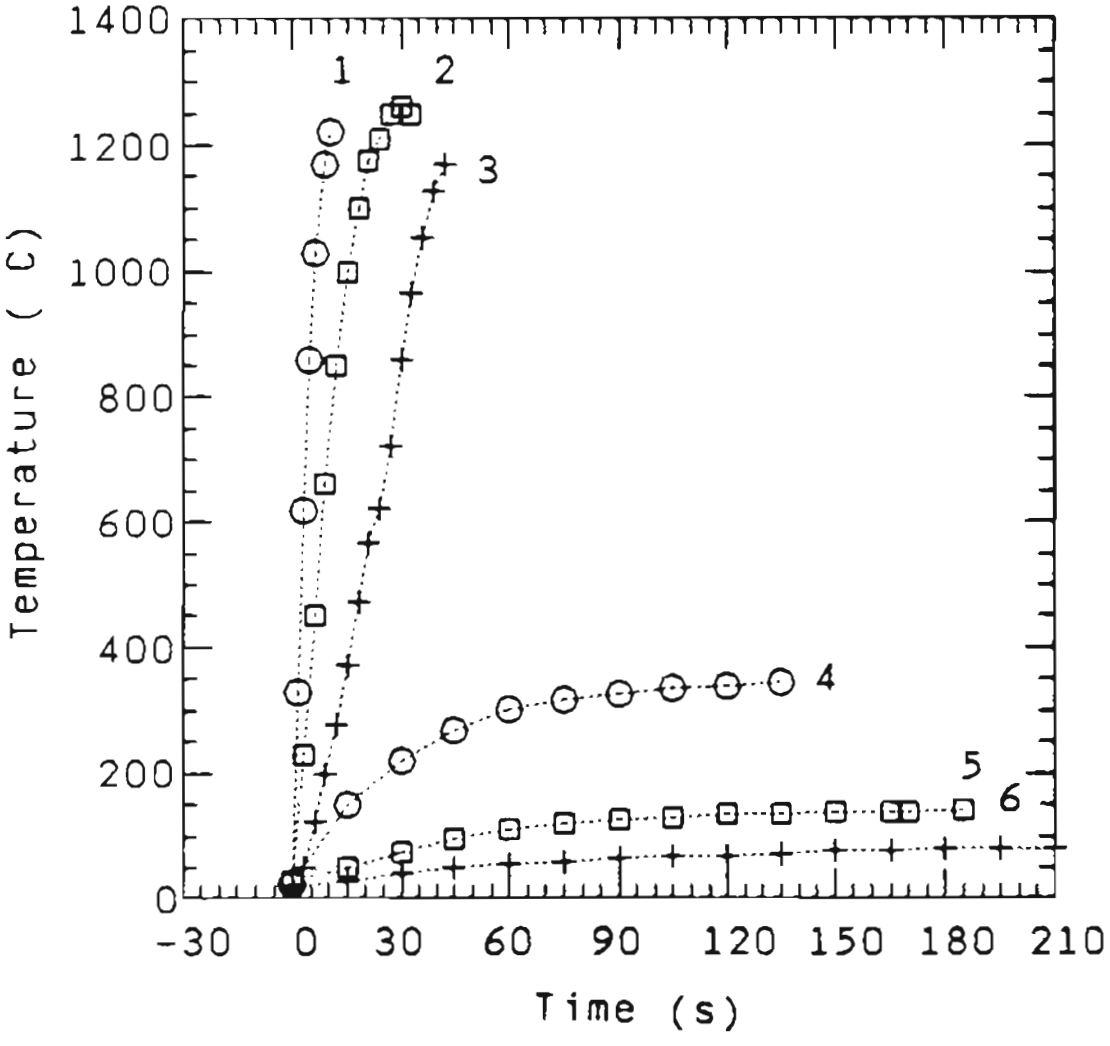

1: Ti-6Al-4V (135A)
2: Stainless steel (135A)
3: Low carbon steel (135A)
4: Ti-6Al-4V (30A)
5: Stainless steel (30A)
6: Carbon steel (30A)

Figure 29. The temperature rise of different alloy electrodes with 3.2 mm diameter produced by the ohmic heating with an applied current.

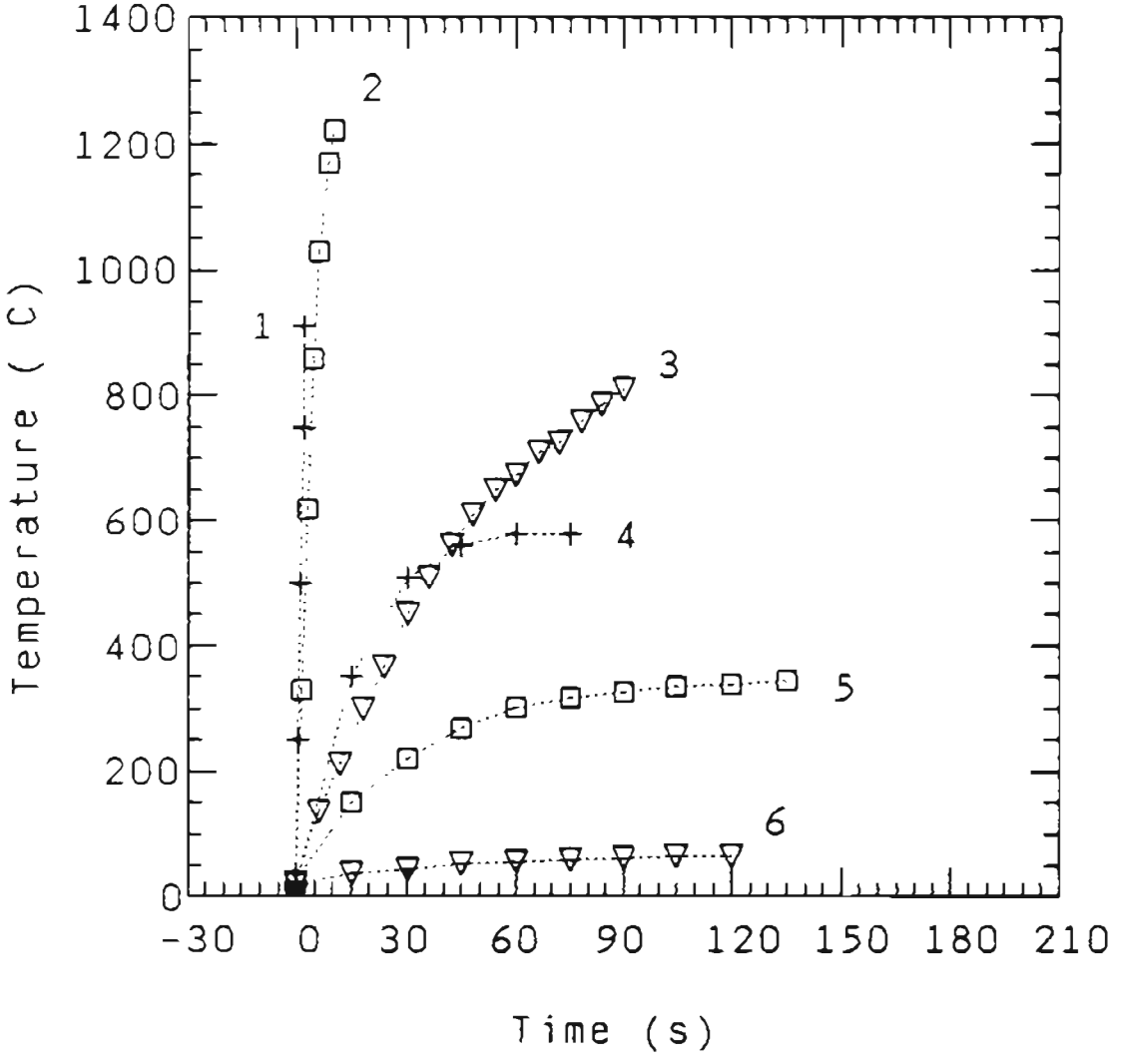

1: 2.4 mm Ti-6211 (135A) 2: 3.2 mm Ti-6Al-4V (135A)
3: 6.4 mm Ti-6211 (135A) 4: 2.4 mm Ti-6211 (30A)
5: 3.2 mm Ti-6Al-4V (30A) 6: 6.4 mm Ti-6211 (30A)

Figure 30. The temperature rise of titanium alloy electrodes with different diameters caused by the ohmic heating with an applied current.

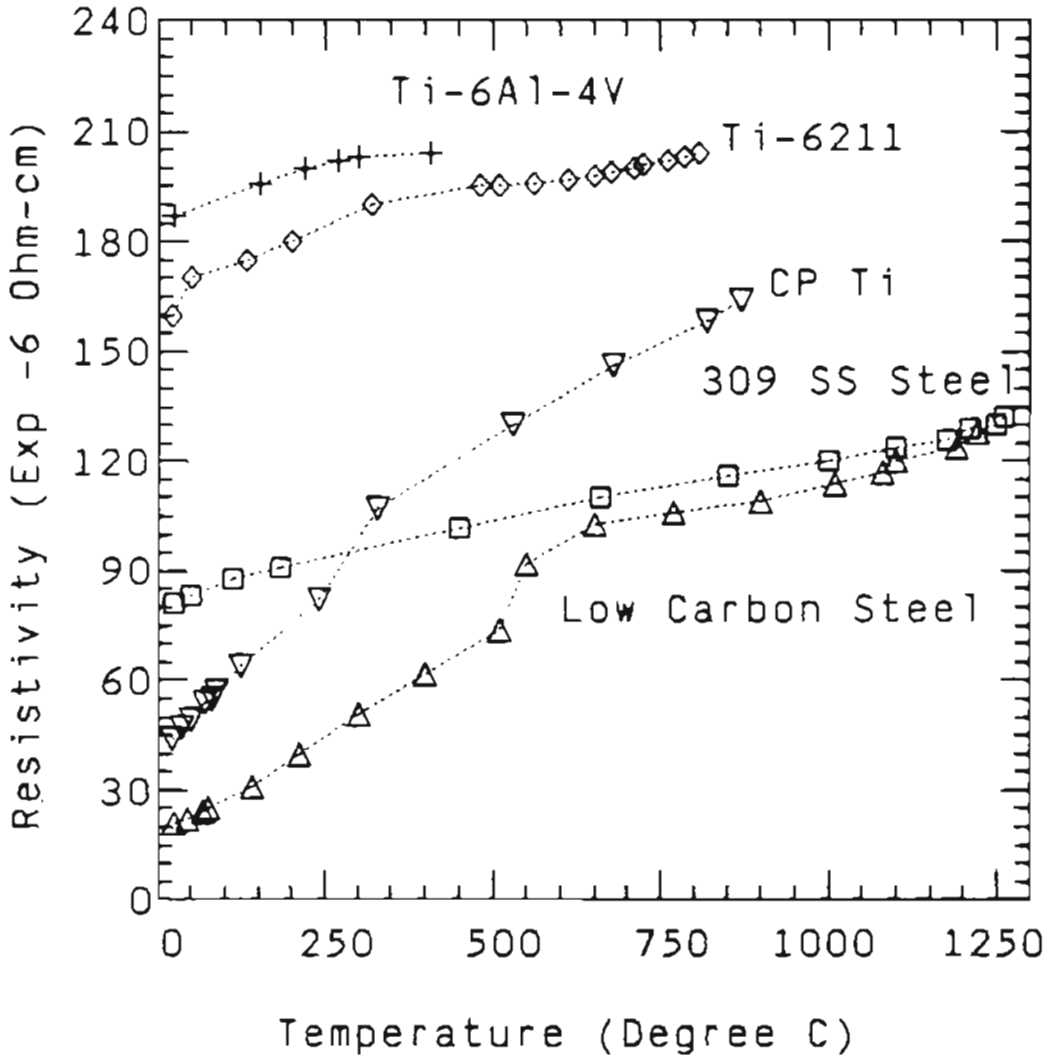

Figure 31. The electric resistivity values for different materials at different temperatures.

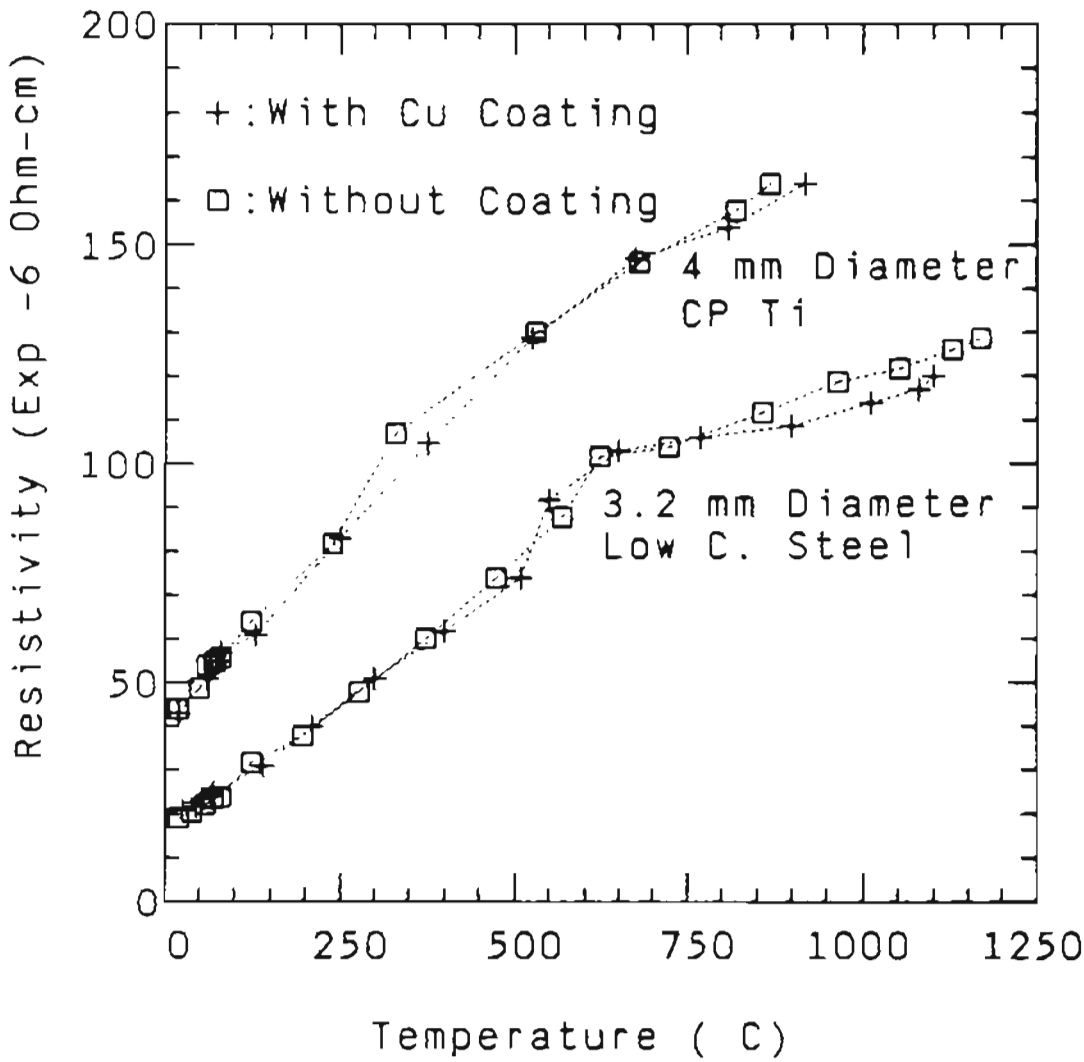

Figure 32. The effect of copper coating on the electric resistivity of commercially pure titanium electrodes and low carbon steel electrodes.

C. Nonconsumable Guide ESW Process

1. ESW in Steel Tube

The nonconsumable guide ESW was used to fill a thick-wall steel tube with a 3.2 mm diameter stainless steel electrode with different welding parameters. It had been successfully joined by both a DC or an AC power source with both pure CaF_2 and Hobart fluxes at different combinations of voltage and current. As shown in Figure 33, using DC CV power source at 40 V, welds made with CaF_2 flux had consistently higher average welding currents than welds made with Hobart 201 flux at the same filler metal melting rate. This was because pure CaF_2 flux had higher conductivity than the Hobart 201 flux and allowed a higher current to pass for the same welding conditions. Another interesting point is that at the lowest filler metal melting rate used in this study, arcing occurred in the weld made by pure CaF_2 flux, but no arcing occurred in the weld made by Hobart flux. This arcing phenomena was caused by the overheating of the electrode due to its own electric resistance.

Figure 34 (A) shows that the welding heat input increased with decreasing filler metal melting rate. Since the average penetration of the welds was directly proportional to the welding heat input, the average penetration increased with decreasing filler metal melting rate as shown in Figure 34 (B). Also shown in Figure 34 (B), the weld where arcing occurred on top of the slag pool had no penetration at all. This was because the heat produced by the arc was concentrated at the top of

the slag pool, resulting in a heat loss by radiation to the air from the arc column, leaving a smaller fraction of heat to melt the filler metal and heat the slag pool. Therefore, no excess heat was available to melt the base metal from the molten slag pool, resulting in lack of penetration to the side wall.

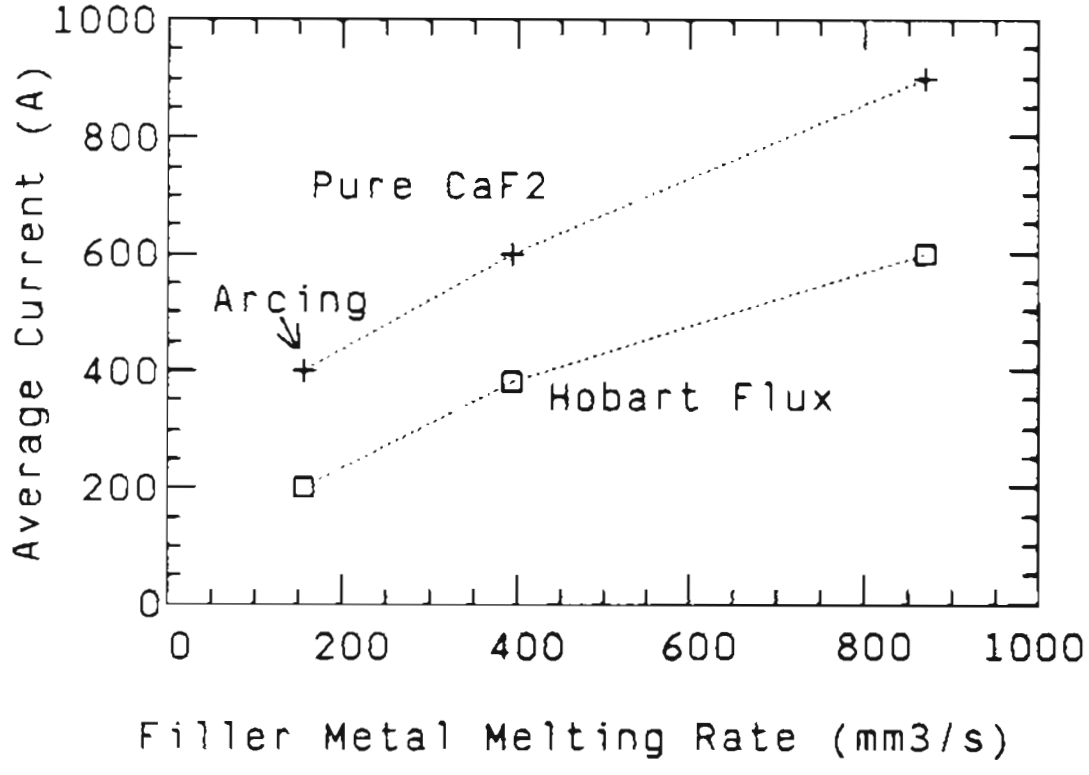

Figure 33. Relationship between the average welding current and filler metal melting rate in nonconsumable guide ESW of steel with either pure CaF_2 or Hobart 201 fluxes at 40V with DC power supply.

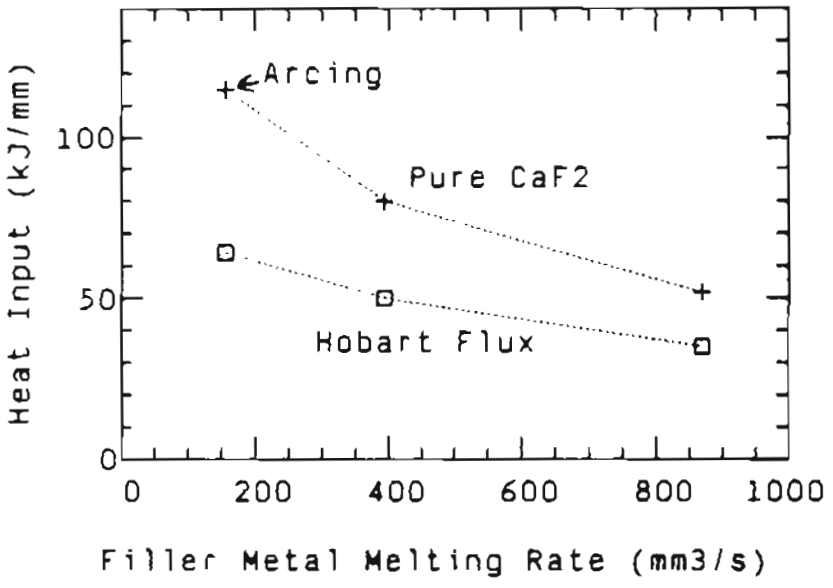

(A)

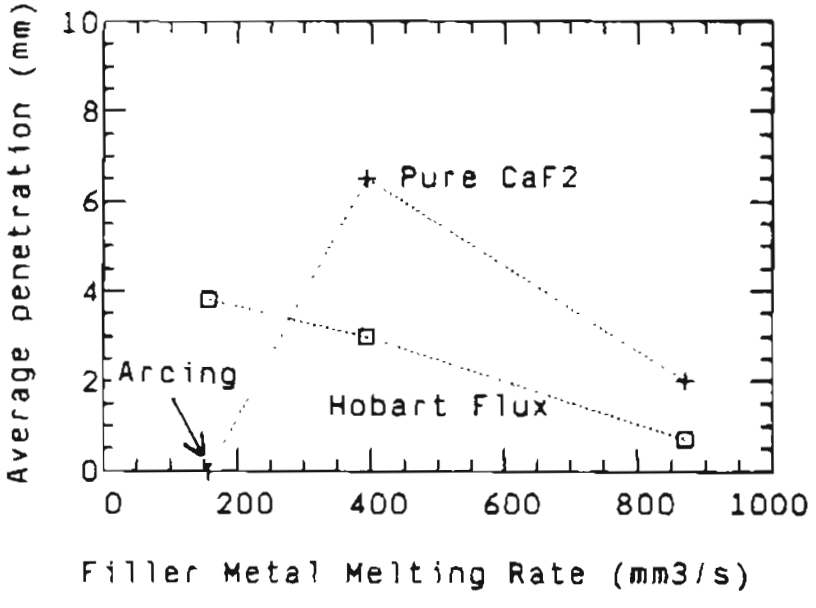

(B)

Figure 34. (A) Correlation between heat input and filler metal melting rate, and (B) Effect of filler metal melting rate on average penetration, in nonconsumable guide ESW of steel with either pure CaF_2 or Hobart 201 fluxes at 40 V with DC power supply.

2. Nonconsumable Guide ESW Titanium Alloy

Contrary to the successful nonconsumable guide ESW of steel, the nonconsumable guide ESW for Ti-6Al-4V alloys proved unsuccessful. Regardless of the combination of current, voltage and welding speed, non-consumable guide ESW of titanium with one 3.2 mm diameter filler metal could not stabilize at any combination of welding conditions to produce a sound weld joint. In most cases, an unstable arc developed above the slag pool and no window of acceptable welding parameters could be established. The weld had lack of fusion problems resulting from slag entrapment as shown in Figure 35.

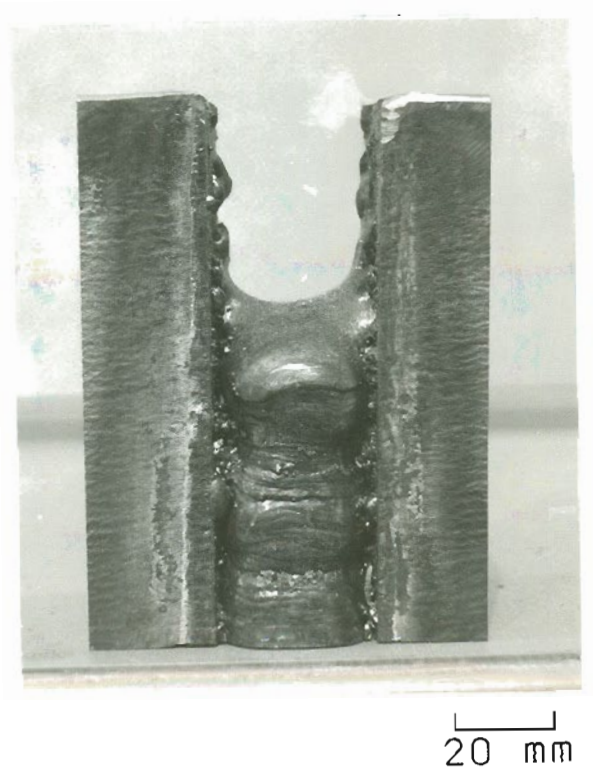

Figure 35. Photograph shows lack of fusion problems resulting from slag entrapment in a Ti-6Al-4V weld made by nonconsumable guide ESW with pure CaF_2 flux and one 3.2 mm diameter filler metal.

D. Weld Evaluation

Weld evaluation consisted of: (a) an analysis of metallurgical structures by optical and electron microscopy, (b) study of the source of interstitial element contamination, (c) tensile testing and hardness testing, (d) Charpy V-notch toughness testing, and (f) fractography. After development of the optimum range of welding parameters for consumable guide ESW of titanium alloys, the following three welds were prepared for evaluation:

1. Ti-6Al-4V high purity CaF_2 flux 50 mm thick
2. Ti-6Al-4V reagent grade CaF_2 flux 50 mm thick
3. Ti-6211 high purity CaF_2 flux 50 mm thick

The optimum welding parameters used to join 50 mm thick Ti-6Al-4V and Ti-6211 plates are given in Table 7 below. These parameters were chosen based on results of the ESW process development study.

Table 7 Optimized welding parameters for consumable guide ESW of 50 mm thick titanium alloys

	Target	Allowable Range
Power Supply	AC Constant Voltage	AC Constant Voltage
Voltage	30 V	25 - 30 V
Current	1000 A	900 - 1250 A
Filler Metal	Single 3.2 mm (Diameter Wire)	Single 2.4 mm and 3.2 mm Dual 2.4 mm and 3.2 mm (Diameter Wire)
Welding Gap	32 mm	30 -35 mm
Deposition Rate	11.1 kg/h	Dependent on Current Setting

1. Analysis of Metallurgical Structures

The transverse-to-weld section macrostructures of all three welds were identical, therefore only the macrostructure of Ti-6Al-4V weld using reagent grade CaF_2 flux is shown in Figure 36. From this figure, it is evident that the welds were symmetric with respect to the weld center. Upon traversing the weld from the weld center into the base plate, the unique manifestations of the prior beta grain macrostructure could be classified into three different zones in each weld joint: (1) columnar grain weld zone, (2) HAZ and (3) unaffected base metal (BM). Although the weld center macrostructure in Figure 36 appeared to be equiaxed in the plane of the photograph, the entire weld structure in 3-dimensions was actually fully columnar.

The microstructures of weld metal, HAZ, and base metal are shown in Figure 37 for the Ti-6Al-4V weld made with reagent grade CaF_2 flux, in Figure 38 for the Ti-6Al-4V weld made with high purity CaF_2 flux, and in Figure 39 for the Ti-6211 weld made with high purity CaF_2 flux. The optical microstructure of Ti-6Al-4V welds made by high purity and reagent grade CaF_2 fluxes were virtually identical as shown in Figures 37 and 38. Ti-6211 alloy is classified as near alpha alloy because it contains a lesser amount of the beta phase than the alpha + beta Ti-6Al-4V alloy, but the microstructures revealed in Figure 39 are similar to the microstructures of Ti-6AL-4V alloy shown in Figure 37 and 38. This is because the beta phase is retained between alpha platelets and it is very difficult to distinguish beta phase from the alpha platelet boundaries by chemical etching used for optical microscopic observation.

Only transmission electron microscopy can be used to distinguish these phases.

The weld zone microstructures for both Ti-6AL-4V and Ti-6211 alloys contained grain boundary alpha, lamellar alpha + beta structure, and Widmanstätten alpha + beta colonies in the grain center. The HAZ microstructures were typified by grain boundary alpha, lamellar alpha + beta structure, and the basketweaved alpha + beta structure in the grain center. The base metal microstructures had the characteristic Widmanstätten alpha + beta colony structure with grain boundary alpha.

The notable difference between the weld, HAZ, and BM microstructures was that the alpha platelets were finest in the HAZ, medium in the weld, and thickest in the BM as seen in Figures 37(B), 38(B), 39(B). One common feature in all the microstructures was the continuous thick alpha film along the prior beta grain boundary.

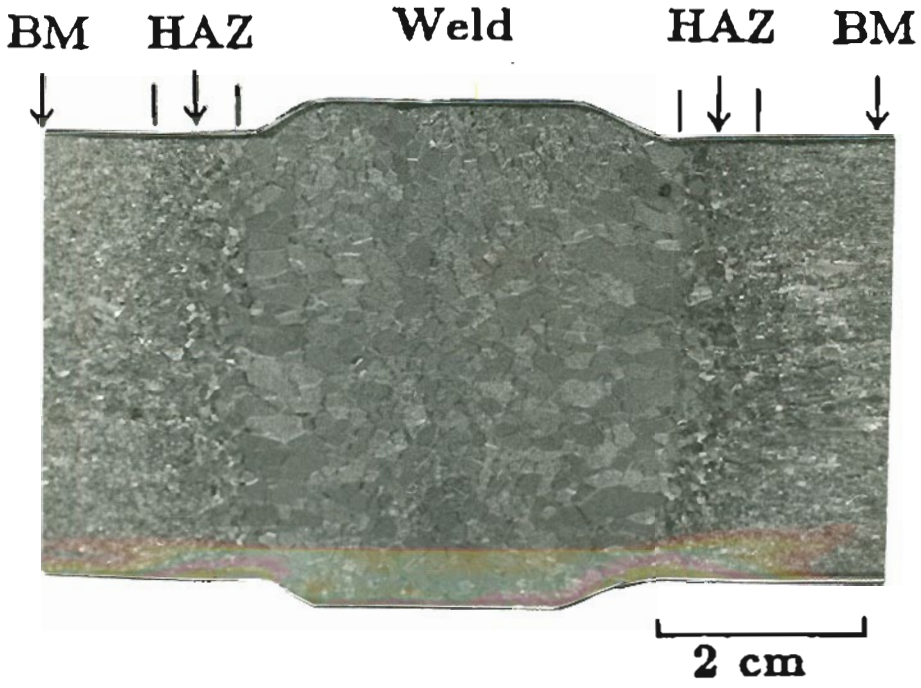

Figure 36. Transverse-to-weld section macrostructure of Ti-6Al-4V electroslag weld using reagent grade CaF_2 flux.

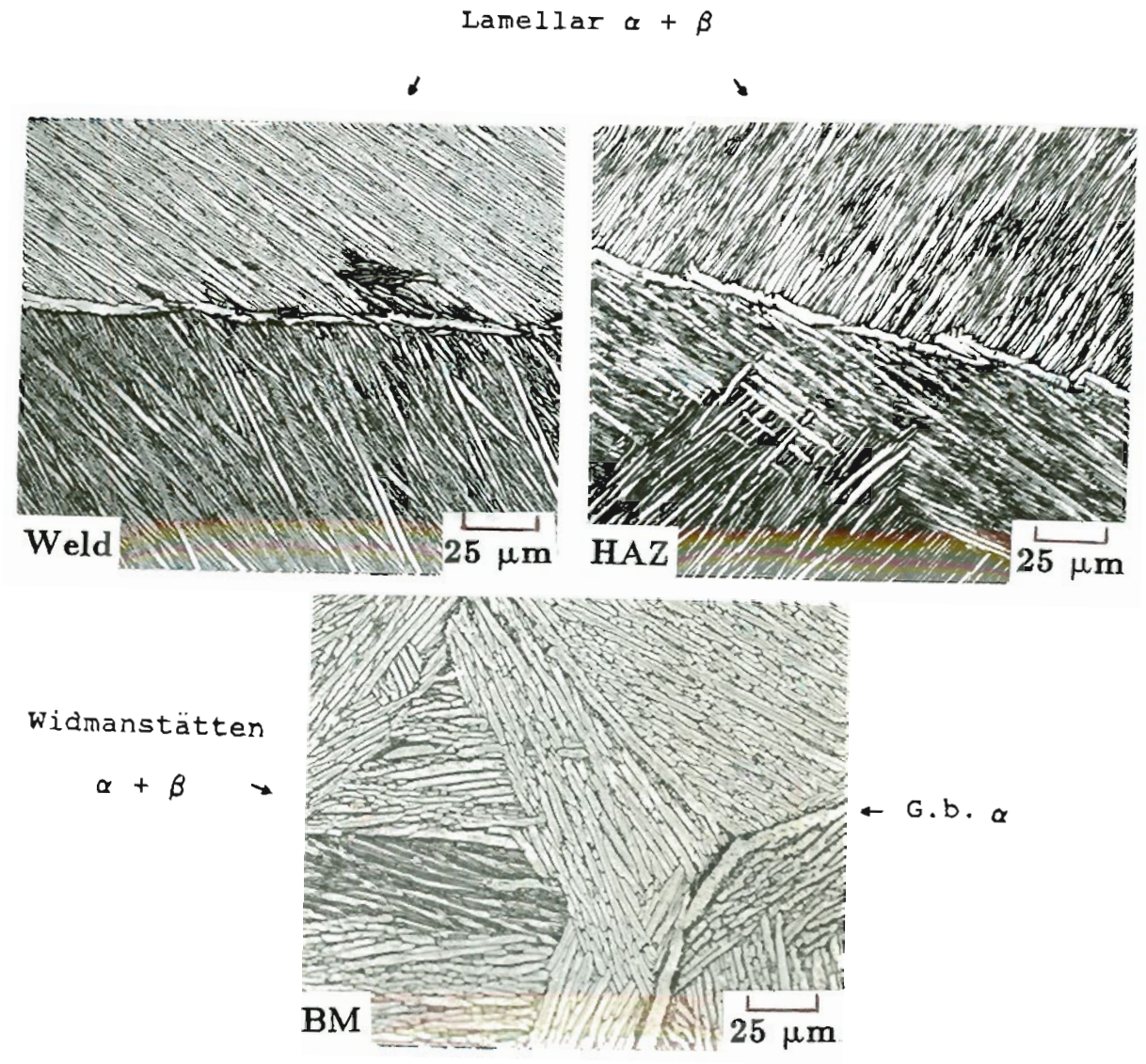

(A)

Figure 37. Microstructures of Ti-6Al-4V weld made with reagent grade CaF_2 flux (A) along prior beta grain boundary, (B) in the center of prior beta grain.

(Figure 37 continued)

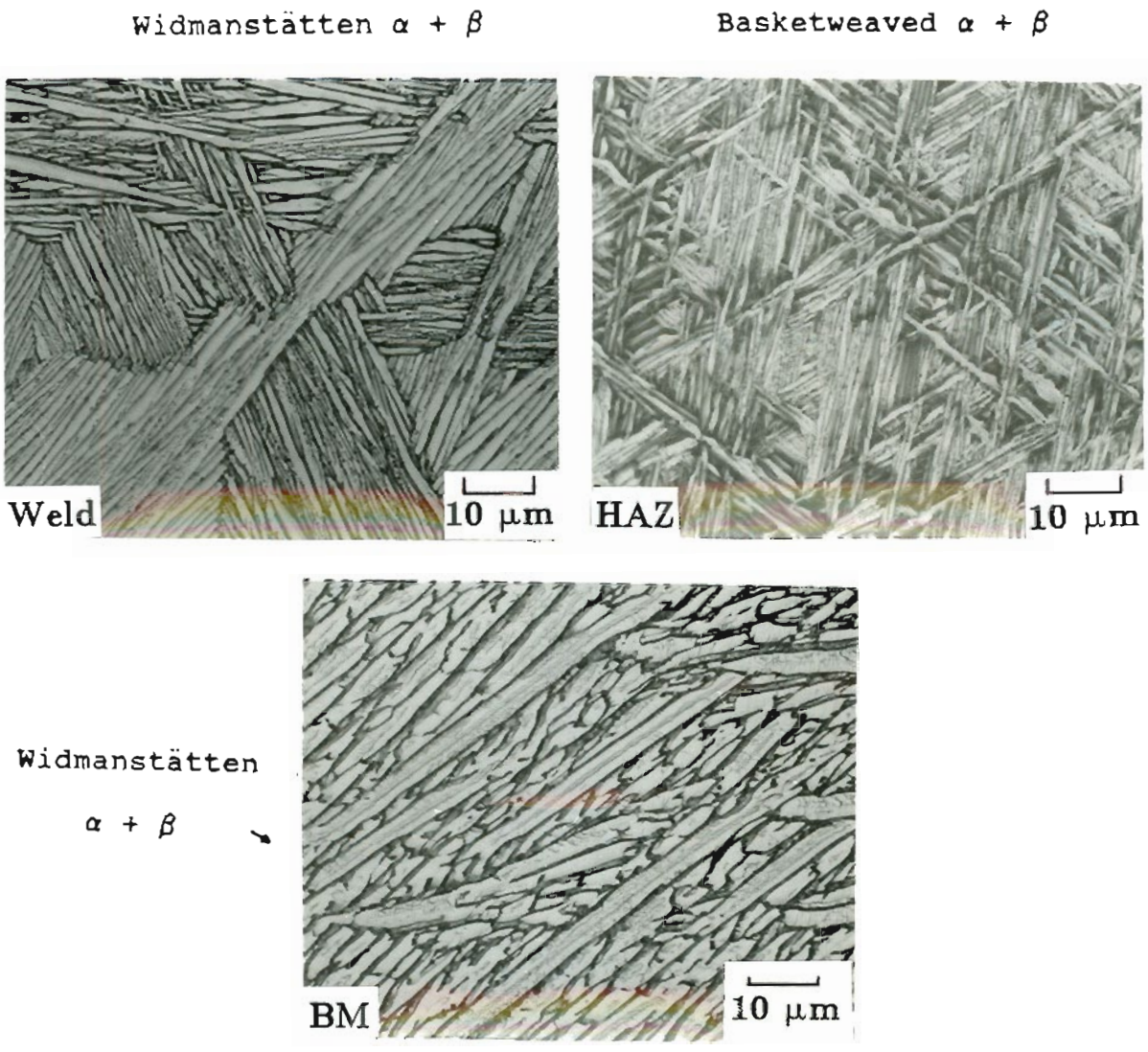

(B)

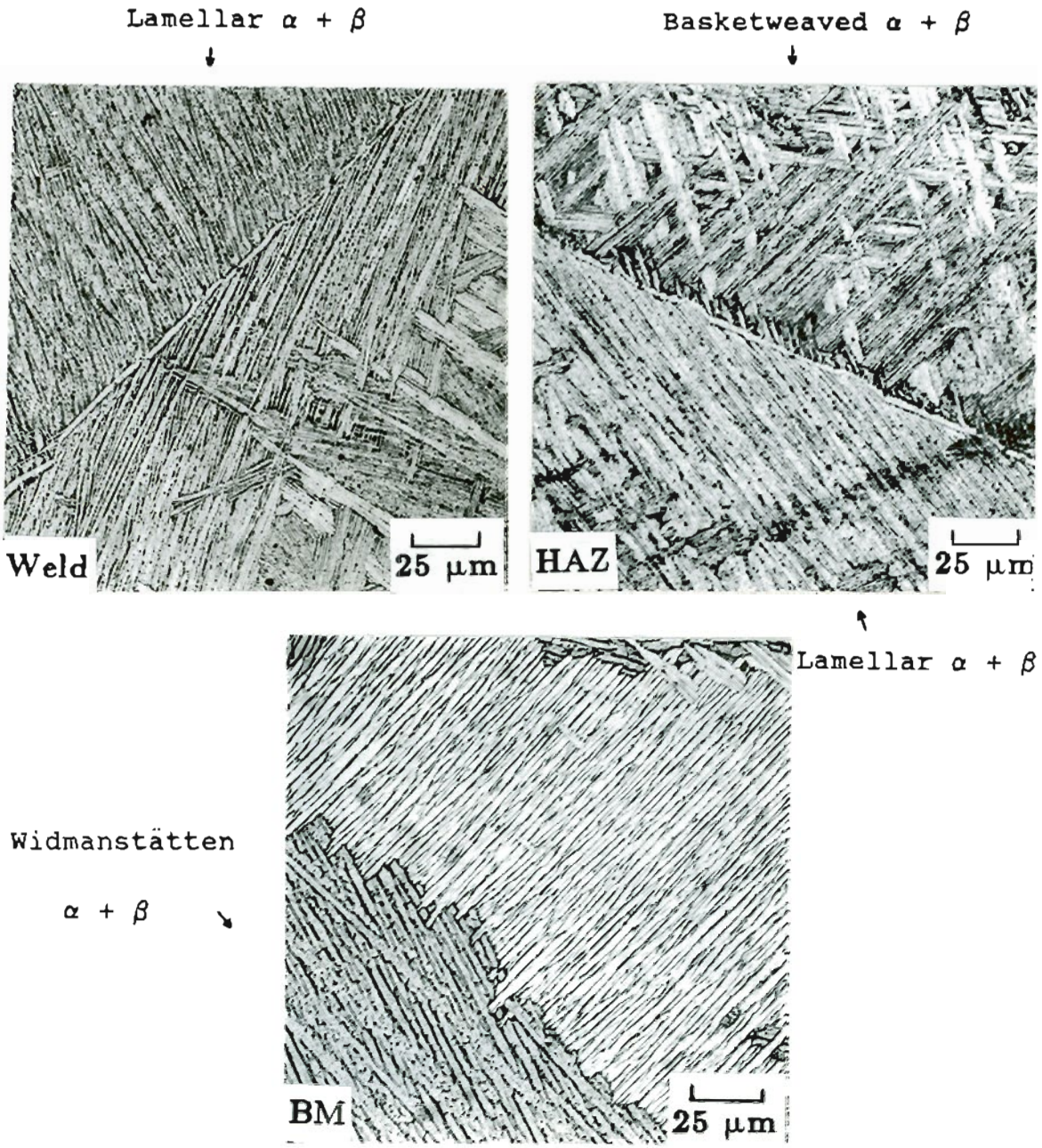

(A)

Figure 38. Microstructures of Ti-6Al-4V weld made with high purity CaF_2 flux (A) along prior beta grain boundary, (B) in the center of prior beta grain.

(Figure 38 continued)

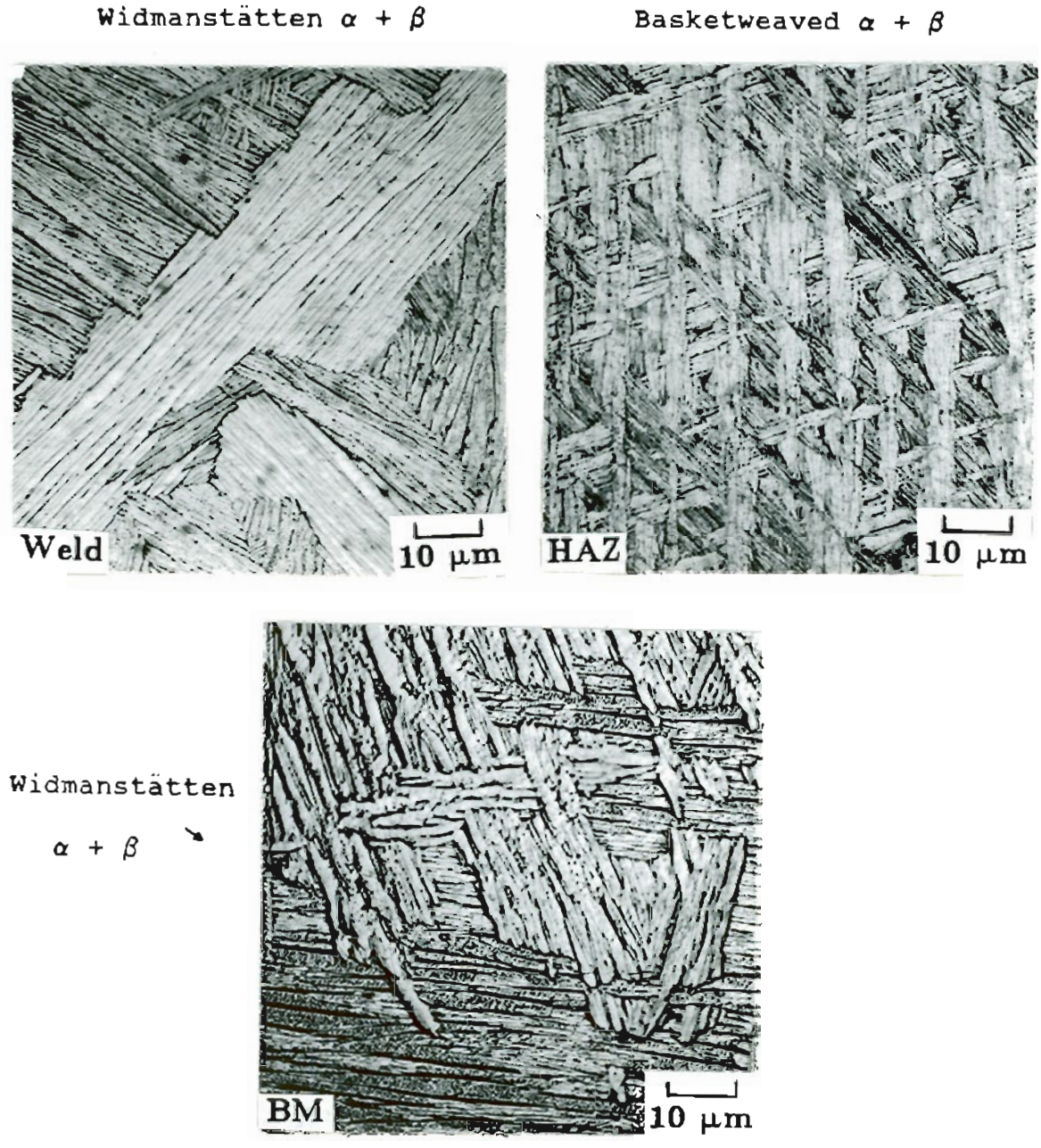

(B)

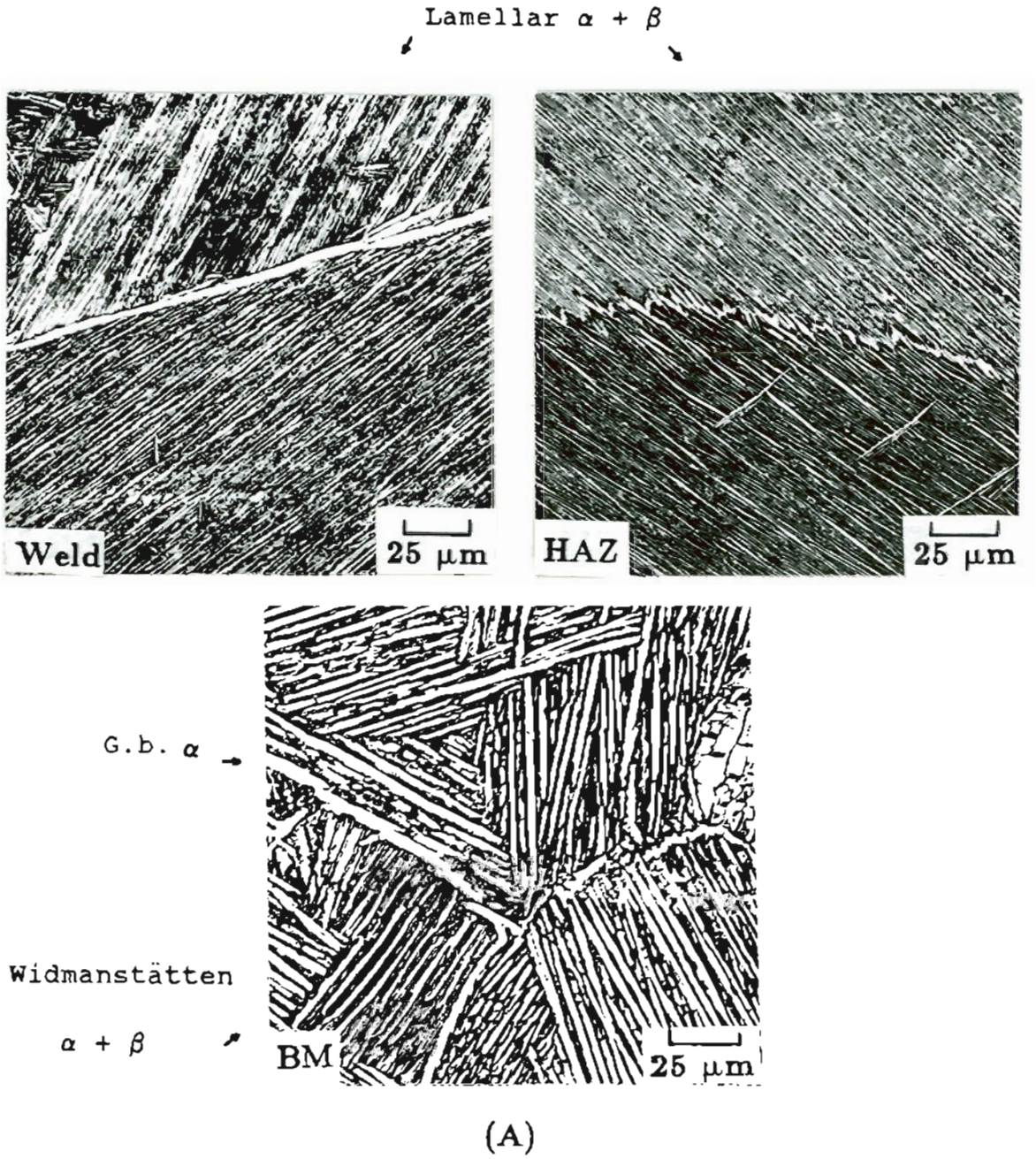

Figure 39. Microstructures of Ti-6211 weld made with high purity CaF_2 flux (A) along prior beta grain boundary, (B) in the center of prior beta grain.

(Figure 39 continued)

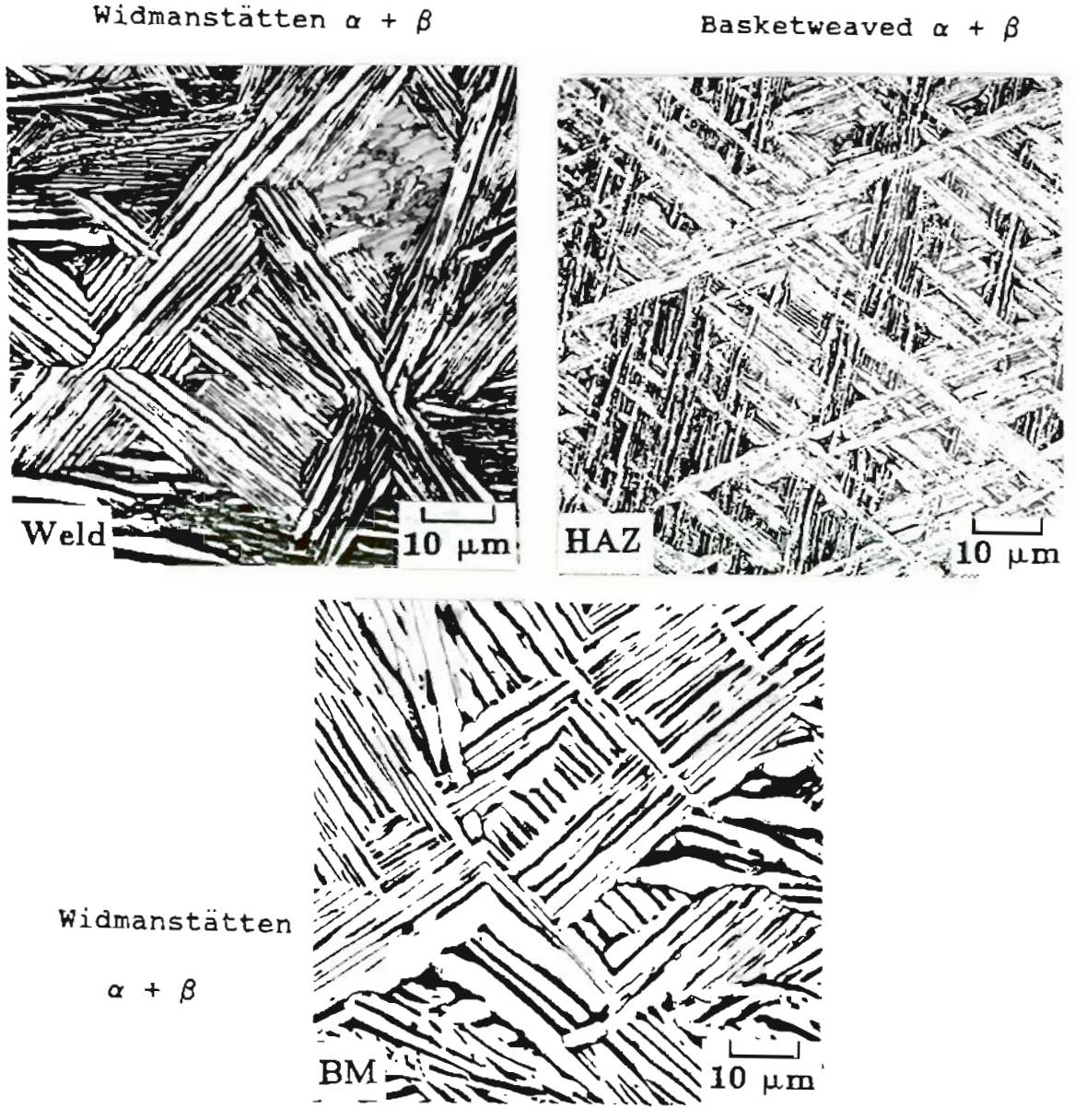

(B)

Weld metal and base metal microstructures observed by TEM are shown in Figure 40 for the Ti-6Al-4V alloy weld using high purity CaF_2 flux and in Figure 41 for the Ti-6211 alloy weld using high purity CaF_2 flux. Base metal microstructure features of the Ti-6AL-4V weld were characterized by a twinned structure in the alpha plate (Figure 40(B)). Twins are commonly observed in beta forged, slow cooled, and annealed alpha + beta titanium alloys.

The classic Burgers relationship: $(101)_\beta \; // \; (0001)_\alpha$; $[1\bar{1}\bar{1}]_\beta \; // \; [11\bar{2}0]_\alpha$ between alpha and beta phases is shown in Figure 42. It shows that the alpha + beta widmanstätten structure in Figure 42(A) is formed by growth of alpha plates parallel to one specific {110} plane of the original beta phase when the Ti-6al-4V alloy is slowly cooled from the beta phase region.

The beta phase region in both Figure 40 and 41 shows a considerable dislocation density and the interface phase as reported by Banerjee et al.[86-88] At a higher magnification, the interface phase is clearly visible as shown in Figure 43. From the diffraction pattern shown in Figure 44, the interface phase has been identified as a hydride with an fcc structure, which agrees with the result reported by Banerjee et al.[86-88] According to the results shown by Banerjee et al., the hydrogen came from the TEM sample preparation technique because the hydrogen content in titanium alloy is below the solubility limit. Though precautions were taken for this study, the interface phase of hydride was still present in all the TEM micrographs. The possible source of hydrogen is the water used for cooling while cutting thin TEM sample.

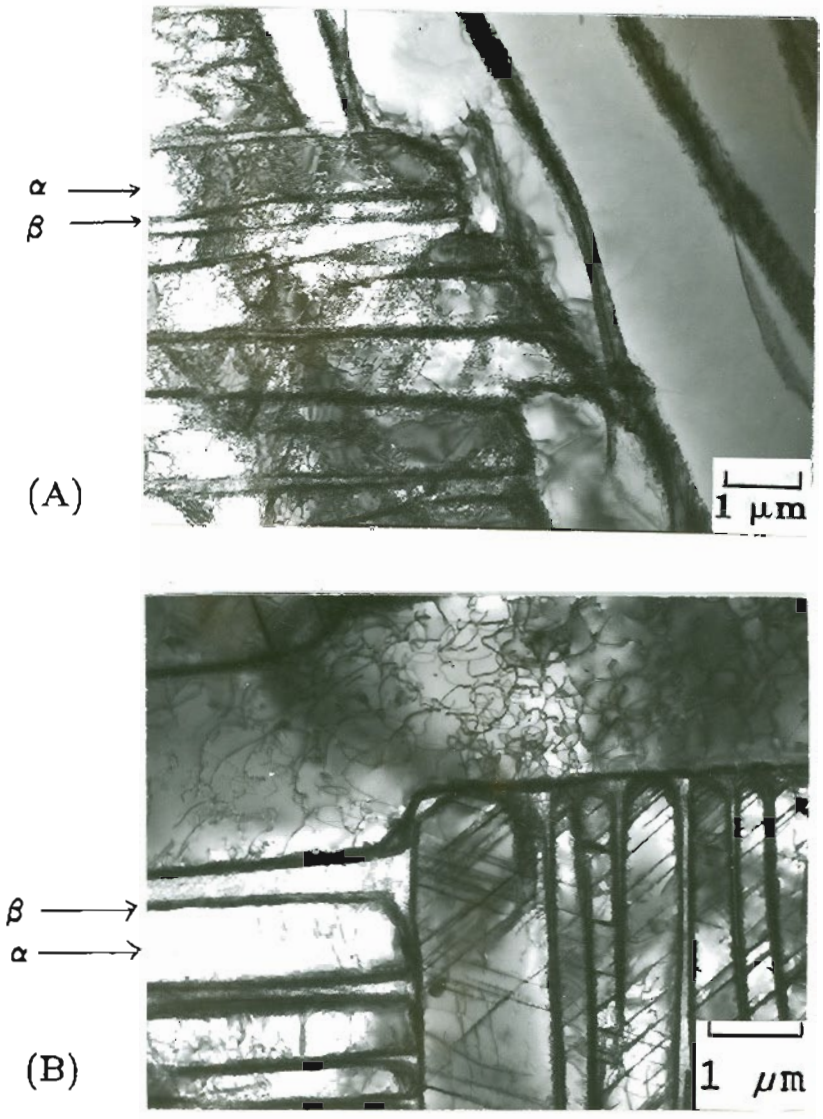

Figure 40. TEM micrographs of Ti-6Al-4V alloy weld made with high purity CaF_2 flux (A) weld metal, and (B) base metal.

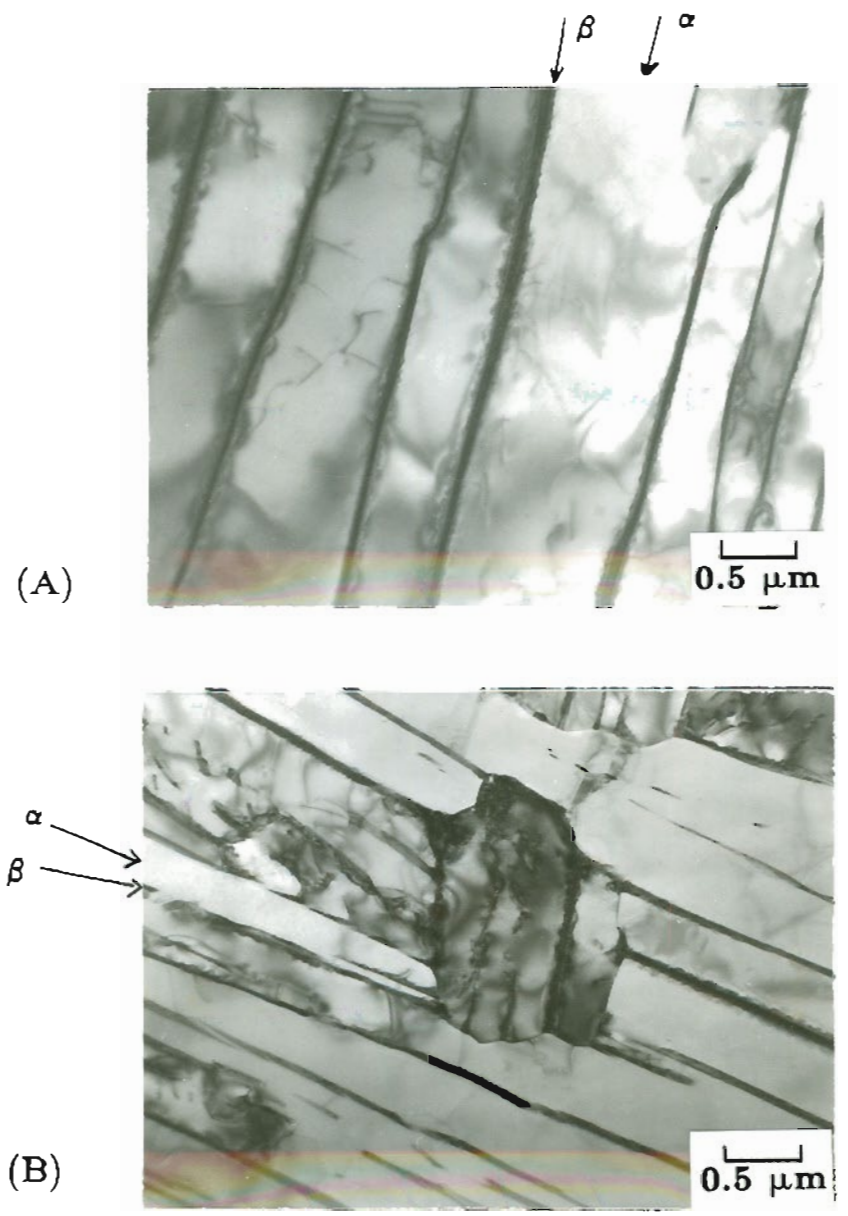

Figure 41. TEM micrographs of Ti-6211 alloy weld made with high purity CaF_2 flux (A) weld metal, and (B) base metal.

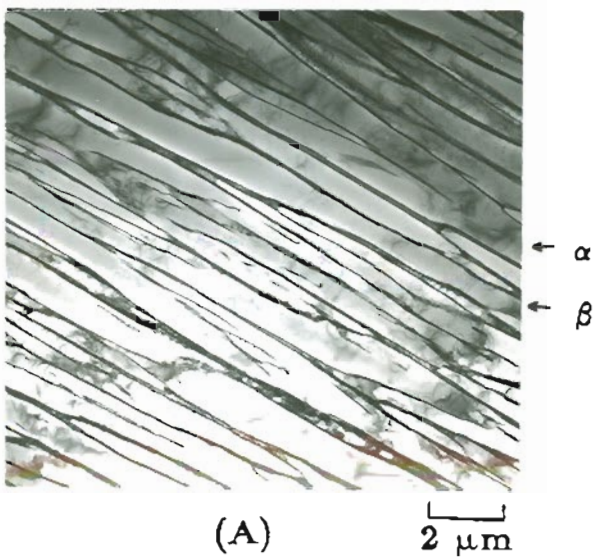

(A)

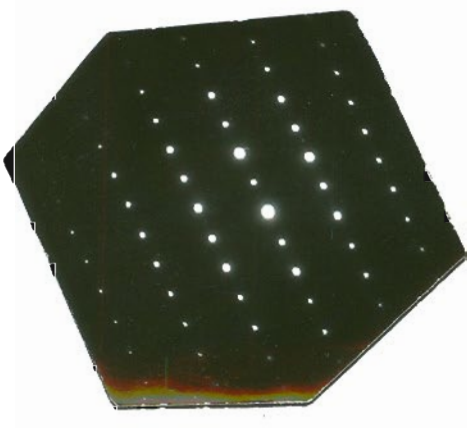

(B)

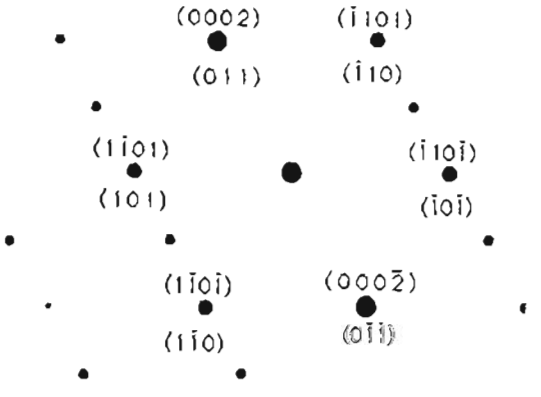

(C)

Figure 42. TEM micrographs of Ti-6Al-4V base metal (A) bright field image, (B) selected area diffraction (SAD) pattern, and (C) schematic illustration of the SAD pattern.

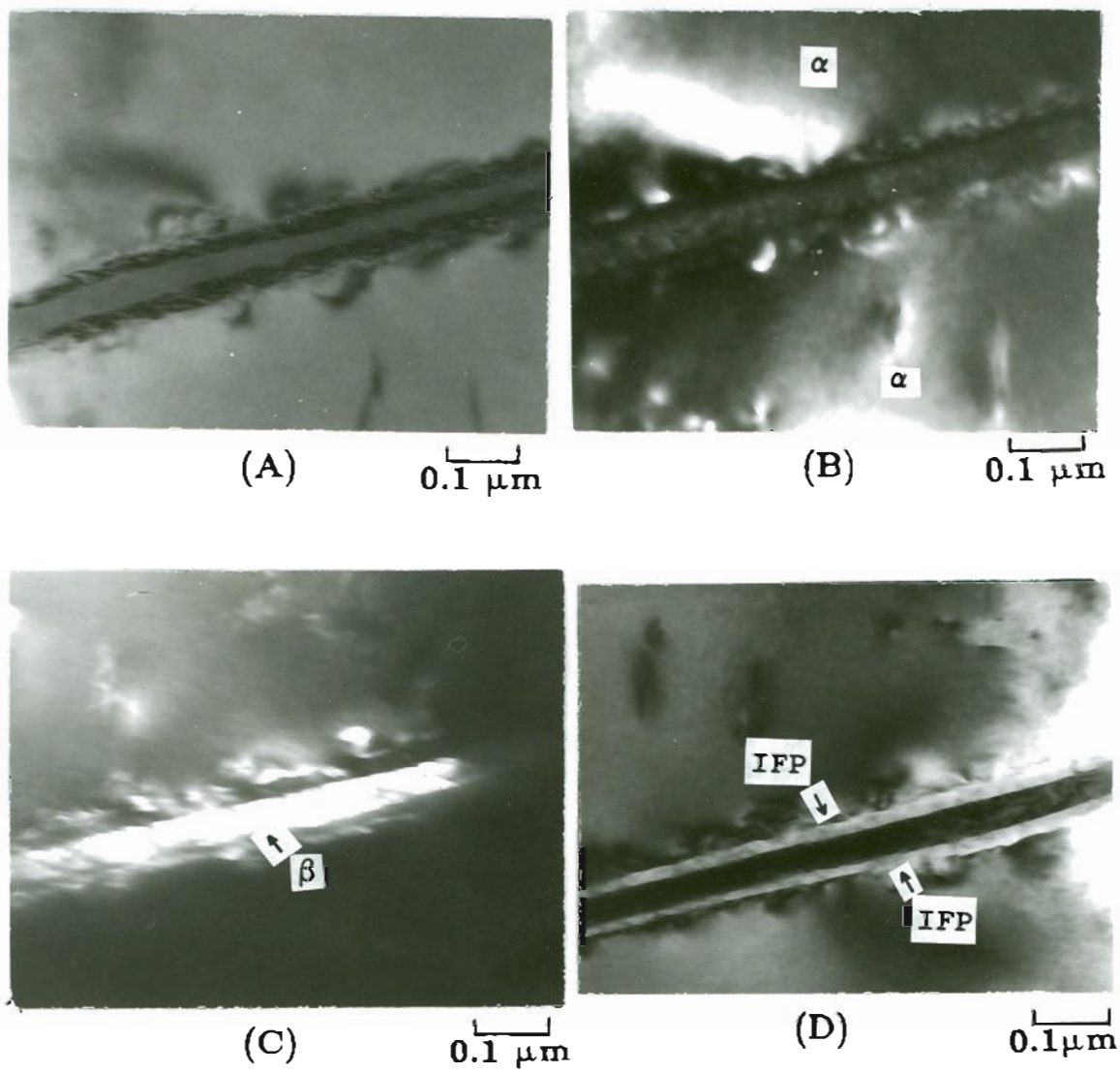

Figure 43. Weld metal TEM micrographs of Ti-6211 weld made with high purity CaF_2 flux (A) bright field image, (B) dark field image shows alpha phase, (C) dark field image shows the beta phase, and (D) dark field image shows interface phase.

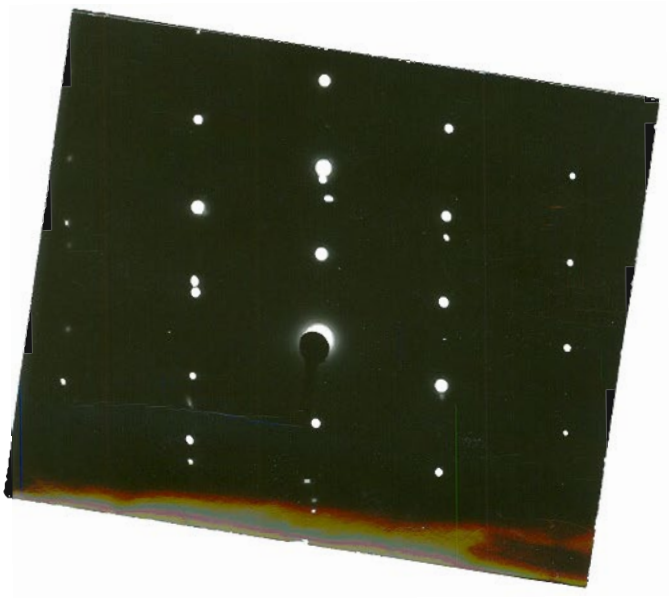

(A)

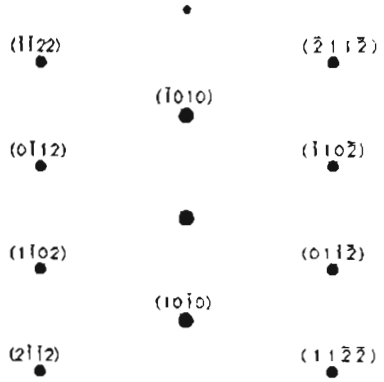

(B)

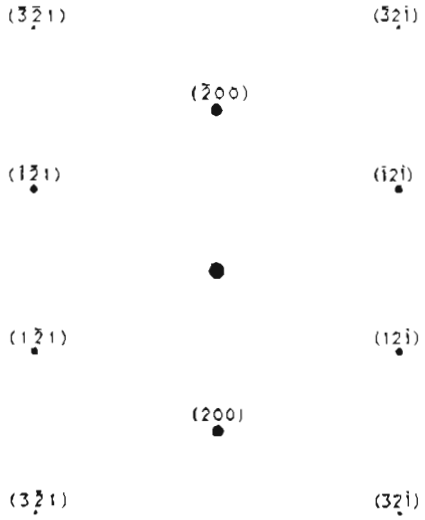

(C)

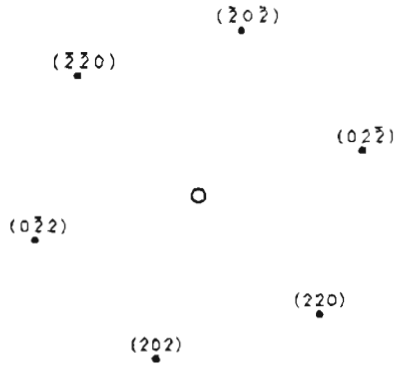

(D)

Figure 44. TEM selected area diffraction pattern of Figure 43 : (A) SAD pattern, and schematic drawing shows (B) hcp alpha phase, (C) bcc beta phase, and (D) fcc interface phase structures contained in the SAD pattern.

2. Interstitial Element Content in Welds

Since the mechanical properties of alpha + beta titanium alloys are strongly dependent on their interstitial element content, chemical analyses of all Ti-6Al-4V and Ti-6211 welds were performed, especially around the area where specimens were taken for mechanical testing. The oxygen and nitrogen contents along the transverse section of all three Ti-6Al-4V and Ti-6211 welds reported in Table 5 were plotted in Figure 45.

Figure 45 shows that the weld metal of Ti-6Al-4V made with high purity CaF_2 flux always developed lower interstitial contents than the weld metal of Ti-6Al-4V using reagent grade CaF_2 flux. This suggested strongly that the use of high purity CaF_2 flux could lower the interstitial element content of electroslag welds. It also shows that in the weld made with reagent grade CaF_2 flux, not only did the weld metal pick up oxygen and nitrogen, but the HAZ close to welding fusion line area also had higher oxygen and nitrogen content than the base metal.

The Ti-6211 welds made with high purity CaF_2 flux had the lowest interstitial elements content as shown in Figure 45. This is because Ti-6211 base metal and filler metal had lower interstitial element content than the Ti-6Al-4V base metal and filler metal.

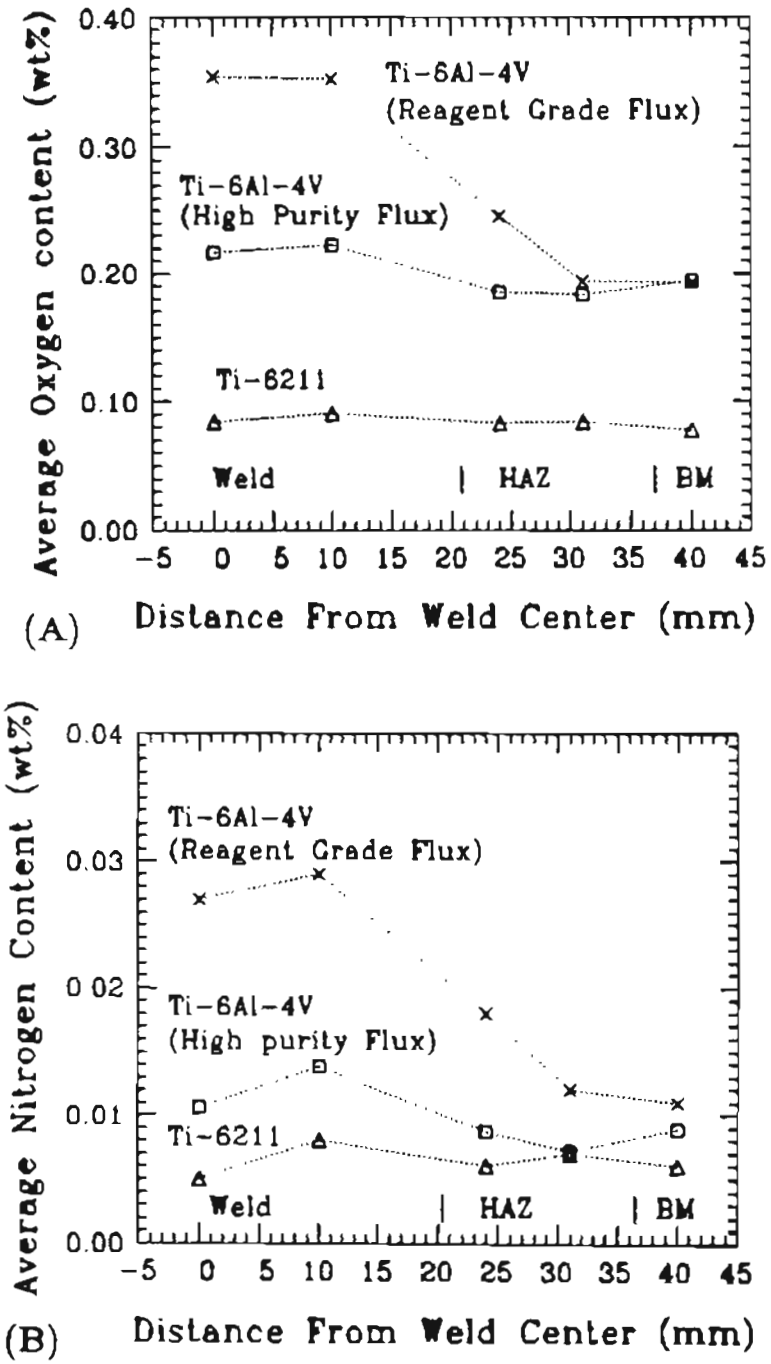

Figure 45. Interstitial elements content along transverse section of electroslag welds: (A) oxygen, (B) nitrogen.

3. Tension test

Most of the transverse-to-weld tension specimens failed in the weld region, primarily due to geometric effects. The gage length of the transverse tension specimens contained 75% to 80% of the weld metal. And after the test was finished, the surface of the broken specimen was macroetched to reveal the actual location where the break occurred. Also some smaller gage length transverse specimens and all weld metal longitudinal specimens were tested to make sure the specimens were tested in the weld metal region.

The tensile and yield strengths of the weld metal for all three welds were always slightly greater than their respective base metal values as shown in Figure 46. However, the reduction in area (%RA) and percent elongation (%E) for the weld metal of all three welds were around 50% lower than the values for their respective base metals. Also, the weld of Ti-6Al-4V alloy using reagent grade CaF_2 flux exhibited the lowest %RA and %E values among these three welds. Because nearly all of the gage length contained weld metal, all of the tensile fractures occurred in the weld metal (near the weld interface).

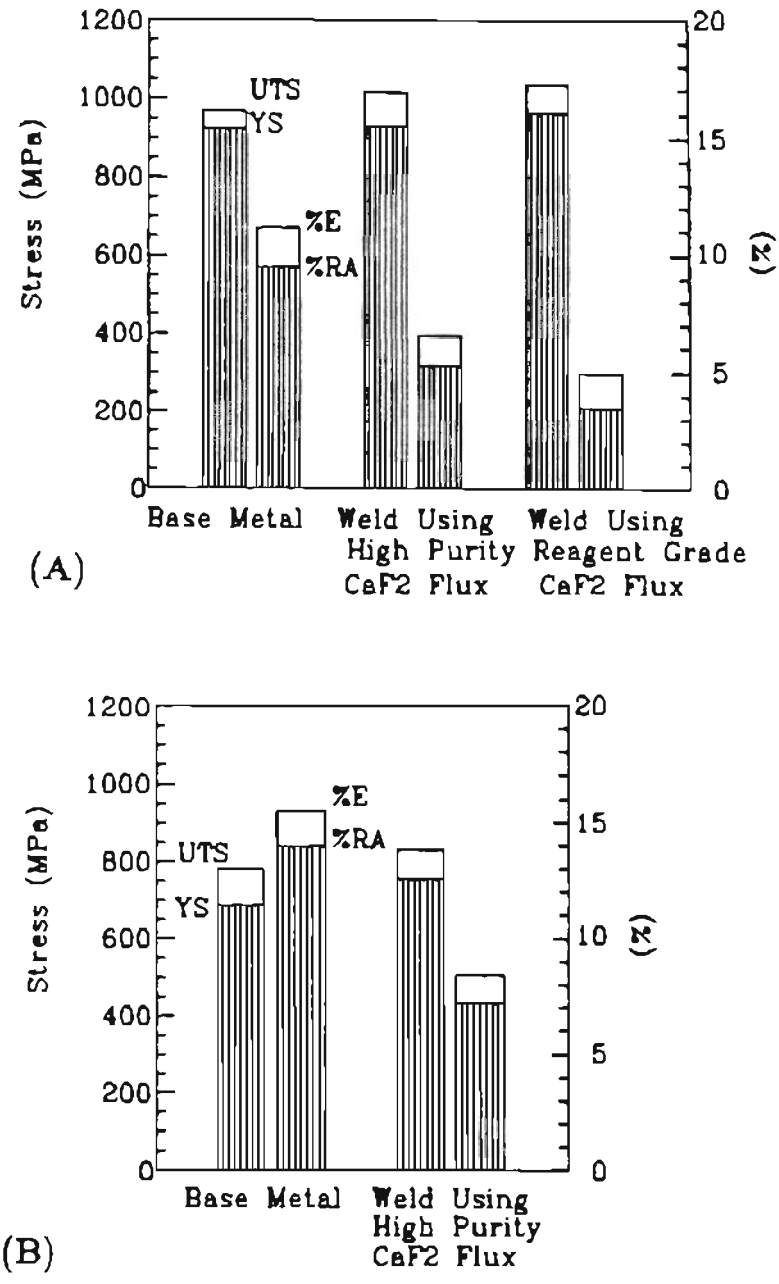

Figure 46. Comparison of tensile properties of electroslag welds with their respective base metals (A) Ti-6Al-4V, (B) Ti-6211.

4. Hardness test

Microhardness measurements made along the transverse section of Ti-6Al-4V welds using reagent grade CaF_2 flux revealed that the hardness was slightly higher in the weld region compared to that of the base metal as shown in Figure 47(a). However, from Figures 47(b), and 47(c), the hardness profiles across Ti-6Al-4V and Ti-6211 welds using high purity CaF_2 flux were generally uniform. Furthermore, the weld metal of Ti-6Al-4V weld using reagent grade CaF_2 flux consistently possessed the highest hardness values among the three welds.

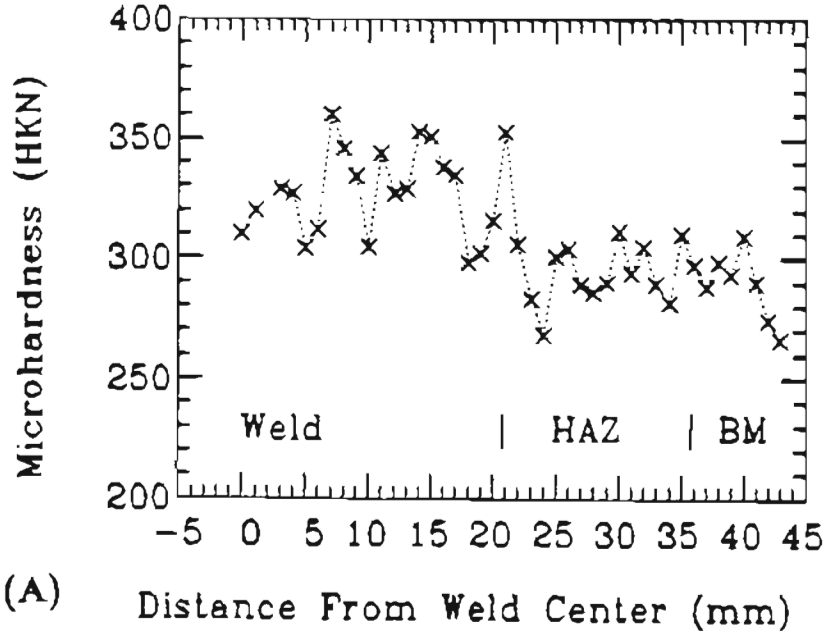

Figure 47. Transverse microhardness profiles across three electroslag welds (A) Ti-6Al-4V weld using reagent grade CaF_2 flux, (B) Ti-6Al-4V weld using high purity CaF_2 flux, (C) Ti-6211 weld using high purity CaF_2 flux.

(Figure 47 continued)

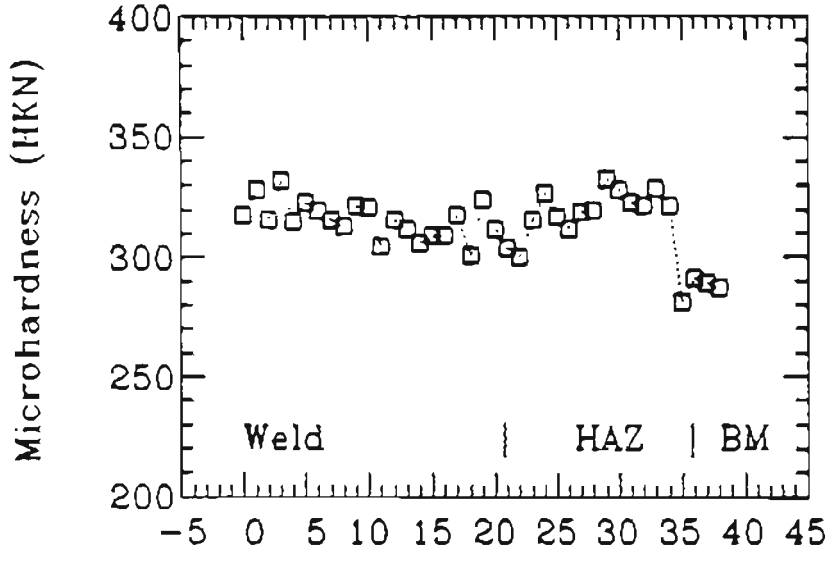

(B)

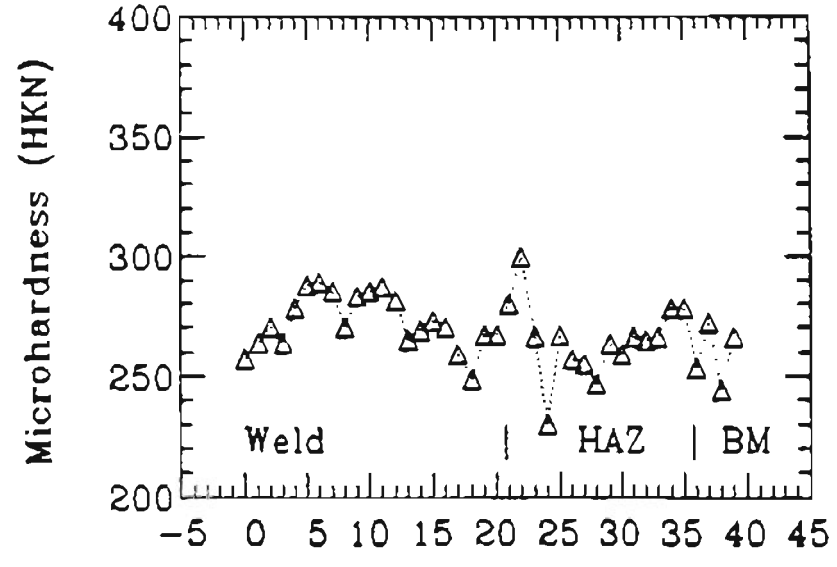

(C)

5. Charpy V-notch test

CVN toughness values at 0°C, 25°C, and 100°C (32°F, 77°F, and 212-°F) along the transverse section of all Ti-6Al-4V and Ti-6211 welds are shown in Figure 48. The CVN toughness values of the weld metal in all Ti-6Al-4V and Ti-6211 welds were lower than the CVN toughness values of BM and HAZ regions. The CVN toughness values at the HAZ of both Ti-6AL-4V welds were even higher than the corresponding values of Ti-6Al-4V base metal as shown in Figure 48(A) and (B). But for the Ti-6211 weld, the CVN toughness values at the base metal region were higher than the corresponding values at the HAZ region as shown in Figure 48(C). Overall, the CVN toughness values of Ti-6211 welds made with high purity CaF_2 flux were about twice as high as the CVN toughness values of both Ti-6Al-4V welds. In all cases, the HAZ and base metal toughness values were always superior to those of the weld metal.

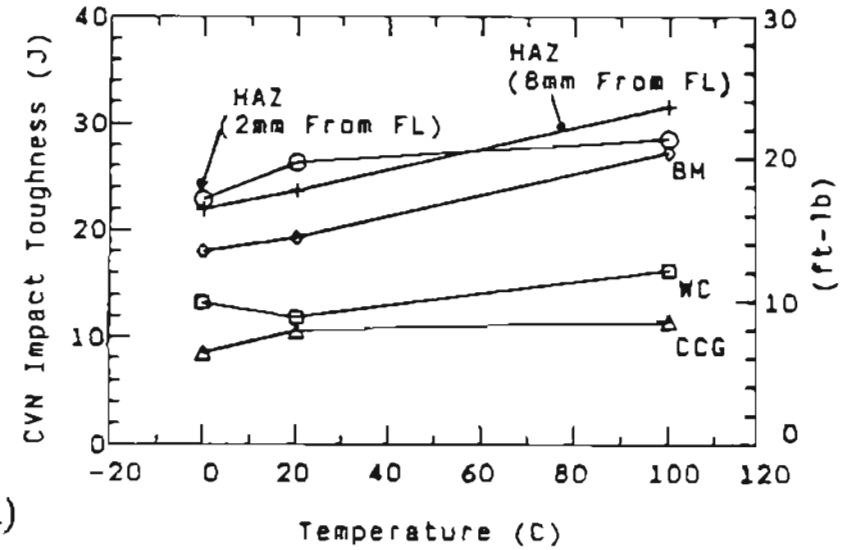

(A)

Figure 48. CVN toughness values at 0°C, 25°C, and 100°C along the transverse section of (A) Ti-6Al-4V weld made with reagent grade CaF_2 flux, (B) Ti-6Al-4V weld made with high purity CaF_2 flux, and (C) Ti-6211 weld made with high purity CaF_2 flux.

(Figure 48 continued)

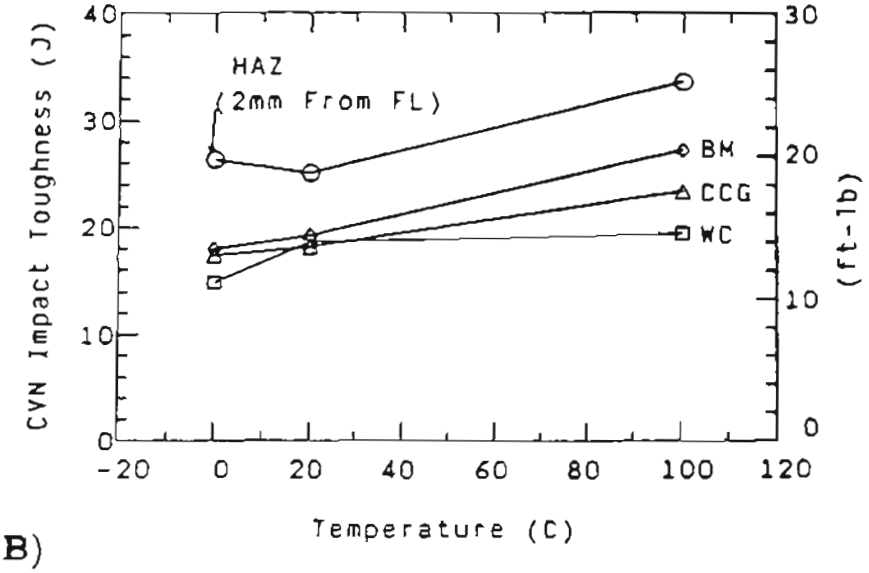

(B)

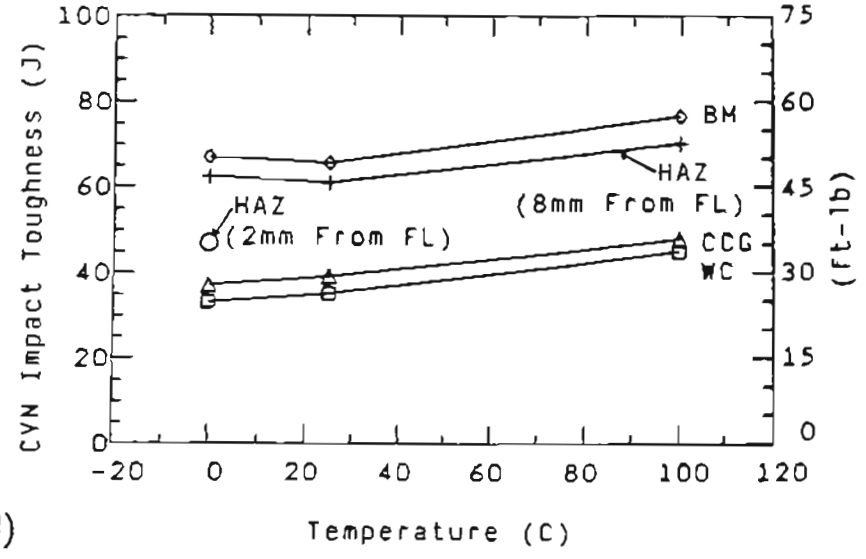

(C)

6. Fractography

From the fractographs of broken CVN toughness specimens in Figure 49, the fracture surfaces of weld metal specimens of Ti-6AL-4V and Ti-6211 welds exhibited a macroscopic brittle fracture appearance (flat and featureless) as compared to the more granular appearance of the HAZ and base metal fracture surface. But at higher magnifications, all fracture surfaces displayed an entirely microscopic ductile dimple type appearance as shown in Figure 50. Also, the weld metal specimens showed large elongated dimples similar to those reported by Chesnutt et al.[89] and Lin et al.[90]. The base metal specimens clearly revealed crack branching in both Ti-6AL-4V and Ti-6211 alloys.

Fractographs of broken tension test weld metal specimens and base metal specimens of both Ti-6Al-4V and Ti-6211 weld joints made with high purity CaF_2 flux are shown in Figure 51. The enlarged fractographs of selected areas in Figure 51 were shown in Figure 52. The fracture appearances of weld metal and base metal specimens were similar to each other in both alloys as shown in Figures 51, and 52, despite the fact that the tensile ductility of the weld metal specimen was only 50% of the tensile ductility of the base metal specimen (for both alloys) as shown in Figure 46 .

Microstructures of sections taken perpendicularly to the fracture surface of CVN impact and tension test specimens are shown in Figures 53 and 54 for Ti-6Al-4V and Ti-6211 welds, respectively. The results in Figures 53(A) and 54(A) indicate that the crack propagation occuring in CVN impact test specimens didn't have any preferred path. But in

tension test specimens, the crack preferred to propagate along the thick alpha film present at prior beta grain boundaries (Figures 53(B) and 54(B)). This is particularly true in the weld metal specimens because of large columnar prior beta grain size. The crack could follow one prior beta grain boundary through the entire diameter of the specimen.

In summary, weld metals made by ESW process had lower tensile ductility and CVN impact toughness than did the corresponding base metals. Although the weld metal CVN specimens exhibited a macroscopic brittle fracture, the microscopic features of the fractures revealed micro-void coalescence and a ductile dimpled fracture surface. Upon tracing the fracture path, the cracks propagated transgranularly in CVN impact test specimens and intergranularly along the prior beta grain boundaries in the tension test specimens.

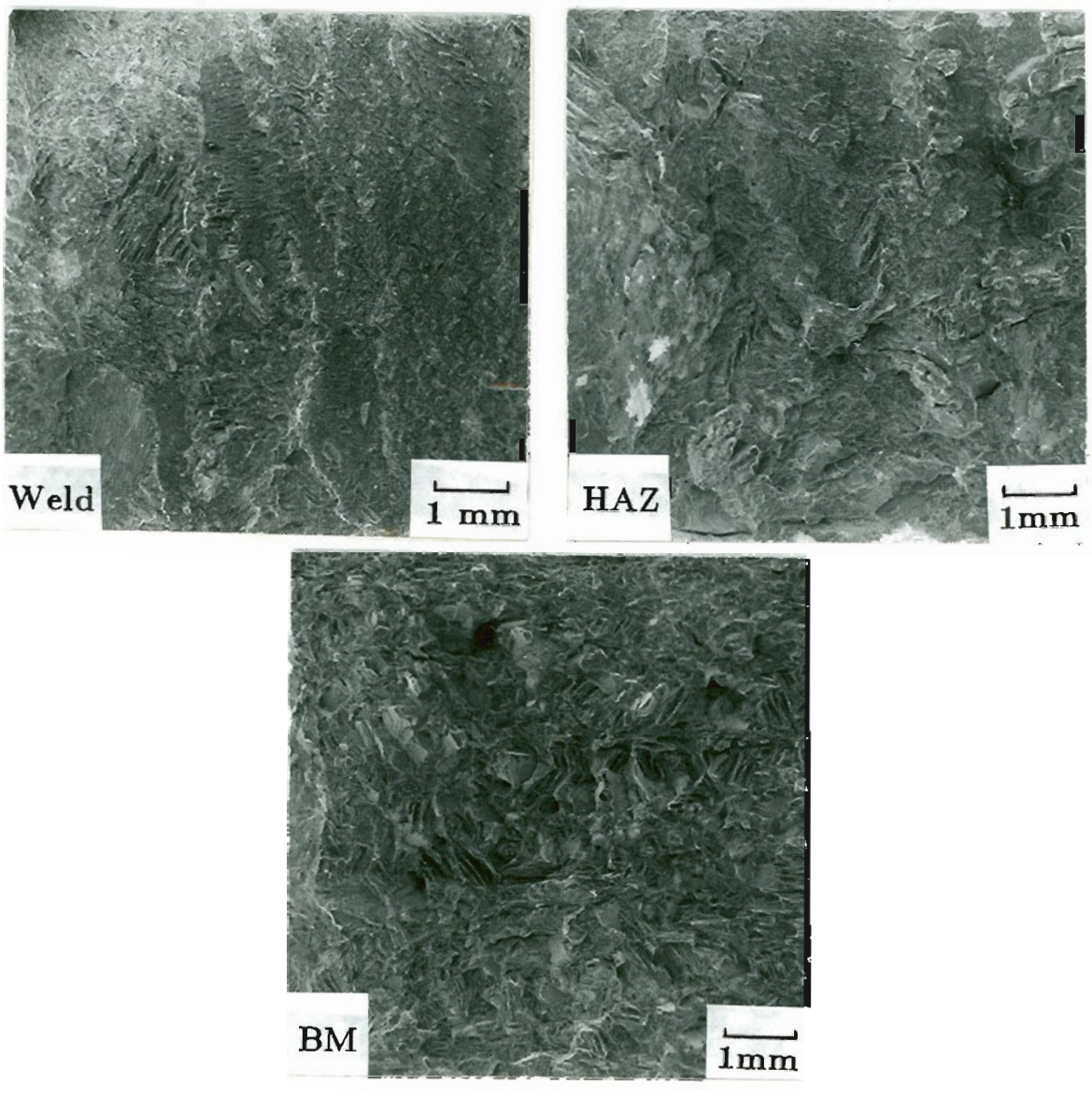

(A)

Figure 49. Fractographs of broken CVN toughness specimens taken at low magnification of the weld metal, HAZ, and BM of (A) Ti-6Al-4V weld made with reagent grade CaF_2 flux, (B) Ti-6Al-4V weld made with high purity CaF_2 flux, and (C) Ti-6211 weld made with high purity CaF_2 flux.

(Figure 49 continued)

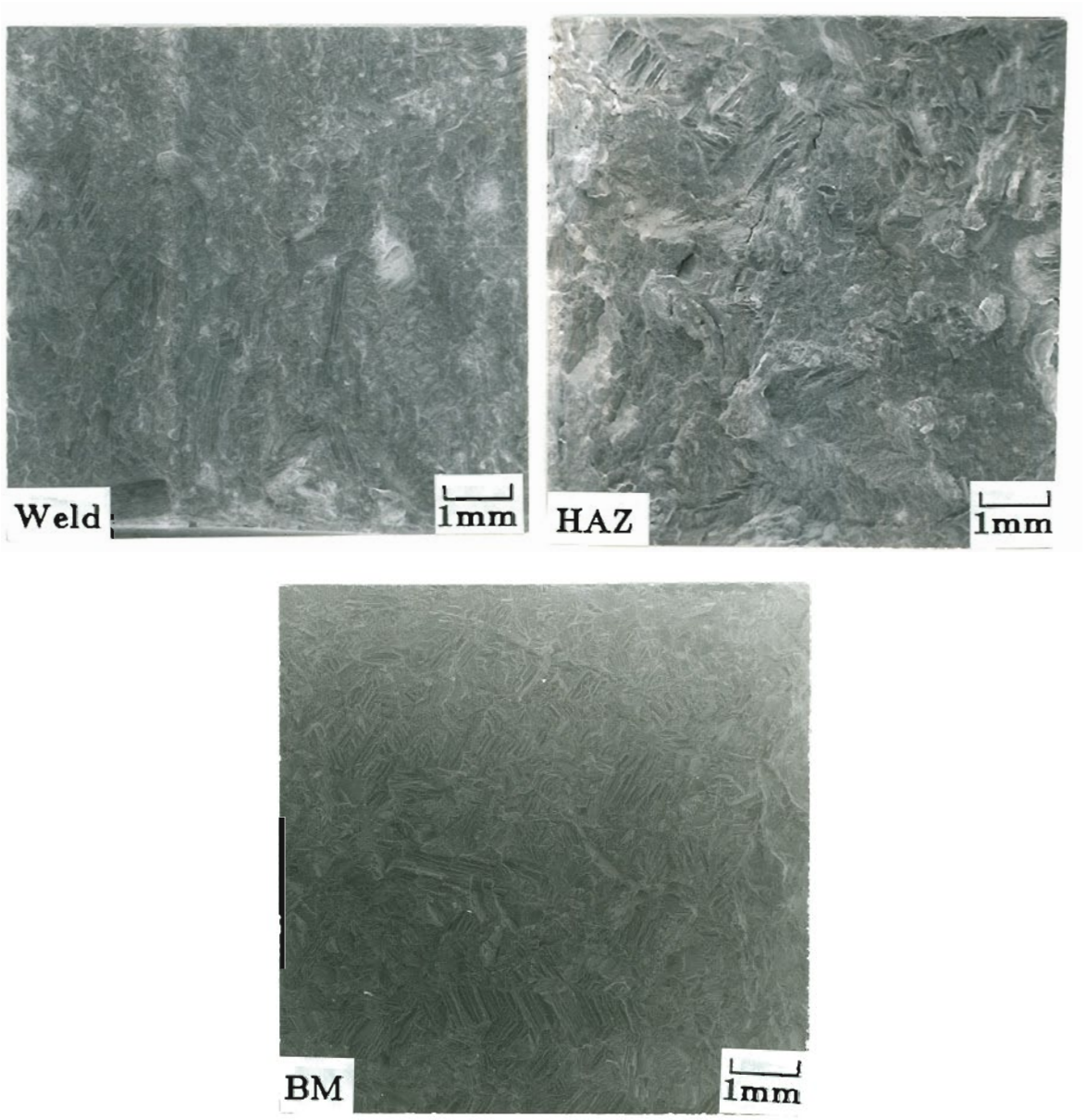

(B)

(Figure 49 continued)

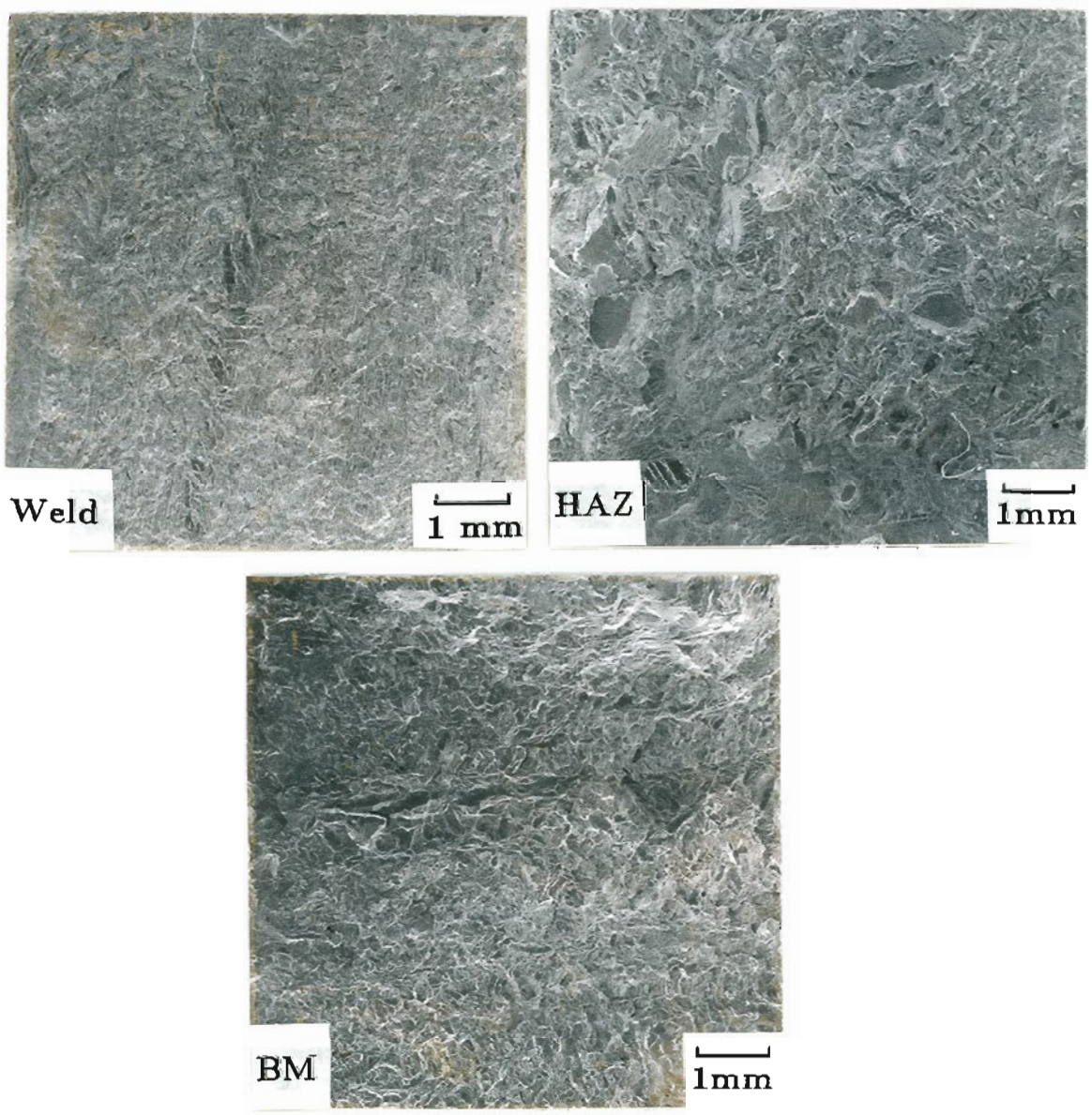

(C)

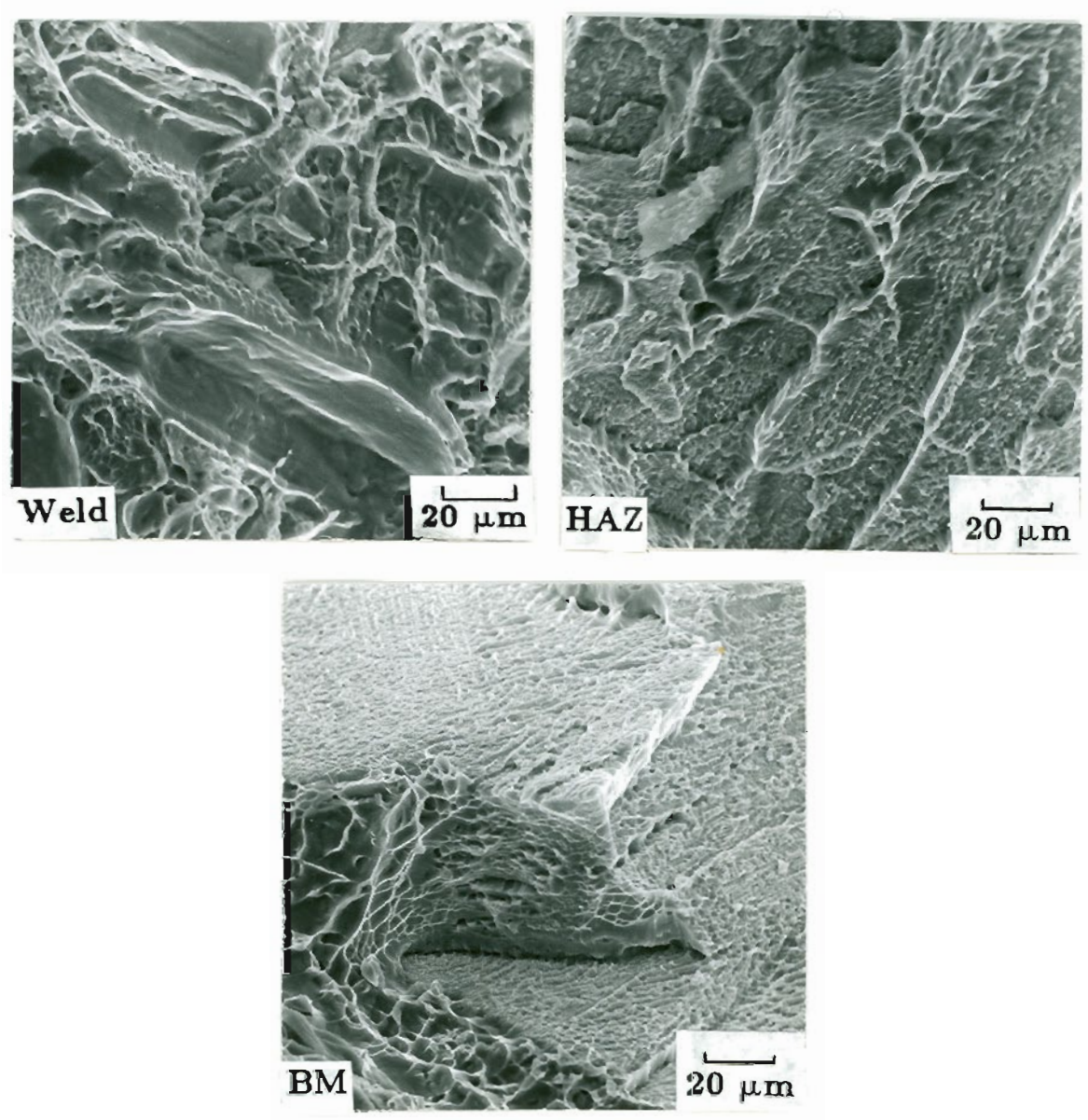

(A)

Figure 50. Enlarged fractographs of the weld metal, HAZ, and BM show a quasi-cleavage fracture and crack branching in: (A) Ti-6Al-4V weld made with reagent grade CaF_2 flux, (B) Ti-6Al-4V weld made with high purity CaF_2 flux, and (C) Ti-6211 weld made with high purity CaF_2 flux.

(Figure 50 continued)

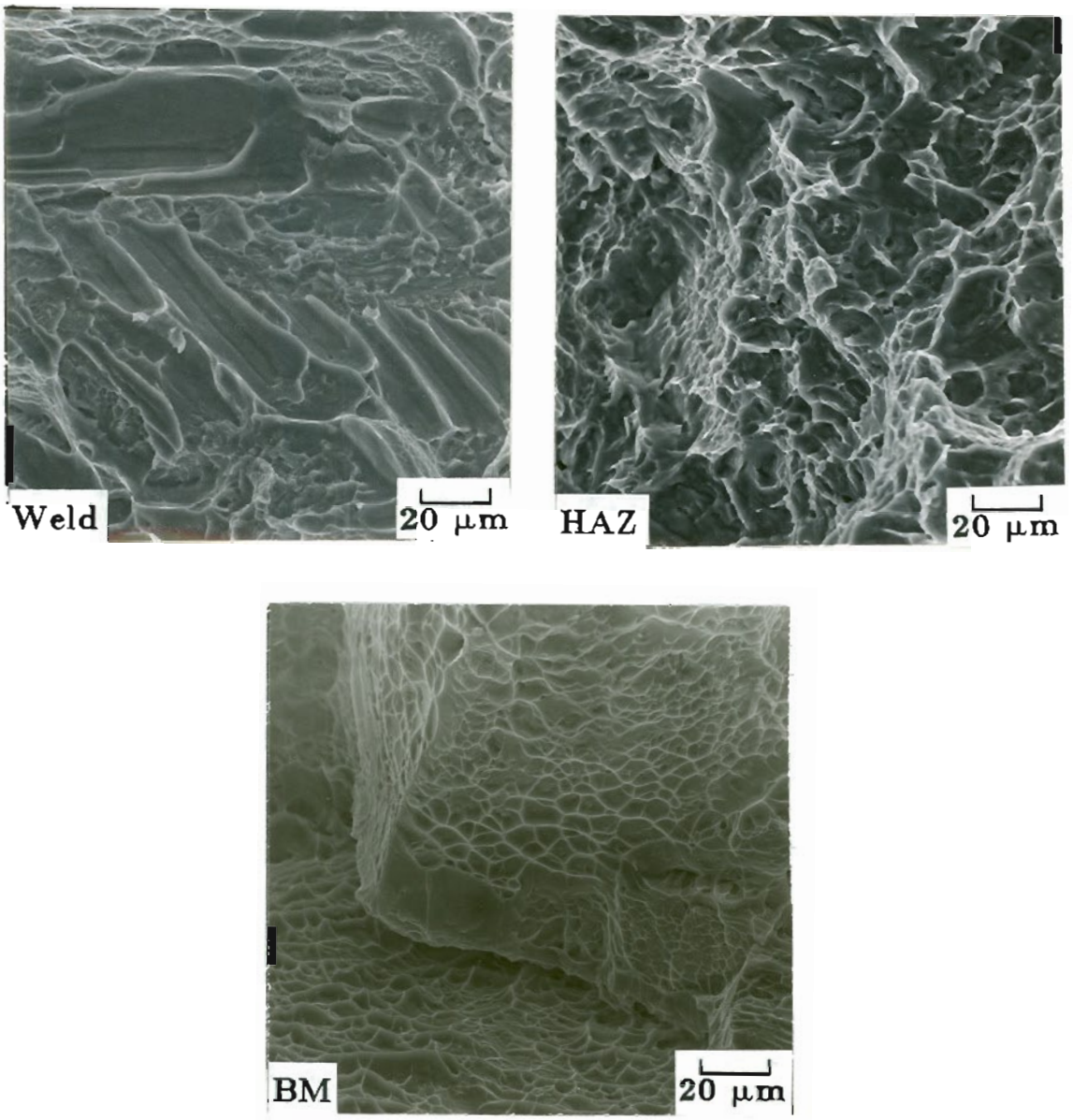

(B)

(Figure 50 continued)

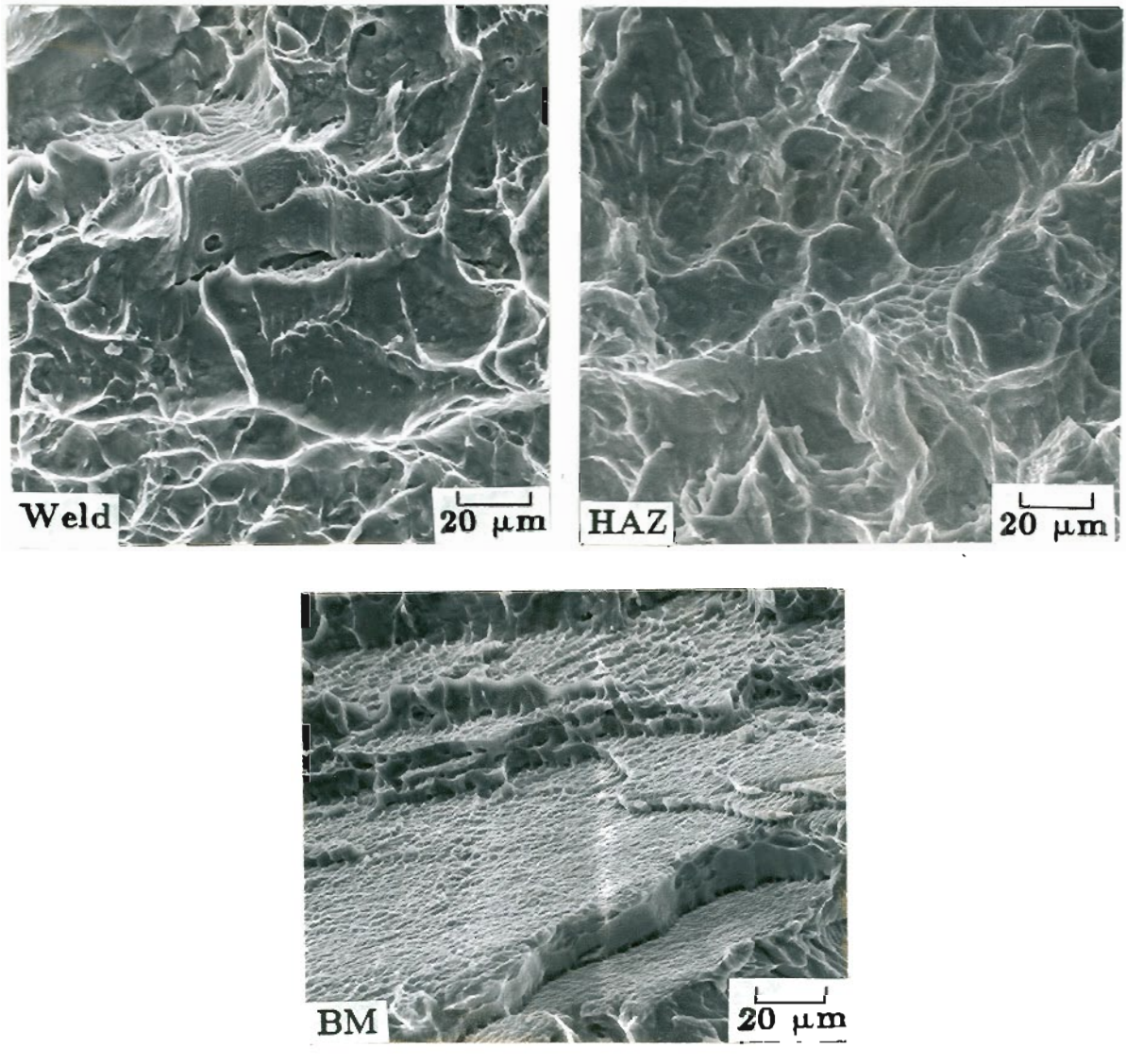

(C)

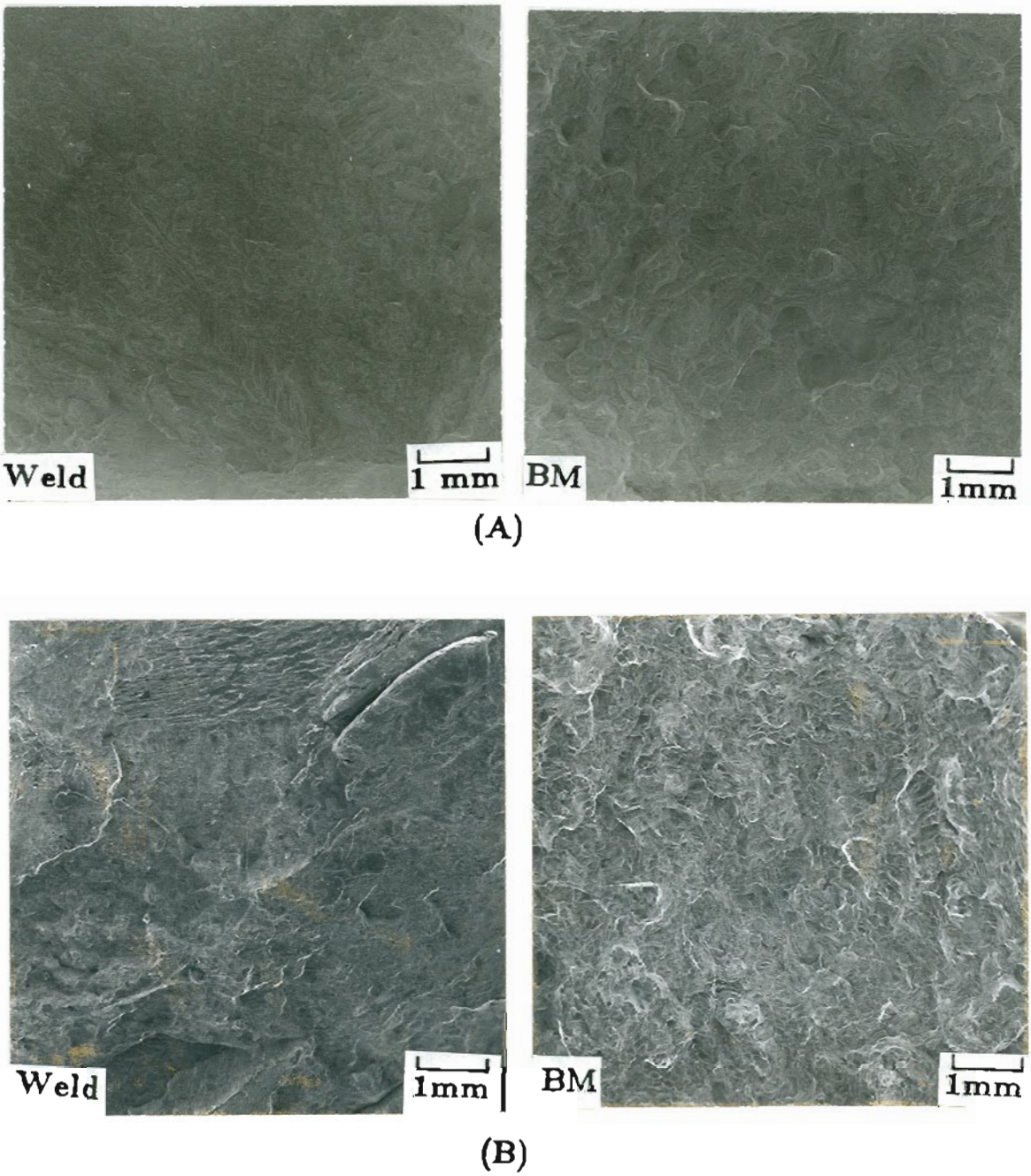

Figure 51. Low magnification fractographs of broken tension test specimens of the weld metal, and BM in : (A) Ti-6Al-4V weld made with high purity CaF_2 flux, and (B) Ti-6211 weld made with high purity CaF_2 flux.

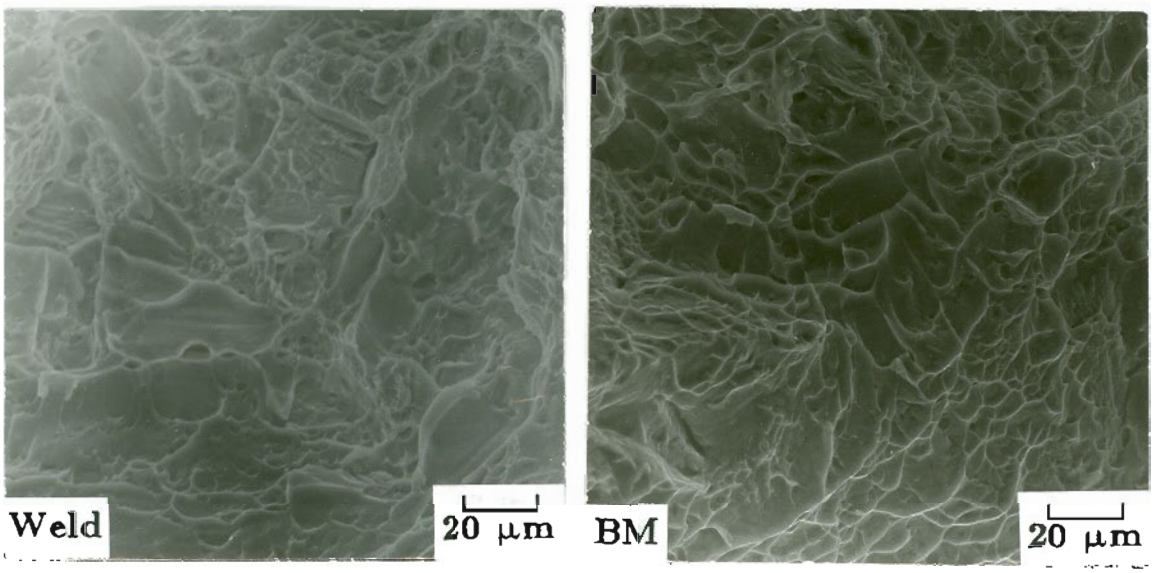

(A)

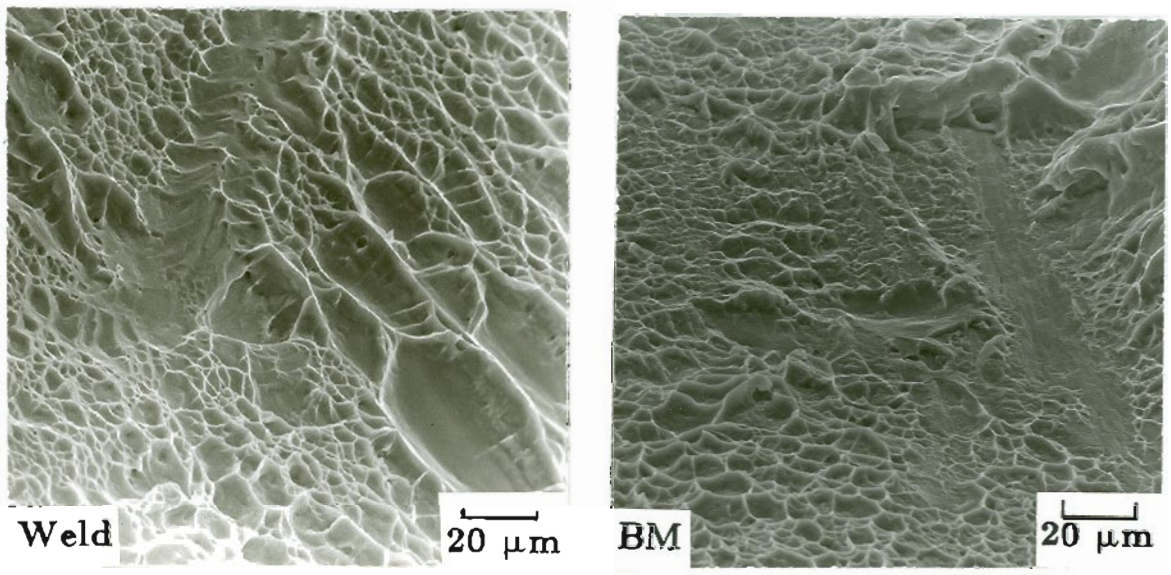

(B)

Figure 52. Enlarged fractographs from selected area in Figure 51, show elongated type of dimple in: (A) Ti-6Al-4V weld made with high purity CaF_2 flux, and (B) Ti-6211 weld made with high purity CaF_2 flux.

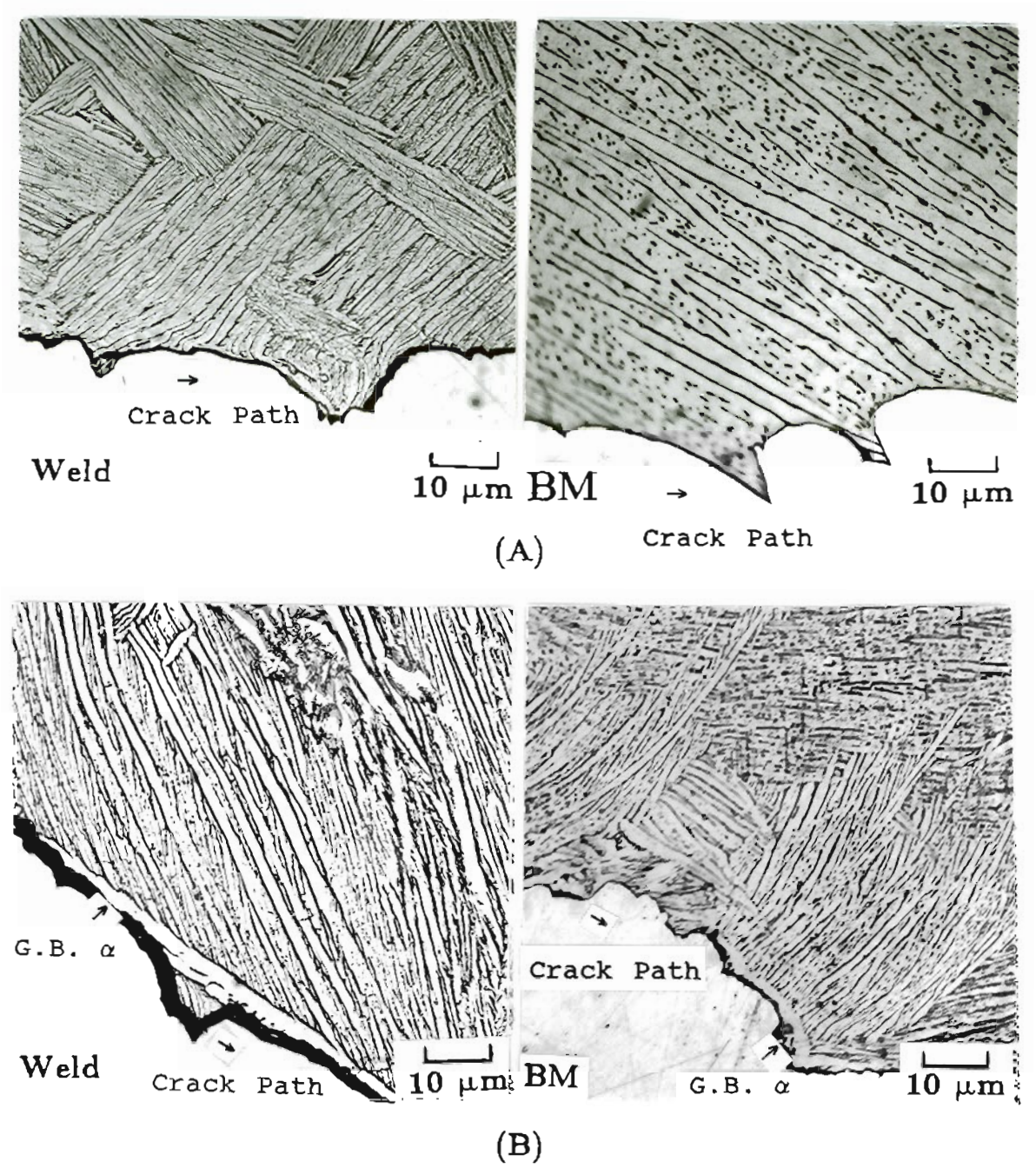

Figure 53. Microstructures of section taken perpendicularly to the fracture surface of: (A) CVN specimen, and (B) tension specimen in Ti-6Al-4V weld made with high purity CaF_2 flux.

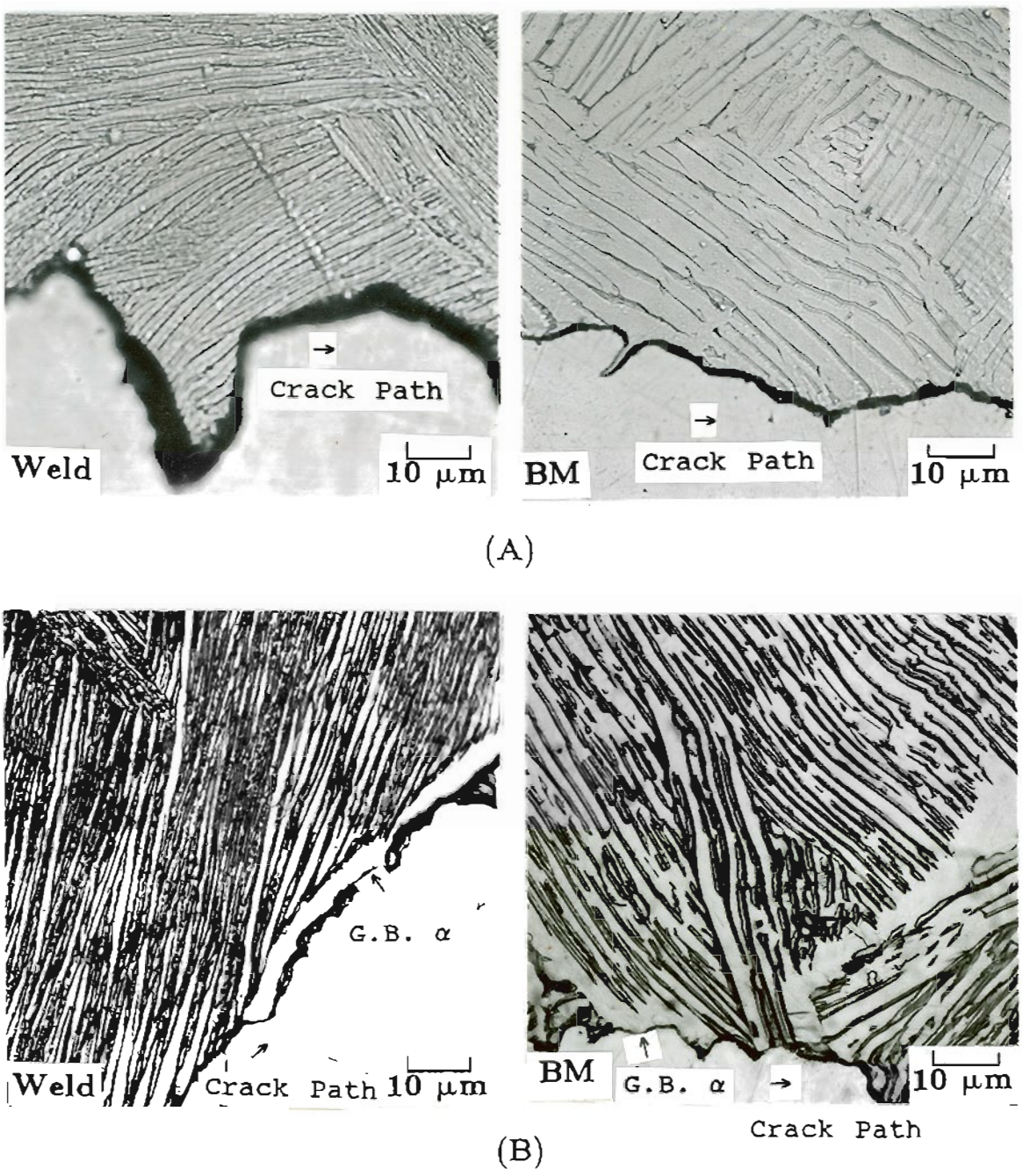

Figure 54 Microstructures of section taken perpendicularly to the fracture surface of: (A) CVN specimen, and (B) tension specimen in Ti-6211 weld made with high purity CaF_2 flux.

V. THEORETICAL ANALYSES OF ESW PROCESS

Unlike ESW of ferrous metals, an AC-CV power source provides the only means to successfully join titanium alloys by consumable guide ESW method. Both DC-en and DC-ep resulted in uncontrollable arcing between the filler/guide and surface of the slag pool and sidewalls. Thus, DC power sources, which are commonly utilized for ESW ferrous metals, always produced poorly fused welds on Ti-6Al-4V.

The mechanism for this striking difference in weldability between titanium and steel by ESW is believed to be electrochemical in nature and related to the presence of three synergistic factors: (1) electrode polarization during the ESW process, (2) the low electrical resistivity of the molten CaF_2 flux, and (3) the high electric resistivity of the titanium electrode (guide and filler metal). The combined effects of these three factors cause the filler electrode and guide to "burn" out of the slag pool to create arcing between the electrode and surface of the slag pool and sidewalls. The following analyses will describe quantitatively the mechanism of ESW of titanium. Point-by-point comparisons will be made between the ESW of titanium and steel to illustrate the differences and difficulties which must be overcome to successfully weld titanium alloys.

A. Characteristics of ESW Steel vs Titanium

To simulate the electric path during ESW of a titanium alloy with AC-CV power, an electric circuit model is created to represent different

parts of the circuit as resistors. For example, the estimated values of resistances (shown in Table 8) for the guide, filler metal, filler metal/slag interface, slag pool, slag/molten metal interface, molten metal pool and plate are calculated based on the geometry and average temperatures of each "resistor" in the ESW circuit. Estimated resistance values (R) are calculated by using Equation 8:

$$R = \rho\ (L/A) \quad \ldots\ldots\ldots\ldots\ldots\ldots\ldots\ldots\ldots\ldots\ldots\ldots\ldots\ldots \quad (8)$$

where L/A is the characteristic length to area ratio over which resistance is measured and ρ is the resistivity. The interfacial polarization resistance (R_p) is calculated using Equation 9.[91]

$$R_p = RT/nFi_o \quad \ldots\ldots\ldots\ldots\ldots\ldots\ldots\ldots\ldots\ldots\ldots\ldots\ldots\ldots \quad (9)$$

Where R is the gas constant, T is temperature, n is number of charges transferred, i_o is the exchange current and F is the Faraday constant. Estimates are also provided for comparable welds (same geometry set-up) made on steel using a standard oxide-based flux (Table 9). The interfacial resistance, molten metal resistance and plate resistance values for ESW both titanium and steel are much smaller than the slag resistance as shown in Table 8 and 9. Therefore, these values could be neglected in order to simplify the electric circuit diagrams as shown in Figure 55(A) for ESW of titanium and Figure 55(B) for ESW of steel.

Figure 55 clearly shows that the slag pool resistance is the major resistance in the ESW process. Due to the lower slag resistance inher-

ent to CaF_2 flux, ESW of titanium with CaF_2 flux must be operated at higher current and lower voltage conditions than similar ESW of steel with oxide-based flux. By the combination of the lower slag resistance and higher wire electrode resistance, the wire electrode provides 19% of the total resistance in ESW of titanium, compared with only 3% in ESW of steel. This high electrode resistance plus the high welding current causes the titanium wire electrode and guide to be susceptible to overheating to the point where the electrode can no longer sustain the electroslag mode. When this condition exists, the titanium electrode can not penetrate into the slag pool as deeply as the comparable steel wire electrode. This increases the chances of the titanium electrode burning out of the slag pool and turning the ESW process into an arc process.

When uncontrollable arcing occurs, most of the welding heat is concentrated above the slag pool to: (a) vaporize the slag surface, (b) overheat the guide and filler metal and (C) radiate energy away from the weld joint. Simultaneously, the lower portion of the slag pool becomes so cold that an inadequate amount of heat reaches the titanium weld pool below to form a sound weld deposit. Furthermore, the high current values needed for ESW titanium limit the length of the consumable guide that can be utilized to approximately 120 cm (4 ft.) due to I^2R heating of the guide.

Table 8 : Estimates of the resistance values during ESW of 50 mm thick Ti-6AL-4V plate using the parameters shown in Table 7.

	T_{Av} (°C)	Resistivity ($\times 10^3 \Omega$-cm)	Length (mm)	Area (mm^2)	Resistance ($\times 10^3 \Omega$)	% of Total Resistance
Guide	500	0.154	508	483	1.62	5.4
Filler Metal Tip	1000	0.227	20	8	5.68	18.9
Filler Metal - Slag Interface *	1727	-	-	-	0.04	0.1
Slag	1727	140.0	13	804	22.64	75.3
Slag - Molten Metal Interface *	1727	-	-	-	0.04	0.1
Molten Metal	1650	0.400	5	1963	0.01	(0.03)
Ti-6Al-4V Plate	500	0.154	150	5000	0.05	0.2

Table 9 : Estimates of resistance values during ESW of 50 mm thick steel plate using AC power, 550 A, 45 V and Hobart 201 flux.

	T_{Av} (°C)	Resistivity ($\times 10^3 \Omega$-cm)	Length (mm)	Area (mm^2)	Resistance ($\times 10^3 \Omega$)	% of Total Resistance
Guide	500	0.059	508	483	0.62	0.7
Filler Metal Tip	1000	0.091	20	8	2.28	2.7
Filler Metal - Slag Interface *	1727	-	-	-	0.04	(0.05)
Slag	1727	500.0	13	804	80.85	96.4
Slag - Molten Metal Interface *	1727	-	-	-	0.04	(0.05)
Molten Metal	1540	0.140	5	1963	0.004	(0.005)
Steel Plate	500	0.059	150	5000	0.02	(0.02)

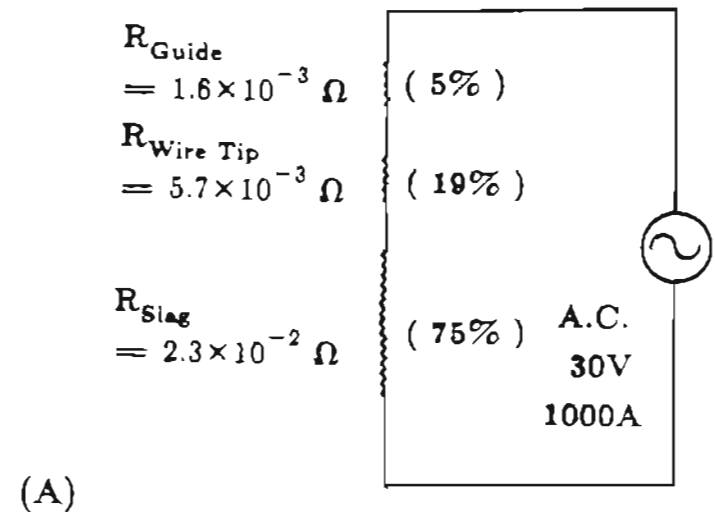

(A)

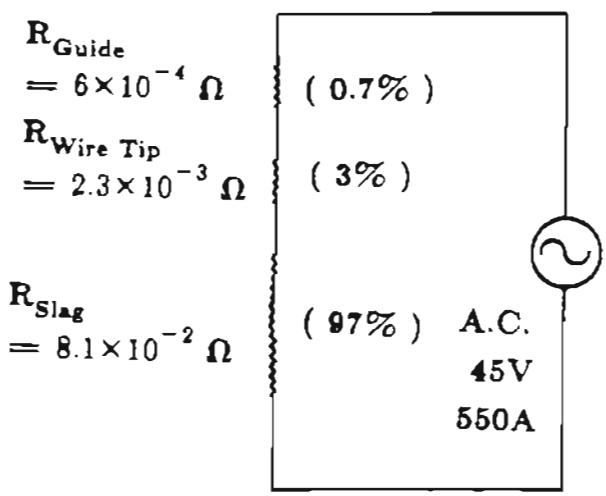

(B)

Figure 55. Simplified circuit diagram for an ESW 50 mm thick plate with AC power supply: (A) ESW titanium with CaF_2 flux and (B) ESW steel with Hobart 201 flux.

B. DC Polarization Effect During ESW

ESW of titanium with DC power was not possible due to polarization effects unless the guide was physically driven into the slag pool. An amplified circuit diagram of the DC-ep (DC electrode positive) system for ESW of titanium is shown in Figure 56. The major difference between the AC and DC processes is that the latter has a more significant interfacial resistance than the former. This is primarily due to the polarization of Ti^{+4} ions at the anode and Ca^{+2} ions at the cathode. The polarization resistance value was estimated to be 6% of the total resistance by using the data for DC polarization of pure iron electrodes reported by Mitchell et al.[61] .

The heat generated by polarization resistance at the interface promotes more rapid melt back of the filler metal tip and consumable guide. At this point, so little of the filler metal is in contact with the slag that only the top of the slag bath is hot, while the bulk slag is cooling (increasing slag resistance). Quickly, an arc is initiated by the combination of filler metal melting out of the slag and gas evolution of TiF_4 and/or CaF_2 at the slag/electrode interface. Formation of gas at the interface further increases the resistance and melt back tendency at that location.

Thus, it is believed that the unstable arcing in DC welding is due to polarization of the flux into calcium metal and fluorine or titanium tetrafluoride gas.[92] Once formed, the fluorine is so reactive that is immediately dissoves into the slag solution. No fluorine gas has ever been reported to be present in the welding fumes under both stable ESW

and unstable arcing conditions. The dissolution of metallic calcium in the flux is believed to further increase the conductivity of the slag which leads to unstable arcing. Using AC current greatly inhibits this electrolysis reaction.

Once arcing is initiated, the circuit diagram changes to that shown in Figure 56(B). Here, heat is concentrated above the slag pool, while arcing is taking place between the electrode and both the slag surface and the sidewalls. Although the bulk slag temperature is so low that lack of fusion results, the top layer on the slag pool is evolving gas and providing a conducting path to the sidewalls. The stability of the arcing process dominates and it is not possible to sustain an electroslag mode of welding.

If the same DC-ep weld shown in Figure 56 were made with steel filler metal/guide and CaF_2 flux, the electroslag mode would dominate over the competitive arcing mode because the electrode resistance is substantially less than that for titanium. The oxide-based high resistivity flux used for ESW steel further enhances the electroslag mode by reducing the current needed for welding and, thus, reducing I^2R heating of the filler metal and melt back. Development of a more resistive halide flux for ESW of titanium alloys would also be helpful in widening the window of usable welding parameters shown in Figure 16.

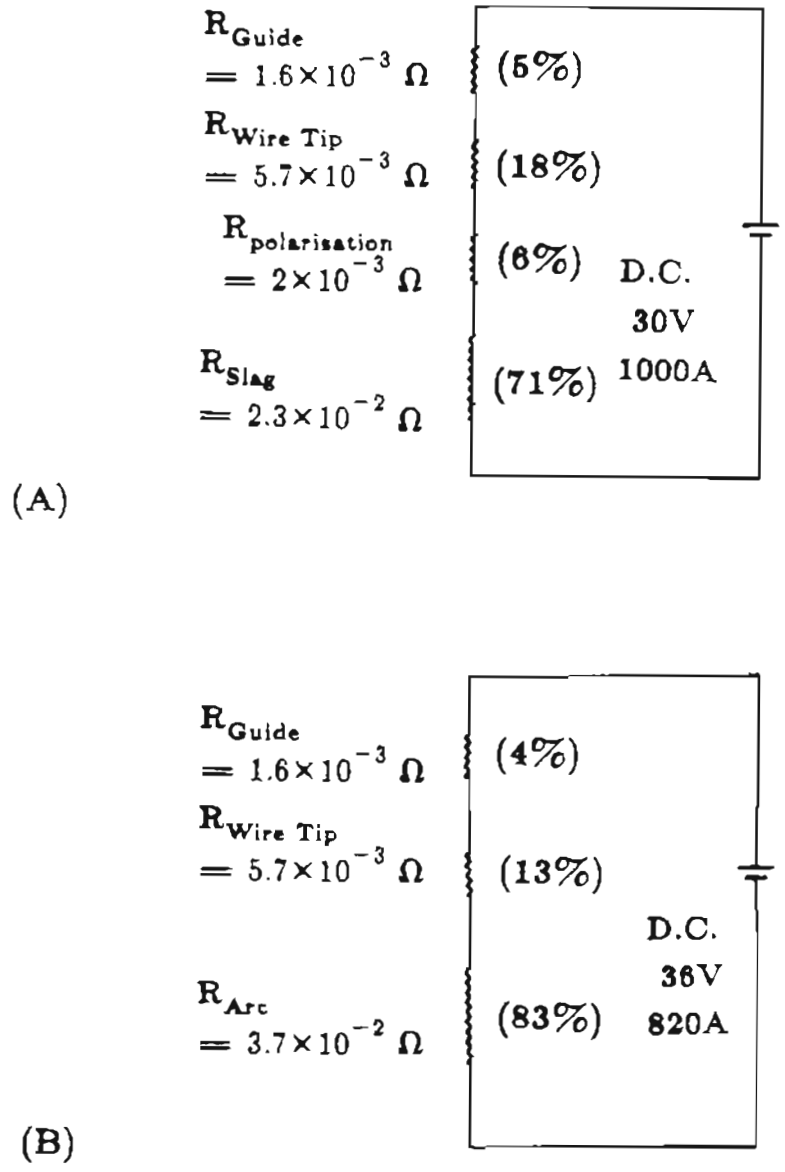

Figure 56. Simplified circuit diagram for ESW 50 mm thick titanium plate with DC power supply and CaF_2 flux : (A) unstable welding in the electroslag mode and (B) stable mode of arcing between the electrode and slag surface.

C. Mechanism of ESW with Low Resistivity Calcium Fluoride Flux

By expanding the resistance term in Equation 1, Ohm's law for the ESW process could be written as shown below :

$$V_w = I_w \rho_{slag} \; l_{eff}/A_{eff} \quad \text{----------} \quad (10)$$

ρ_{slag} : resistivity of slag
l_{eff} : Effective inter-electrode distance
A_{eff} : Effective electrode contact area

l_{eff}/A_{eff} is known to have an inverse relationship with electrode feed rate (V_e),[33] therefore, it can be expressed as:

$$l_{eff}/A_{eff} = 1/f(v_e) \quad \text{----------} \quad (11)$$

$f(v_e)$: a function related to v_e

Then, substituting Equation 11 into Equation 10, the result is as follows:

$$V_w = I_w \; \rho_{slag} \; / \; f(v_e) \quad \text{----------} \quad (12)$$

Also equations 2 and 3, can be combined as shown below:

$$W_s = (n \; v_e \; A_e)/(A_g - A_p) \quad \text{----------} \quad (2)$$

$$H_{input} = (V_w \; I_w)/W_s \quad \text{----------} \quad (3)$$

$$\Rightarrow \quad H_{input} = (V_w \; I_w)/Cv_e \quad \text{----------} \quad (13)$$

$C : n \; A_e/(A_g - A_p)$

At constant voltage (Vw = Constant), Equation 12 can be rewritten as:

$$I_w = C_v \; f(v_e)/\rho_{slag} \quad \text{----------} \quad (14)$$

C_v : constant voltage value

Substituting Equation 14 into Equation 13, the result is:

$$H_{input} = C_v^2 \, f(v_e)/\rho_{slag} \; Cv_e$$

$$= C_1 \, f(_2v_e)/\rho_{slag} \; v_e \quad \ldots\ldots\ldots\ldots\ldots\ldots\ldots\ldots \quad (15)$$

$$C_1 = C_v^2/C$$

1. Flux Resistivity Effect on the Welding Current

The constant voltage power supply was used for ESW of both titanium and steel alloys. At a fixed value of voltage and electrode feed rate, the weld using a low resistivity flux (such as CaF_2 flux) requires a higher current than the weld using high resistivity flux (such as oxide-base flux). The reason is that the current is inversely proportional to the resistivity as shown in Equation 14. This result was observed in consumable guide ESW of steels (Figure 26) and in non-consumable guide ESW of steels (Figure 33); both were made by low resistivity CaF_2 flux.

Besides having a higher current, the weld deposited with low resistivity CaF_2 flux also generates a higher heat input than the weld using a high resistivity oxide-based flux at a fixed values of voltage and electrode feed rate as shown by Equation 15. The weld with a higher heat input will have a higher base metal dilution as shown in Figure 34. Similar results were reported by Ann[17] for consumable guide ESW of steels using different percentages of CaF_2 addition in Hobart 201 oxide-base flux.

2. Flux Resistivity Effect on the Welding Voltage

Equation 15 shows that the heat input of the ESW process increases when the welding voltage is increased. But the welding voltage can not be increased indefinitely, because there is a limit imposed by the slag pool geometry. When the voltage is being increased and the current is constant in the ESW process, the inter-electrode distance increases according to Equation 10, until the electrode is out of the slag pool and an explosive arc breaks out between the electrode and slag pool. Since the result of arcing is a lack of fusion and slag entrapment defects in the weld, the welding voltage has to be kept below the threshold to avoid arcing.

This threshold voltage for ESW with a lower resistivity flux is lower than that for ESW with a higher resistivity flux, because voltage is directly proportional to resistivity as shown in Equation 10. This result can be easily illustrated by the following examples. In consumable guide ESW of Ti-6Al-4V alloys using low resistivity CaF_2 flux, the typical values used to calculate the voltage threshold are:

I_w = 1100 A (average current among working range),

ρ_{slag} = 0.14 ohm-cm (resistivity of CaF2 at 1700 C),

l_{eff} = 1 cm (maximum gap between guide and base metal plates), and

A_{eff} = 4.84 cm^2 (cross-section area of guide plate)

substituting all these values into Equation 10, the result is:

V_{max} = (1100 x 0.14 x 1)/4.84 V

= 32 V

For ESW of steel using high resistivity Hobart 201 oxide-base flux, the typical welding variables are listed below:

I_w = 600 A (average current among working range),

ρ_{slag} = 0.5 ohm-cm (resistivity of Hobart 201 flux at 1700 C),

l_{eff} = 1 cm (maximum gap between guide and base metal plates), and

A_{eff} = 4.84 cm^2 (cross-section area of guide plate)

substituting all these values into Equation 10, the result is:

$$V_{max} = (600 \times 0.5 \times 1)/4.84 \text{ V}$$
$$= 62 \text{ V}$$

These results are in good agreement with experimental observations. As shown above, arcing is rarely ever encountered in ESW of ferrous alloys. The voltage limit for stable ESW of Ti-6A-4V alloys using low resistivity CaF_2 flux is determined to between 30 V and 35 V as shown in Figure 16. The ESW process is stable at 30 V and changes to an arc process at 35 V. Similar results have also been observed for ESW of steel using low resistivity CaF2 flux; the ESW process is stable at 30 V and changes to an arc process at 35 V as shown in Table 6.

Table 6 also shows that ESW of steel using high resistivity Hobart 201 flux is stable at 38V and 45V without arcing. The working range for voltage during ESW of steel using high resistivity Hobart 201 flux has been reported to be 36-45 V by Ann[17] (for 50 mm thick plates) and 35-50 V by Frost et al.[35] (for 100 mm thick plates). Therefore, the estimated limiting voltage value (62 V) may be a little higher than the actual

value.

In summary, the welds made by low resistivity flux have a lower voltage working range than the welds made by high resistivity flux. The consequence of having a lower voltage working range is that the welds will have a lower heat input (Equation 15) and welding procedures will have to specify the upper limit of voltage for actual use. If arcing occurs more than about once per 10-20 seconds, the voltage will need to be reduced.

D. Electrode Ohmic Heating Effect

1. Equations for Ohmic Heating

From the ohmic heating experiments, the initial ohmic heating rate of the electrode can be calculated by the following equations. Assuming no heat losses to the environment, all the heat produced by ohmic heating is used to heat up the electrode. Therefore, the heat balance for a small section of electrode can be expressed as shown in Equation 16.

$$A\ L\ D\ C_p\ dT = I^2\ L\ (R_o + aT)\ dt / A \quad \ldots\ldots\ldots\ldots\ldots\ldots \quad (16)$$

$$\Rightarrow \quad dT / (1 + aT/R_o) = I^2\ R_o\ dt / A^2\ D\ C_p$$

$$\text{let} \quad C = I^2\ R_o / A^2\ D\ C_p \quad \ldots\ldots\ldots\ldots\ldots\ldots\ldots\ldots\ldots\ldots\ldots \quad (17)$$

$$\Rightarrow \quad dT / (1 + aT/R_o) = C\ dt$$

$$\Rightarrow \quad d\{\ln(1 + aT/R_o)\}\ R_o/a = C\ dt$$

Integrating both sides:

$$\Rightarrow \quad \ln(1 + aT/R_o)\ R_o/a = C\ t$$

$$\Rightarrow \quad (1 + aT/R_o) = \exp(a\ C\ t\ /\ R_o)$$

The resulting temperature rise as a function of time is derived in Equation 18 as shown below :

$$\Rightarrow \quad T = \{\exp(a\ C\ t\ /\ R_o) - 1\}\ R_o/a \qquad \ldots\ldots\ldots\ldots\ldots\ldots\ldots \quad (18)$$

The heating rate is expressed as :

$$\Rightarrow \quad dT/dt = C \exp(a\ C\ t\ /\ R_o) \qquad \ldots\ldots\ldots\ldots\ldots\ldots\ldots\ldots \quad (19)$$

at t = 0, the initial heating rate is equal to:

$$\Rightarrow \quad dT/dt)_{t=0} = C$$

$$= I^2\ R_o\ /\ A^2\ D\ C_p$$

let j = I/A

$$\Rightarrow \quad dT/dt)_{t=0} = j^2\ R_o\ /\ D\ C_p \qquad \ldots\ldots\ldots\ldots\ldots\ldots\ldots\ldots \quad (20)$$

A : Cross-sectional area of electrode
L : Length of the electrode where temperature is measured
D : Density of the electrode
C_p: Heat capacity of electrode
T^p: Temperature of the electrode
I : Applied current
R_o: Resistivity of the electrode at room temperature
a : Temperature coefficient of resistivity
t : Time
C : Parameter as defined in Equation 17
ln : Natural logarithm function
exp : exponential function
j : current density

Equation 20 shows that the initial heating rate of the electrode is equal to the square of current density times the resistivity of the electrode at room temperature divided by the heat capacity and density of the electrode. Figure 57 shows that the measured initial heating rate values are in good agreement with the values calculated using Equation 20.

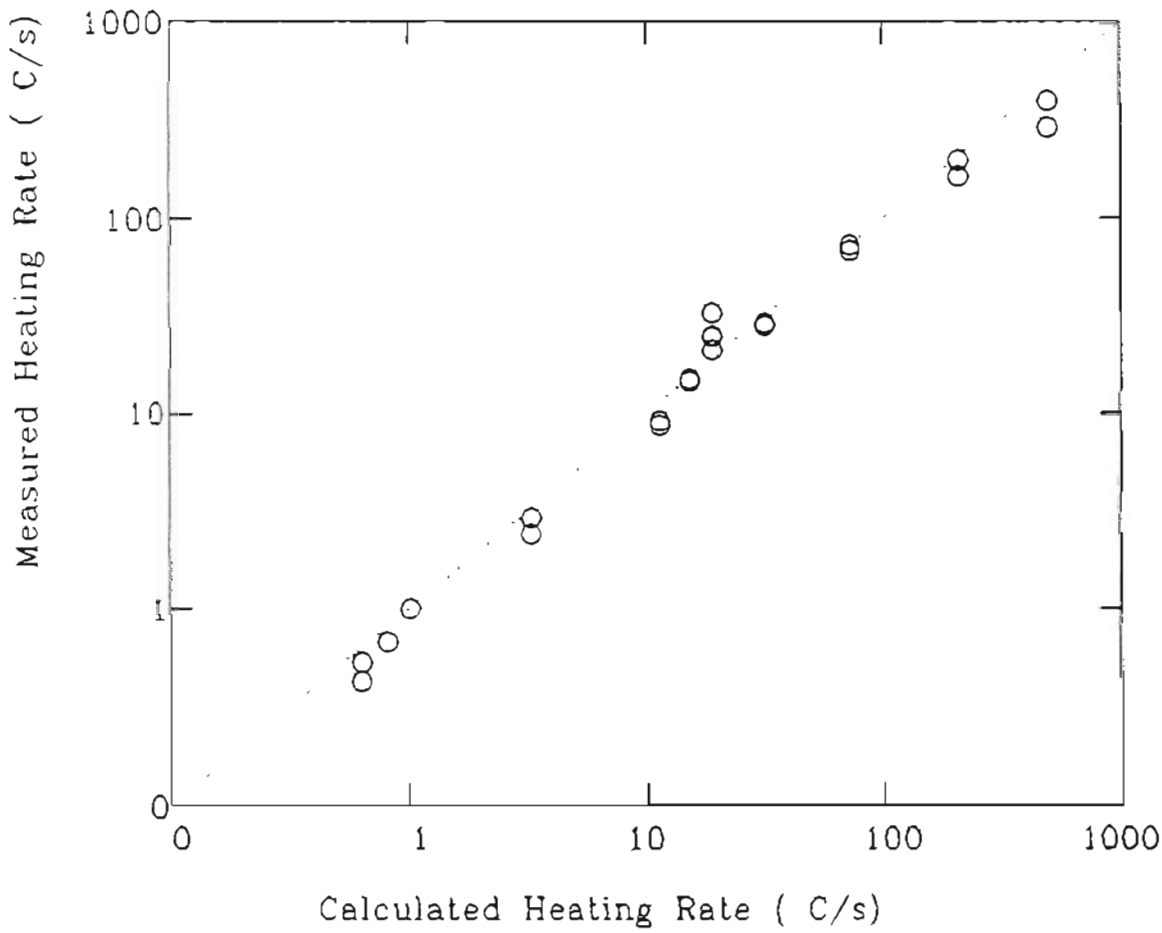

Figure 57. Correlation between the calculated using Equation 20 and measured values of initial ohmic heating of different electrodes.

2. Ohmic Heating Effect on Arcing Instability in Non-Consumable Guide ESW Process

The ohmic heating rate results were further applied to calculate the amount of ohmic heating contribution to the electrode melting rate in the non-consumable ESW process. Figure 58 shows a simplified diagram of the electrode feeding model for the non-consumable guide ESW process. The temperature increase of the electrode before it enters the slag pool is equal to the ohmic heating rate times the duration time for the electrode to travel through the total dry stickout distance.

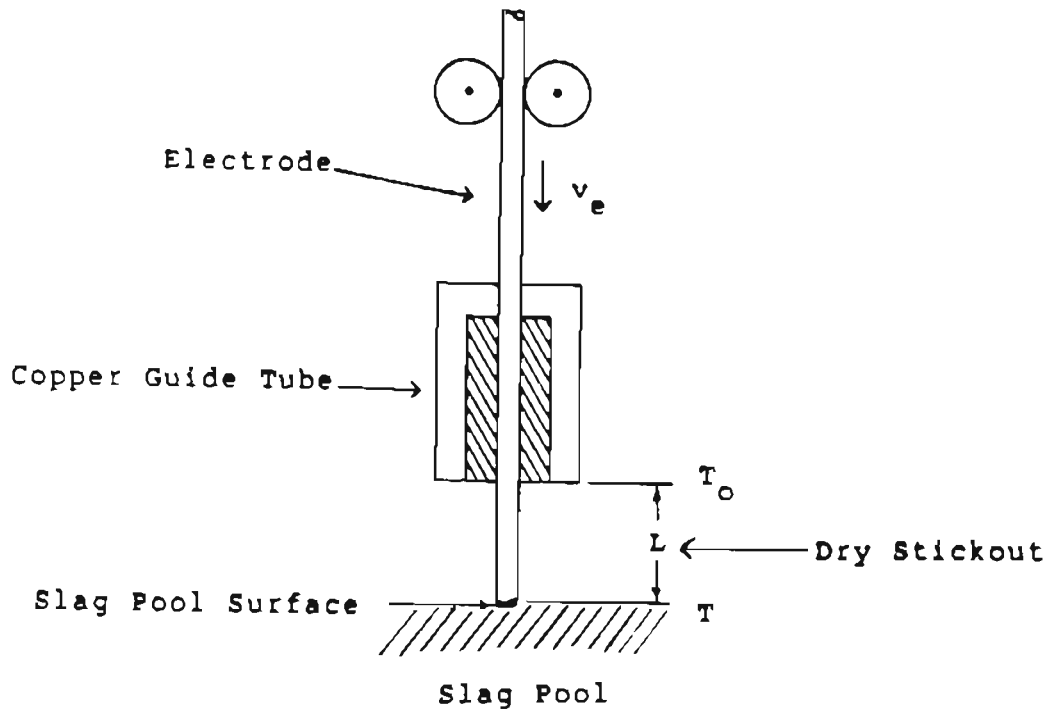

Figure 58. A simplified diagram shows the wire feed system used in the non-consumable guide ESW process.

Assuming no heat losses to the environment, the temperature can be expressed as :

$$T - T_o = (dT/dt)\, L/v_e \quad \ldots\ldots\ldots\ldots\ldots\ldots\ldots\ldots\ldots\ldots \quad (21)$$

T : Electrode temperature before it enters the slag pool
T_o: Electrode temperature after it leaves the copper guide tube (assumed to be at room temperature)
dT/dt: Ohmic heating rate of the electrode
L : Dry stickout distance
v_e: Electrode feed rate

In the ESW process the L/v_e value is small, therefore, the initial ohmic heating rate can be used to approximate the steady state ohmic heating rate. So, by substituting Equation 20 into Equation 21, the temperature rise is equal to:

$$T - T_o = \{dT/dt)_{t=0}\}\, L/v_e$$
$$= j^2 R_o L / D C_p v_e \quad \ldots\ldots\ldots\ldots\ldots\ldots\ldots\ldots \quad (22)$$

This equation is the same as the one-dimensional analytical solution reported by Myers et al.[93] Equation 22 can be converted to the percentage ohmic heating contribution of the total electrode melting rate, by dividing the heat caused by ohmic heating with total amount of heat required to melt the electrode. The result is as followed :

$$P_{ohm}\ \% = \{C_p (T - T_o) / H_m\} \times 100\% \quad \ldots\ldots\ldots\ldots\ldots\ldots \quad (23)$$

And, substituting Equation 22 into Equation 23:

$$P_{ohm}\ \% = j^2 R_o L / D H_m v_e \quad \ldots\ldots\ldots\ldots\ldots\ldots\ldots\ldots \quad (24)$$

$P_{ohm}\ \%$: percentage ohmic heating contribution of electrode melting rate

H_m : Heat required to melt the electrode

The electrode melting rate and welding current correlation have been reported by several researchers[93-95] to have a parabolic relationship as shown in the equation below:

$$MR_e = a\ I + b\ I^2 + c \quad \ldots\ldots\ldots\ldots\ldots\ldots\ldots\ldots\ldots\ldots \quad (25)$$

MR_e: Electrode melting rate
aI_2: Heat conduction from the slag pool
bI^2: ohmic heating of the electrode
c : constant

For stable ESW, the electrode feed rate is equal to the electrode melting rate. If the ohmic heating contribution was higher than 100%, which means the electrode melts faster than the electrode feed rate, the electrode would burn out of the slag pool and the ESW process would turn into an arc process. Arcing on top of the slag pool is not desirable in ESW process because the resulting weld will have lack of fusion due to slag entrapment. To avoid arcing, a limiting electrode feed rate can be obtained from Equation 25 by setting the percentage ohmic heating contribution to 100%. The result is shown below in Equation 26 :

$$v_{lim} = j^2\ R_o\ L\ /\ D\ H_m\ v_e \quad \ldots\ldots\ldots\ldots\ldots\ldots\ldots\ldots\ldots\ldots \quad (26)$$

v_{lim} : Limiting electrode feed rate

If the electrode feed rate is slower than the limiting value, then arcing will occur on top of the slag pool.

To demonstrate the ohmic heating effect on arcing instability in

non-consumable guide ESW process, examples for ESW of steel and titanium alloys are discussed below. The welding variables; current, electrode feed rate, dry stickout distance and electrode diameter are shown in Figure 59(A) for steel (taken from ASM Metal Handbook[96]), and in Figure 59 (B) for titanium alloy (taken from Gurevich's report[20]). Using Equation 24, the corresponding percentage ohmic heating contribution of the electrode melting rate are calculated and plotted in Figures 60(A) for steel and in Figure 60(B) for titanium alloy.

The results in Figure 60 show that the titanium alloy is far more susceptible to arcing caused by ohmic heating than steel even though a larger diameter electrode is used for ESW of the titanium alloy. This is because titanium alloy has an electrical resistivity value (180×10^{-6} ohm-cm) that is nine times the value (20×10^{-6} ohm-cm) of steel as shown in Figure 31.

Figure 60 also shows that the percentage ohmic heating contribution to the electrode melting rate is directly proportional to dry stickout distance, but inversely related to electrode diameter and welding current (electrode feed rate). The inverse effect of welding current on percentage ohmic heating contribution of electrode melting rate is because current and electrode feed rate are interrelated in the ESW process, and the increase of electrode feed rate is faster than the corresponding increase of current as shown in figure 59. Also, when increasing the current, the electrode penetrates deeper into the slag pool and the contribution of electrode melting rate due to the heat conducted from slag pool increases.

In summary, the percentage ohmic heating contribution of electrode melting rate gives an indication of arcing instability in non-consumable guide ESW process. ESW of titanium alloys is more susceptible to arcing than ESW of steel due to its high electric resistivity and the requirement that titanium be welded with low resistivity halide fluxes.

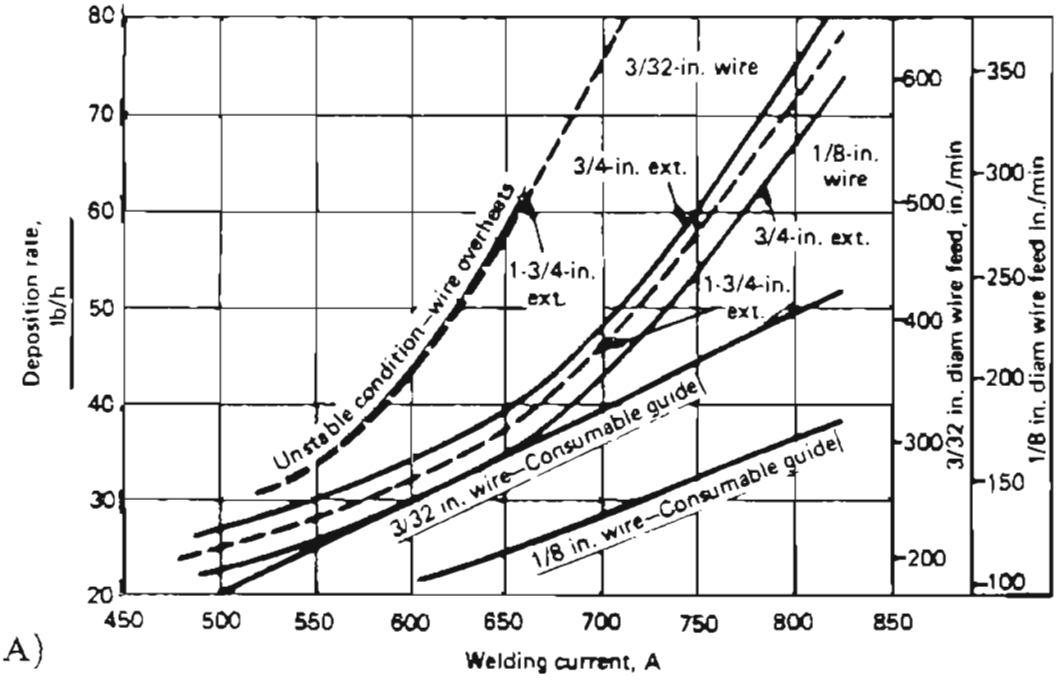

(A)

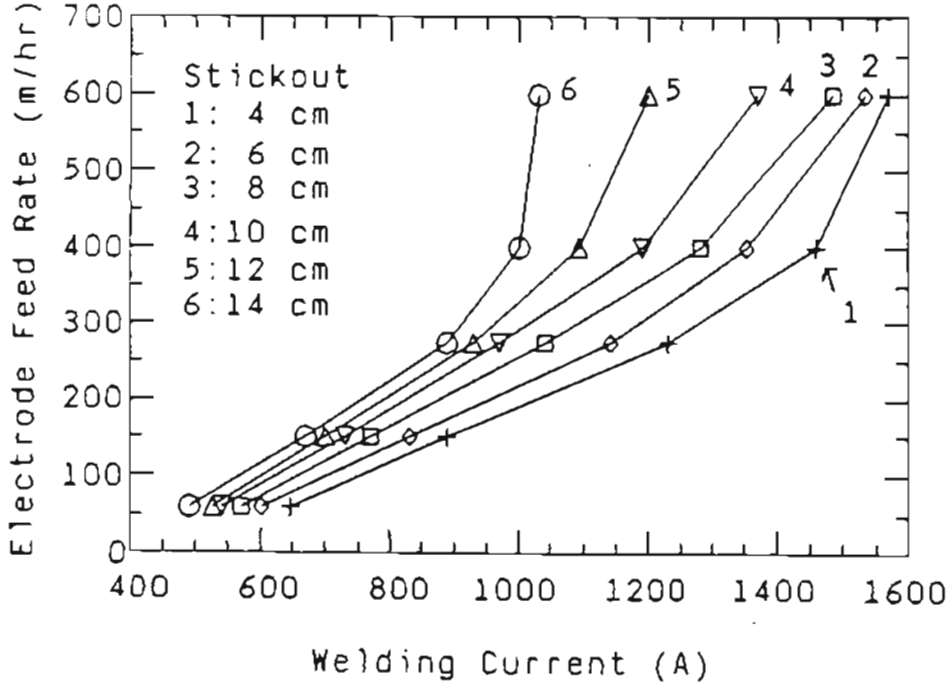

(B)

Figure 59. Welding variables for : (A) ESW of steel (After ASM Metal Hand Book[96]) and (B) non-consumable guide ESW of titanium alloy (after Gurevich[20]).

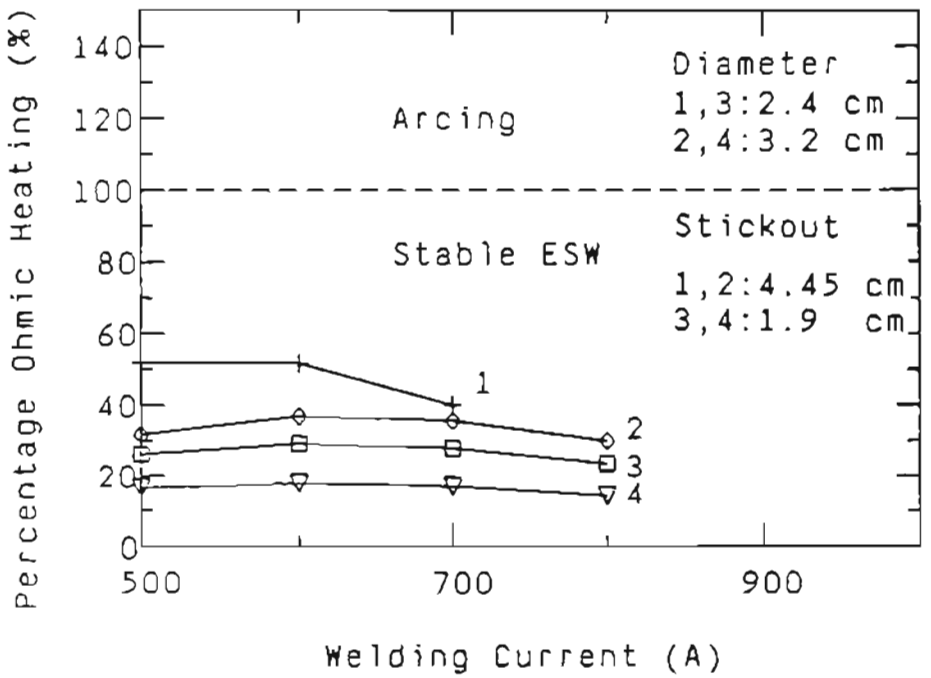

(A)

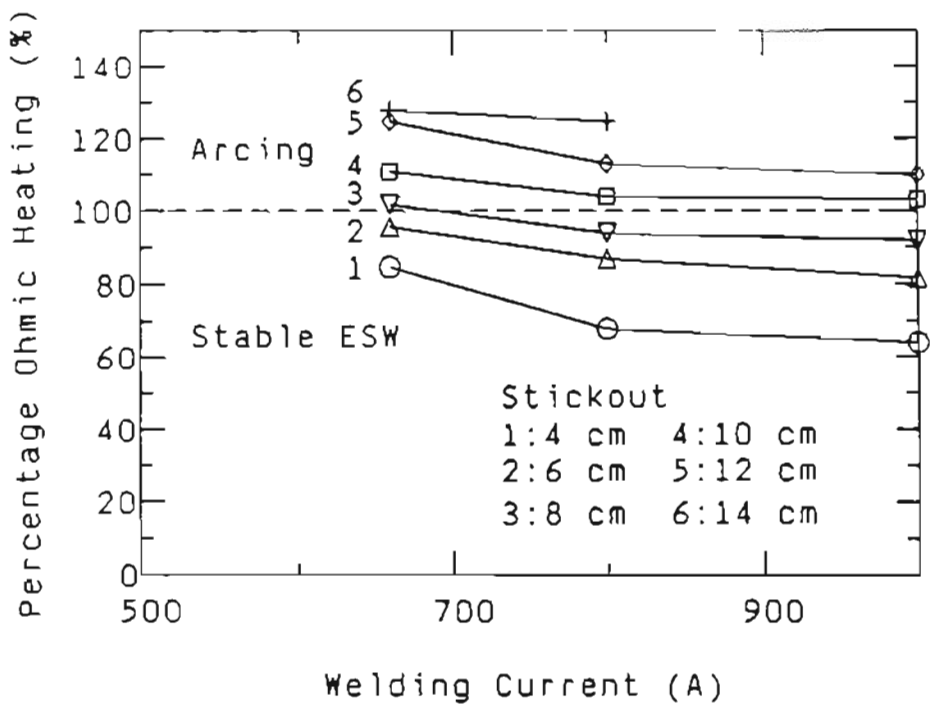

(B)

Figure 60. Ohmic heating effect on arcing instability in non-consumable guide ESW process using data shown in Figure 59 : (A) steel and (B) titanium alloy.

VI. DISCUSSION

A. ESW Process Optimization

1. Working Range for ESW

In the ESW process, the working range concept shown in Figure 4 reported by Frost et al.[35] was simplified and shown in Figure 61(A). Boundary A represents a lower voltage limit for minimum base metal dilution. Boundary B is the higher current (associated with electrode feed rate) limit, beyond this limit short circuiting occurs. The higher voltage limit (Boundary C) is proportional to the resistivity of the flux as discussed in Chapter V. Arcing occurs on the top surface of the slag pool when the voltage exceeds this limit. Boundary D is the lower current (electrode feed rate) limit. When the current is set below the limit, arcing initiate on top of the slag pool due to ohmic heating of the electrode.

Since boundary A is mainly dependent on the material properties as reported by Frost et al[35]., it does not change by simply adjusting the welding variables. Boundary B was replaced by the machine limiting current value because at the higher welding current levels caused by the low resistivity slag, the machine limit was reached first before the short circuiting limit. In this study, only boundary C and D were targeted because the low resistivity CaF_2 flux and high resistivity wire electrode and guide plate used for ESW of titanium alloys had a great effect on boundary C and D.

For clarity, the working range for the consumable guide ESW of 50 mm (2") thick titanium (shown in Figure 16) was compared with the working range for ESW of steel reported by Venkataraman[16]. A substantial difference in the working range for titanium and steel was shown in Figure 61(B). The working range of welding parameters for the titanium was much smaller and shifted to a higher current and lower voltage area than the working range for ESW steel. This result was due to the combined effect of low resistivity CaF2 flux and high resistivity titanium electrode used for ESW titanium alloys. The low resistivity CaF_2 flux lowered the voltage limit (threshold for uncontrollable arcing) from 62 V (using Hobart 201 oxide-base flux) to 32 V as calculated in Chapter V. The high resistivity titanium electrode elevated the lower current limit from 500 A (for steel electrode) to 850 A due to the ohmic heating effect.

Figure 61(B) shows that the working range for ESW of titanium alloy using CaF_2 Flux is only one eighth that of the working range for ESW of steel using Hobart 201 (oxide-based) flux. Similarly, due to the lower working voltage, ESW of titanium alloys generates significantly lower heating power resulting in a lower base metal dilution value than ESW of steel (based on Equation 15).

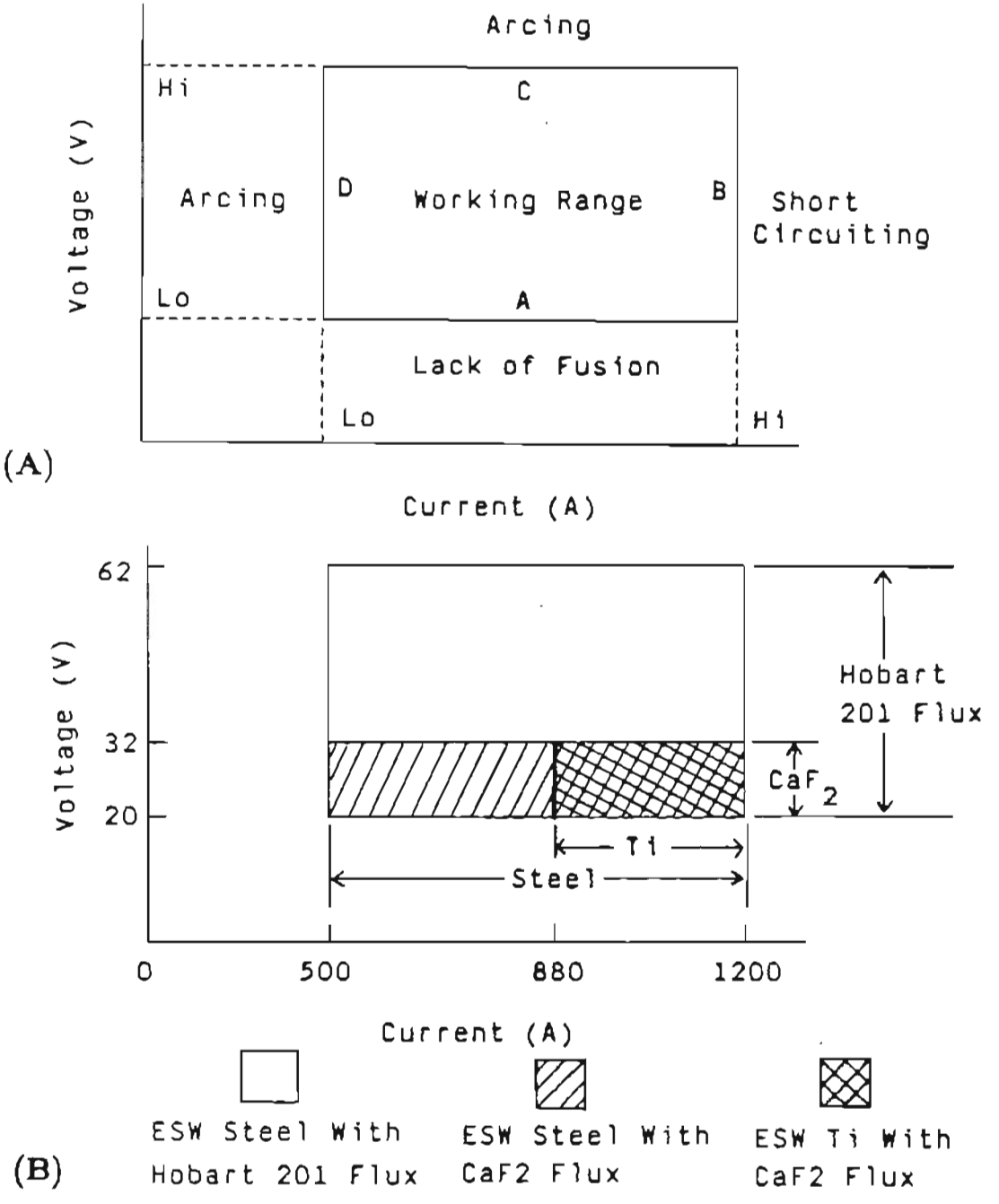

Figure 61. ESW working ranges for : (A) schematic drawing, and (B) comparison between consumable guide ESW of steel using Hobart 201 oxide-base flux and of titanium alloys using CaF_2 Flux.

2. Current and Electrode Melting Rate Correlation

The current and electrode melting rate correlation is shown in Equation 25. One of the requirements for a stable ESW process is that the electrode feed rate be approximately equal to electrode melting rate, so the process could maintain a steady state.

$$MR_e = a\,I + b\,I^2 + c \quad \ldots\ldots\ldots\ldots\ldots\ldots\ldots\ldots\ldots\ldots \quad (25)$$

MR_e: Electrode melting rate
aI: Heat conduction from the slag pool
bI^2: Ohmic heating of the electrode
c : Constant

In ESW of steel, several investigators[13,16,34] have reported a linear relationship between the electrode feed rate and welding current, but some other researchers[17,35,36] have reported a parabolic relation between the electrode feed rate and welding current. In this study, consumable guide ESW of titanium alloys resulted in a linear relation as shown in Figure 20. But in non-consumable guide ESW of steel, a parabolic relationship (Figure 33) was found. Figure 59(A) (taken from ASM Handbook[96]), clearly shows that a linear relationship exists between the electrode feed rate and welding current for consumable guide ESW of steel while a parabolic relationship is characteristic for the non-consumable guide ESW of steel.

The explanation for this difference lies in Equation 25. For the non-consumable guide ESW process, the ohmic heating term (I^2R) is sufficiently large such that the current and electrode feed rate develop a parabolic correlation. On the other hand, in the consumable

guide ESW process ohmic heating affected mainly the guide plate and not the electrode, so, the electrode was melted by the heat conducted from slag pool and the electrode melting rate was linearly proportional to the welding current as shown in Equation 25.

3. Heat Input and Its Effect on Base Metal Dilution during ESW

In consumable guide ESW, welding current and electrode feed rate have the linear relationship: $MR_o = aI$. Substituting this into Equation 13 yielded:

$$H_{input} = V_w / C \quad \ldots\ldots\ldots\ldots\ldots\ldots\ldots\ldots\ldots\ldots\ldots\ldots \quad (27)$$

The heat input is proportional to welding voltage only. Figure 17 clearly shows that the percentage base metal dilution (direct proportional to heat input) increases with increasing voltage, but independent of current.

In non-consumable guide ESW, the welding current and electrode feed rate have a parabolic relationship. Substituting this relation into Equation 13 yielded:

$$H_{input} = (V_w v_e^{1/2})/C v_e \quad \ldots\ldots\ldots\ldots\ldots\ldots\ldots\ldots\ldots\ldots \quad (28)$$
$$= V_w / C v_e^{1/2}$$

This equation shows that the heat input or base metal dilution value increases when voltage increases, also, when electrode feed rate decreases. This result was shown in Figure 34 for non-consumable guide ESW of steel. The base metal dilution value increased when the

electrode feed rate decreased except when arcing occurred on the top surface of slag pool. If arcing occurred, no base metal dilution resulted.

Equation 25 also shows that the electrode melting rate is independent of welding voltage. Therefore, in consumable guide ESW process, welding voltage and current played their roles independently. Welding current governed the electrode melting rate and also the welding speed. But, welding voltage was responsible for the heat input and base metal dilution level. Since consumable guide ESW of titanium alloy had a lower working voltage than did ESW of steel, it had a low heat input and low base metal dilution problem. Figure 17 shows that the maximum base metal dilution obtained for consumable guide ESW of titanium alloys is 38% compared to the 40% to 60% base metal dilution in standard consumable guide ESW of steel.[16,17]

4. Wire Diameter and Plate Thickness Effect

In the consumable guide ESW of titanium, melting rate was insensitive to the filler wire diameter due to the presence of the 12 mm (1/2") thick plate guide. Generally, a large diameter filler wire was thought to be less susceptible to ohmic heating and could be used to widen the operational window by reducing the lower current limit. But, since the ohmic heating effect was predominantly controlled by the guide plate, increasing diameter of the electrode did not lower the lower current limit.

Plate thickness usually only had an indirect effect on the ESW

process. The required welding current for good weld was directly proportional to the plate thickness. The maximum plate thickness was bound simply by the maximum current output of the power supply. Theoretically, any thickness of plate can be welded by ESW. The lower limit of the plate thickness (20 mm) was however limited by the physical dimensions of the welding head used with in ESW process. In this study, 25 mm (1") thick Ti-6Al-4V plate was successfully welded by the consumable guide ESW process.

5. Flux Alloying Addition Effect

The flux resistivity effects on the ESW process have been discussed in Chapter V. The main conclusion is that ESW of titanium using a low resistivity CaF_2 flux has a lower heat input than ESW using a high resistivity flux primarily because of the voltage limitation (30 V) required to prevent arcing. In order to increase the resistivity of flux for ESW, CaF_2 flux was alloyed with LaF_3 or YF_3 and AlF_3 fluxes additions. Bacon et al.[97] has reported the beneficial increases in resistivity of $CaF_2$2 with increasing amounts of LaF_3 or YF_3 and AlF_3 fluxes addition as shown in Figure 62. Among them, the AlF_3 flux was discarded due to its high volatility above 1200 °C.

The addition of LaF_3 and YF_3 fluxes was maintained below 25% because the density values of the LaF_3 (4.4 g/cm^3 at 1675 °C) and YF_3 fluxes were higher than the density value of molten titanium (4.1 g/cm^3-).[30] When LaF_3 or YF_3 flux additions exceeded 25%, the denser flux tended to segregate from the slag pool into the weld metal.

Although the additions of 20% to 25% LaF_3 or YF_3 fluxes increased the resistivity of CaF_2 flux by approximately 50% (Figure 62), the increased resistivity slag only slightly increased welding performance as shown in Figure 22. The working range of welding parameters shown in Figure 23 remained essentially identical to that shown in Figure 16 for pure CaF_2 flux. One possibility is that the resistivity values of the alloyed flux are not high enough, because their values are still only half that of the Hobart 201 oxide-based flux. Another possibility is that the increase in the upper voltage limit is too small and is overshadowed by the scatter of the voltage output.

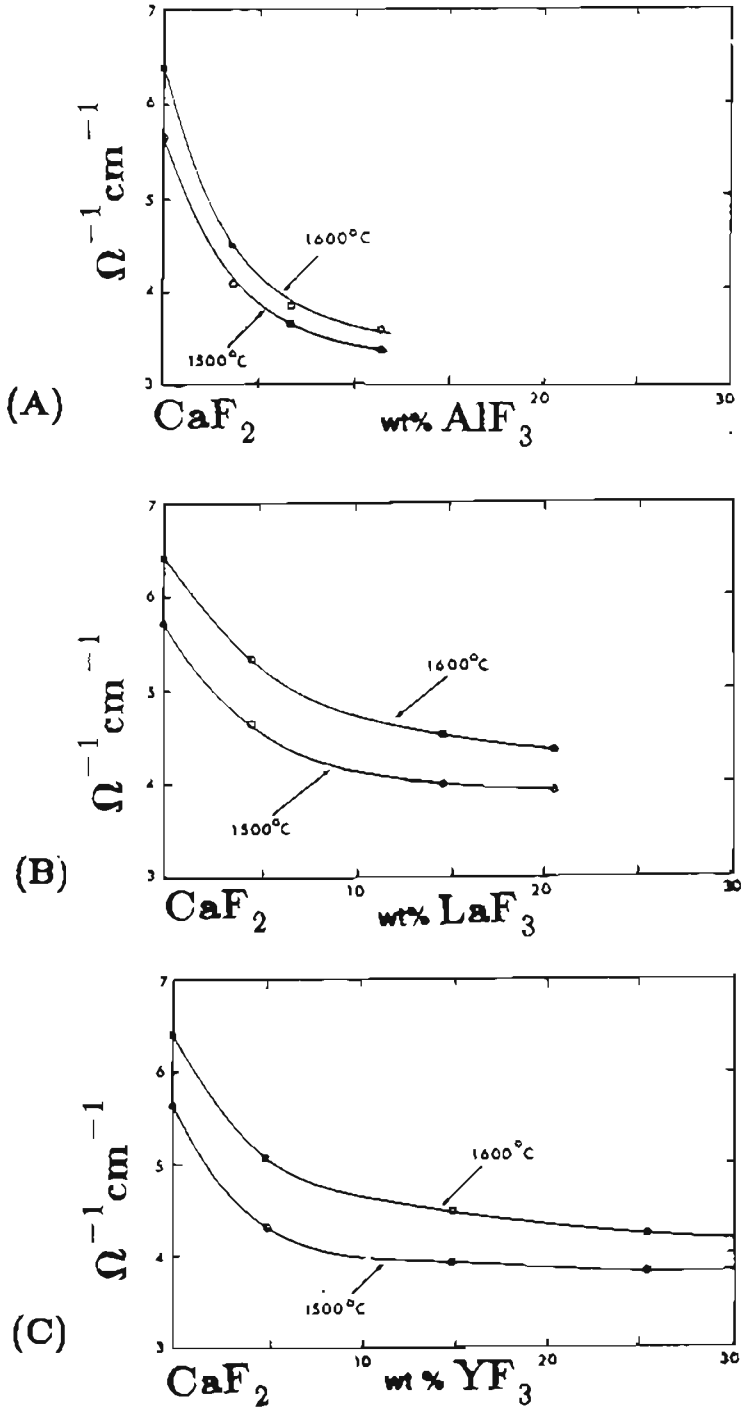

Figure 62. Electrical conductivity (reciprocal of resistivity) of CaF_2 flux with addition of : (A) AlF_3 flux, (B) LaF_3 flux and (C) YF3.(after Bacon et al.[97])

6. Non-Consumable Guide ESW of Titanium Alloy

Although consumable guide ESW worked well with a single 3.2 mm filler wire, similar ESW with the non-consumable guide proved unsuccessful. The main reason for the unsuccessful non-consumable guide ESW of Ti-6Al-4V alloys was uncontrollable arcing on top of the slag pool caused by using an inadequate diameter electrode (3.2 mm) and not using any slag pool level control system to maintain a short dry stickout distance of only a few mm's. For comparison, researchers at Paton Institute[20] successfully welded titanium because they used a very large diameter electrode (5 mm) and a special technique for slag pool level control to reduce the arcing instability caused by electrode ohmic heating. Equation 24 shows that the ohmic heating contribution to the total electrode melting rate is proportional to the square of the current density. The advantage of using a larger diameter electrode (5 mm) is that the ohmic heating for a 5 mm electrode is six times lower than that for a 3.2 mm (1/8") electrode. Therefore by using a larger diameter electrode, the chance of arcing on top of slag pool was greatly reduced.

In non-consumable guide ESW Ti-6Al-4V alloy, the other important variable affecting the ohmic heating of the electrode was the dry stickout distance. As shown in Figure 60 when the dry stickout distance increases, the percentage of the ohmic heating contribution to electrode melting rate increases, even over 100%. Therefore, without a slag pool level control system, the dry stickout distance will vary greatly and the ESW process will lose its stability.

D. Weld Evaluation

1. Metallography

The large prior beta grain size of the as-deposited weld macrostructure shown in Figure 36 is due to the very high heat input (75 kJ/mm for 50 mm thick plate, Table 7) used to make these welds. The symmetry in macrostructure (about the weld center) occurs because of the symmetric placement of the base plates and cooling shoes which were the major heat sinks in the ESW process. The HAZ of titanium electroslag welds is relatively large as compared to steel electroslag welds, because the thermal diffusivity values for Ti alloys are lower than the values for steel.

Unlike weld metal deposited by the GTAW process where martensite was commonly observed in the microstructure of Ti-6Al-4V and Ti-6211 alloys as shown in Figure 63, no martensite was observed in the electroslag welds of either alloy. This was due to the substantially slower cooling rate resulting from the high heat input used for the ESW process.

The beta-to-alpha transformation in Ti-6Al-4V alloys is well documented.[98-101] In the weld metal, the weld zones had coarse microstructure similar to that of a small casting except that the prior beta grains emanating from the HAZ continued to grow into the weld zone by epitaxial growth. The three-fold increase in grain width in the weld (compared to the coarse grained HAZ) was a result of competitive grain growth. Upon cooling during ESW, the substructure within the large beta

grains had been shown to develop in three distinct steps:

(1) the alpha phase first grew heterogeneously from the prior beta grain boundary and advanced by a planar interface,

(2) the lamella alpha + beta phases grew from the grain boundary into the grain because the undercooling broke down the planar interface and

(3) at the grain center, some new nuclei formed due to further undercooling and subsequently grew and interlocked with each other to form the Widmanstatten alpha + beta colony structure.

In the HAZ, the first two steps were similar; only the microconstituents were finer than those in the weld regions. During the last step in the HAZ, the basket weave Widmanstatten structure developed because many new nuclei formed and grew due to the higher undercooling produced by the fast cooling rate in the HAZ.

(A) 25 μm

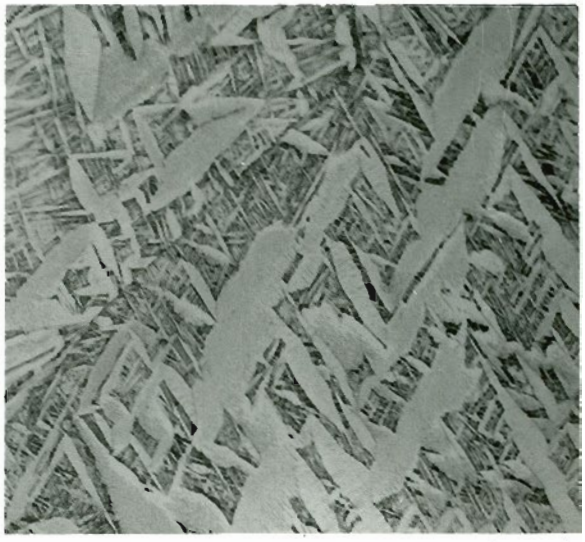

(B) 25 μm

Figure 63. Martensitic microstructure of weld metal made by GTAW in (A) Ti-6Al-4V and (B) Ti-6211.

2. Interstitial Element Contamination

The Ti-6Al-4V weld deposited with the reagent grade CaF2 flux contained 100% more oxygen and 200% more nitrogen than did the base metal as shown in Figure 45. This shows that the use of reagent grade CaF2 flux was inadequate to protect the molten metal from interstitial element contamination. In the Ti-6Al-4V and Ti-6211 welds deposited with high purity CaF2 flux, the weld metal contained the same interstitial element content as did the base metal as shown in Figure 45. This indicated that the ESW process was not a source of contamination if a good level of workmanship was maintained.

The weld metal tensile ductility and CVN impact toughness of the Ti-6Al-4V and Ti-6211 welds using high purity CaF_2 flux were lower than their respective base metal values (Figures 46 and 48), in spite of the fact that they had the same levels of interstitial content as their respective base metals (Figure 45). This shows that the interstitial element content of the weld is not the main controller of the weld metal tensile ductility and CVN impact toughness losses.

But, the weld metal of the Ti-6Al-4V welds using reagent grade CaF_2 flux has the lowest tensile ductility and CVN impact toughness values among these three welds (Figures 46 and 48), while having the highest interstitial element content among them (Figure 45). Therefore, the interstitial content of the weld metal still playes a secondary role in explaining the losses in weld metal tensile ductility and CVN impact toughness.

3. Tensile Properties

Terlinde et al.[102] have reported that increasing prior beta grain size decreased both tensile strength and ductility. Raising the interstitial content, particularly oxygen, increased the tensile strength while decreasing tensile ductility.[73,74] Also, reducing the alpha plate thickness was reported to increase both tensile strength and ductility.[90,103-104] The tensile strength values of all weld metal of Ti-6Al-4V and Ti-6211 electroslag welds were only slightly higher than their respective base metal values as shown in Figure 7. This was a combined result of the larger prior beta grain size, higher interstitial content and finer alpha plate thickness in the weld metal as compared to that of the respective base metal.

In weld metal tensile specimens, the cracks followed the alpha phase film along the prior beta grain boundary through almost the entire diameter of the specimen as shown in Figures 53(B) and 54(B). In the base metal tensile specimens, the cracks only followed the alpha phase along the prior beta grain boundary occasionally. This shows that the large prior beta grain width (3-5 mm) in the weld metal produced by the ESW process (compared to the smaller prior beta grain size of 0.5 mm in the base metal) is responsible for the sharply lower tensile ductility.

4. Microhardness

It is well established that the microhardness values of titanium alloys increase with increasing interstitial content and decreasing alpha plate thickness.[73] Although the alpha plate thickness was finest

in the HAZ, medium in the weld, and thickest in the BM in all three welds (Figures 37, 38, and 39), the microhardness values were hardly affected. Also, the interstitial contents were uniform across the Ti-6Al-4V and Ti-6211 welds deposited with high purity CaF2 flux as shown in Figure 45. These are the reasons why the microhardness profiles across the Ti-6Al-4V and Ti-6211 welds (using high purity CaF2 flux) are uniform (Figures 47(B), and 47(C)). But, the Ti-6Al-4V weld metal deposited with reagent grade CaF2 flux had higher microhardness values than did either the HAZ or BM (Fig. 8a), due to its higher interstitial content as shown in Figure 6.

5. CVN Toughness

The 0°C (32°F) CVN toughness profiles are shown in Figure 64. All weld metal specimens had a lower CVN impact toughness than their respective base metal and HAZ values. The low CVN impact toughness in the weld metal specimens of all three welds was due to the macroscopically transgranular fracture with little crack branching as shown in Figure 49. In the base metal and HAZ specimens, the crack front branched along the prior beta grain boundaries and the inter-Widmanstatten colony boundaries (Figures 49 and 50). When branching occurred, the crack required more energy to propagate so the CVN toughness value increased as compared to the one fracturing with little or no branching. In the weld metal specimens, it was not the grain boundary alpha film (along the coarse prior beta grain boundary) causing the loss of CVN toughness because, if it were, the weld would have fracture

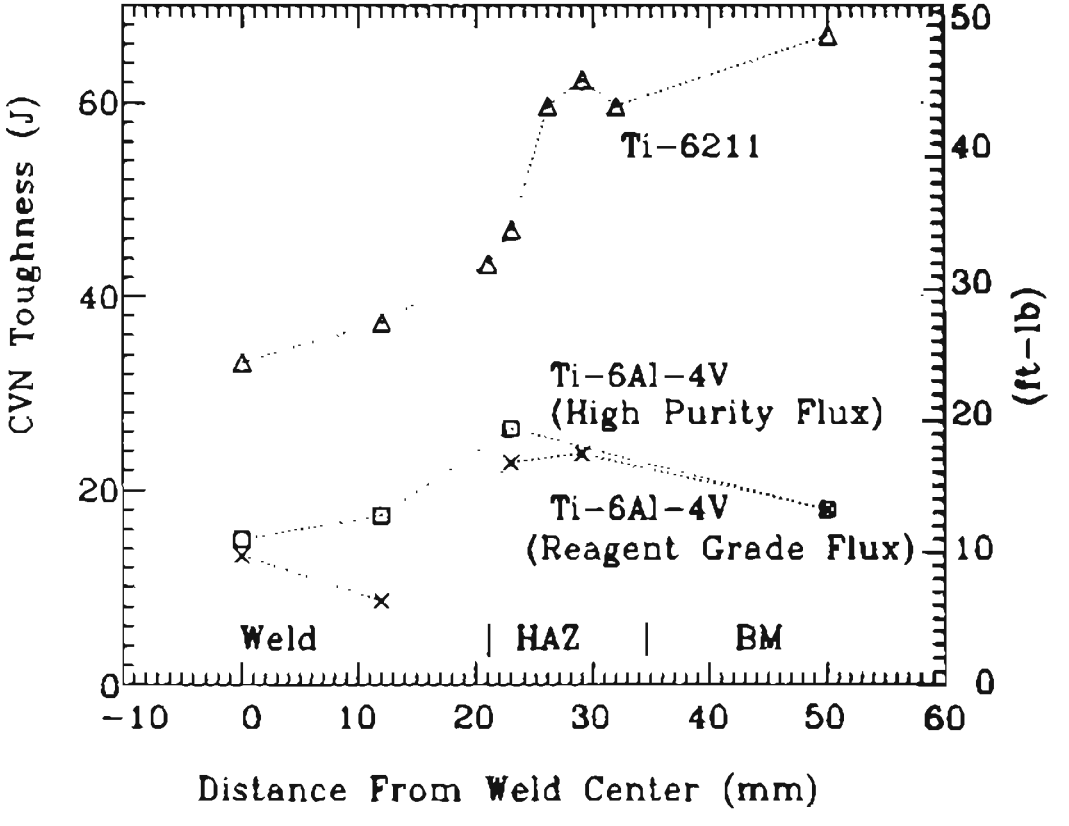

Figure 64. CVN impact toughness profiles at 0°C across three electroslag welds.

intergranularly, rather than transgranularly as shown in Figure 49. It is proposed that the coarse prior beta grain size and the large area of lamella alpha + beta microstructure (Figures 37-39) provided the path for crack to propagate long distances without branching. This was the reason why the welds fractured transgranularly and had lower CVN toughness values than did the HAZ and BM.

The CVN toughness values for the HAZ of Ti-6Al-4V welds deposited with both high purity and reagent grade flux were slightly higher than their corresponding BM values. But this was not true for the Ti-6211 weld. This might be explained by the finer alpha + beta microstructure in the HAZ than BM (Figures 37 and 38), because the finer microstructure produced a greater alpha/beta interphase area to absorb more energy when a crack propagates through them. In the near-alpha Ti-6211 alloy, the amount of beta was less than that observed in the Ti-6Al-4V alloy so the effect of the alpha/beta interface might be minor compared with the effect of grain size on the CVN toughness values.

In summary, the mechanical properties of the weld and HAZ were directly related to interstitial content, prior beta grain size, and microstructure. The large prior beta grain size and the lamellar alpha + beta structure associated with it had the most detrimental effect on the toughness of the Ti-6Al-4V and Ti-6211 electroslag welds.

C. Cost-Effectiveness of ESW Ti Alloys

In determining the economy of ESW of titanium, a simple comparison can be drawn between consumable-guide ESW and the only other practical welding process: gas-tungsten arc welding (GTAW). Consider, for example, a butt joint weld on 50-mm-thick Ti-6Al-4V plates. The total length of weld is 1 m long. Both processes use run-off tabs.

The factors in any cost comparison of welding processes include: joint preparation, shielding gas, deposition rate, total welding time, labor and flux consumption. Joint preparation for the ESW process is simply a square-groove butt joint with a root opening of 32 mm and guide plate preparation. The GTAW process requires machining a double-u groove or double-V groove with a minimum 45-deg inclined angle and adequate root opening. The entire GTAW system, including plates to be welded, spools of filler metal, etc., must be mounted in a chamber filled with argon to prevent atmospheric contamination of the weld pool on such a thick section.

To greatly simplify the cost comparison between ESW and GTAW, we can justifiably assume that the greatest costs by far are labor costs and production time. Although both processes would be used in a completely automatic mode, the operator of the GTAW system must perform a multiple pass operation. The GTAW operator must stop, manually reset and wait until the specified interpass temperature is attained before proceeding to the next pass. The number of passes by ESW is only one, regardless of the plate thickness, but the number of passes by GTAW

exceeds 160. For comparison, the deposition rate for ESW of 50 mm thick titanium in this study was approximately 11.1 Kg/h while that for GTAW is approximately 0.4 Kg/h.

The welding time for ESW a joint of 50-mm-thick Ti-6Al-4V plate that is 1 m long would be approximately 39 min, while GTAW would require at least 20 h. Even though the cost of labor for GTAW will be greater than ten times that for ESW, the more important aspect of production time must be considered. ESW process requires less than 1/30 of the welding time required by GTAW process.

Regarding interstitial contamination and defects in welding, both ESW and hot-wire GTAW are high-quality processes. However, it is statistically more significant that both interstitial contamination and weld defects will more likely occur in the deposits by GTAW than ESW. This is because (1) argon cover can be lost when a slight breeze is encountered (unless the entire plate is placed in a chamber flooded with argon) and (2) each of the 160 passes by GTAW is susceptible to under-cutting and lack of fusion type defects. The nature of ESW of titanium alloys is such that the only possible defects are lack-of-fusion types which are always visible at the surface. That is, if the surface of the electroslag weld is sound, the probably that the interior is also sound is nearly 100%. Thus, ESW is a very good alternative to GTAW for thick plate welding operations, and ESW becomes more cost-effective as the plate thickness increases.

VII. CONCLUSIONS

From the investigation of ESW of Ti-6Al-4V and Ti-6211 alloys, the following are concluded:

1. Titanium alloy plate, 25 mm (1") and 50 mm (2") thick, can be successfully welded by the consumable guide ESW process.

2. The ESW process is a contamination-free method for welding titanium alloys provided good workmanship standards (cleanliness of consumables and plate) are met. Weld metals free from interstitial element contamination were obtained by consumable guide ESW using; AC-CV power source, high purity CaF_2 flux, argon protection over the slag pool, and good welding practice.

3. The welding current and electrode melting rate are related linearly for the consumable guide ESW process and parabolically for non-consumable guide ESW of titanium alloys.

4. In consumable guide ESW, the base metal dilution increases with increasing welding voltage, but remains unchanged with increasing or decreasing welding current.

5. The electric path model clearly shows that 24% of the heat is concentrated on the electrode and guide plate in consumable guide ESW of titanium alloy, compared to only 3% for similar welding of steel. This high percentage of heat causes the titanium electrode and guide plate to overheat and to possibly generate arcing on the

slag pool surface.

6. Predictive equations describing the mechanism of ESW with low resistivity CaF_2 flux reveals that the maximum welding voltage above which unstable arcing occurs is limited to 32 V (as compared to 62 V for ESW steel using an oxide-base flux).

7. The model also predicts that ESW titanium operates at a lower maximum available heat input than does similar welding on steel. As the slag resistivity decreases, the maximum available heat input (using high purity CaF_2 flux) can only be maintained by reducing the voltage and raising the current levels.

8. Despite the lower heating power generated by ESW with pure CaF_2, excellent weld quality and soundness was obtained.

9. The ohmic heating model for the consumable guide ESW process shows that the arcing susceptible of a high resistivity titanium electrode is much greater than that for a low resistivity steel electrode. With a larger diameter electrode, shorter dry stickout distance and higher resistivity flux, the ohmic overheating of the electrode can be greatly reduced and stable welding conditions can be achieved for non-consumable ESW titanium alloys.

10. The percentage of the ohmic heating that contributes to the electrode melting rate increases with increasing current density, electrode resistivity and dry stickout distance, but decreases

with increasing electrode feed rate and heat content of the electrode. Arcing occurs on top of the slag pool when the percentage ohmic heating contribution of electrode melting rate exceeds 100%.

11. An AC power supply is mandatary for ESW of titanium alloys, because AC power reduces the electrode polarization. Conversely, DC power can not be used because the highly polarized slag generates uncontrollable arcing and electrode burn-back.

12. Due to the high heat input of the ESW process, the weld and HAZ were characterized by large prior beta grain sizes, and weld metal and HAZ microstructures consisting of grain boundary alpha, lamellar alpha + beta, and widmanstätten alpha + beta as compared to grain boundary alpha and widmanstätten alpha + beta in the base metal.

13. Yield and tensile strength levels of the weld metal are similar to those of the base material.

14. Tensile ductility values for the weld metal of both Ti- 6Al-4V and Ti-6211 alloys are typically less than those of the base plate due primarily to the coarse prior beta grains size and secondarily to the interstitial content. The fracture path in the weld metal follows the alpha phase film along the prior beta grain boundaries.

15. CVN impact toughness values in the weld metal of both Ti- 6Al-4V

and Ti-6211 alloys are less than those of the plate due to the coarse prior beta grain size and lamellar alpha + beta structure, which cause the crack to propagate transgranularly with less branching.

RECOMMENDATIONS FOR FUTURE WORK

1. Results from this study clearly show that lower tensile ductility and CVN impact toughness in the titanium weld metal is a result of a large prior beta grain produced by very high heat input of the ESW process. Grain refinement techniques such as magnetic stirring, ultrasonic stirring, mechanical vibration, metal power addition could be adopted to improve both tensile ductility and CVN impact toughness of the titanium weld metal.

2. Based on the arcing instability model proposed in this study, non-consumable guide electroslag welds of titanium alloys can be successfully made by using a combination of a large diameter electrode and a short dry stickout with a thermally insulated and water cooled copper guide tube.

3. To widen the working range (V = 25-30, I = 850-1200) in consumable guide ESW of titanium alloys, a higher (electric) resistivity flux is necessary in order to raise the maximum allowable voltage and reduce the minimum current level without the arcing problem. Also, by using an AC constant voltage power supply capable of delivering high current at lower voltage (such as I = 300-2000 at V=15), the working range could be increased by widening the current range at lower voltage levels.

REFERENCES

1. M.J. Donachie, Jr. "Introduction to Titanium and Titanium Alloys", Titanium and Titanium alloys, ed. by M.J.Donachie, Jr. ASM, 1982, p3-9.

2. W. Abbott, "Hints for Welding titanium", Titanium and Titanium Alloys, ed. by M.J.Donachie, Jr., ASM, 1982, p315-317.

3. "Electroslag Welding", ed. by B.E. Paton, Mir Publisher, 1980. p11-18.

4. W.P. Benter, Jr., and C.G. Schilling, "Acceptance Criteria for Electroslag Weldments in Bridges", NCHRP Report 201, May, 1979, p3-4.

5. Hobart Brothers Co., "Technical Guide for Electroslag Welding", 1980, p1-4.

6. S.M. Gurevich, Ya.Yu. Kompman, and Yu.K. Novikov, " Technological Possibilities of Electroslag Welding of Titanium Alloys", Titanium and Titanium Alloys II, ed. by J.C. Williams, and A.F. Belov, 1976, p12259-1267.

7. R.P. De Vries, and R.W. Hornbaker, " Consumable Electroflux Melting - the Hopkins Process: Part 1", Ind. Heating, v. 33, No. 9, Sep., 1966, p 1685-1969.

8. K.E. Dorschu, et al., "Unusual Electroslag Welding Applications", Welding Journal, Vol.52, No.11, 1973, p710.

9. E.R. Bangs : "A Comparative Literature Survey of the Technology in Welding Thick-Sectioned Titanium Alloys in the USA and Foreign Countries Phase III" Report IITRI-J06536, IIT Research Institute, Feb., 1982, p48-64.

10. T.W. Eagar, et al. "Heat Source - Materials Interations During Fusion Welding", Annual Technical Report AD-A118776, Apr., 1982.

11. Shou-Kong, Fan : "Electroslag Welding of Titanium" M.S. Thesis, Massachusetts Institute of Technology, Dec., 1982.

12. P.J. Konkol, "Effect of Process Parameters on Thermal Distribution During Electroslag Welding" Welding Journal, Dec., 1977, p371s-379s.

13. M.Solari, and H. Biloni, "The Effect of Wire Feed Speed on the Structure in Electroslag Welding of Low Carbon Steel", Welding Journal, Sep., 1977, p274s-280s.

14. A.L. Liby, and D.L. Olson, "Metallurgical Aspects of Electroslag Welding : A Review", Quarterly of the Colorado School of Mine, vol.69, No.1, 1974, p41-69.

15. A.I. Pugin and G.A. Pertsovskii, "Calculation of the Thermal Cycle in the HAZ When Welding Very Thick Steel by Electroslag Process", Automatic Weelding, No.6, 1963, p12-21.

16. S. Venkataraman, "Effect of Process Variables and Microstructures on Properties of Electroslag Weldments", Ph.D thesis, Oregon Graduate Center, 1981.

17. H.S. Ann, "Solidification Study and Improved Structural Integrity of Electroslag welds" Ph.D thesis, Oregon Graduate Center, 1987.

18. D.W. Yu, "Welding Metallurgy and Toughness Improvement for Mild and Low-Alloyed Steel Electroslag Weldments", Ph.D thesis, Oregon Graduate Center, 1988.

19. E.G. Thompson, "Welding of Reactive and Refractory Metals", WRC Bulletin, No.85, 1963.

20. "Metallurgy and Technology of Welding Titanium and its Alloys", ed. by S.M. Gurevich, Naukova Dumkka, Kiev, 1979, p96-148

21. J.H. Devletian, and S.J. Chen, "Joining of Thick-section Titanium Alloys by Electroslag Welding", Welding Journal, Vol.68, Sep., 1989, p37-42.

22. Y.Y. Kompan, S.M. Gurevich, and Y.K. Novikov, "Bubbling Argon Through the Molten Pool During the Electroslag Welding of Titanium Alloys", Avt. Svarka., No.10, 1972, p15-16.

23. K. Yonesawa, "Welding of titanium and titanium alloys", Welding International, No.12, 1987, p20-31.

24. K.C. Mill, and B.J. Keene, "Physicochemical Properties of Molten CaF_2 - Based Slag", International Metal Reviews, No.1, 1981, p21-69.

25. S. Hara, H. Hashimoto, and K. Ogino, "Electical conductivity of Molten Slags for Electro-slag remelting", Transactions ISIJ, Vol. 23, 1983, p1053-1058.

26. V.P. Didkovskii, and S.M. Gurevich, "The Electroslag Welding of Titanium Using Electrode Wires", Avtom. Svarka, No.1, 1961, p48-51.

14. A.L. Liby, and D.L. Olson, "Metallurgical Aspects of Electroslag Welding : A Review", Quarterly of the Colorado School of Mine, vol.69, No.1, 1974, p41-69.

15. A.I. Pugin and G.A. Pertsovskii, "Calculation of the Thermal Cycle in the HAZ When Welding Very Thick Steel by Electroslag Process", Automatic Weelding, No.6, 1963, p12-21.

16. S. Venkataraman, "Effect of Process Variables and Microstructures on Properties of Electroslag Weldments", Ph.D thesis, Oregon Graduate Center, 1981.

17. H.S. Ann, "Solidification Study and Improved Structural Integrity of Electroslag welds" Ph.D thesis, Oregon Graduate Center, 1987.

18. D.W. Yu, "Welding Metallurgy and Toughness Improvement for Mild and Low-Alloyed Steel Electroslag Weldments", Ph.D thesis, Oregon Graduate Center, 1988.

19. E.G. Thompson, "Welding of Reactive and Refractory Metals", WRC Bulletin, No.85, 1963.

20. "Metallurgy and Technology of Welding Titanium and its Alloys", ed. by S.M. Gurevich, Naukova Dumkka, Kiev, 1979, p96-148

21. J.H. Devletian, and S.J. Chen, "Joining of Thick-section Titanium Alloys by Electroslag Welding", Welding Journal, Vol.68, Sep., 1989, p37-42.

22. Y.Y. Kompan, S.M. Gurevich, and Y.K. Novikov, "Bubbling Argon Through the Molten Pool During the Electroslag Welding of Titanium Alloys", Avt. Svarka., No.10, 1972, p15-16.

23. K. Yonesawa, "Welding of titanium and titanium alloys", Welding International, No.12, 1987, p20-31.

24. K.C. Mill, and B.J. Keene, "Physicochemical Properties of Molten CaF_2 - Based Slag", International Metal Reviews, No.1, 1981, p21-69.

25. S. Hara, H. Hashimoto, and K. Ogino, "Electical conductivity of Molten Slags for Electro-slag remelting", Transactions ISIJ, Vol. 23, 1983, p1053-1058.

26. V.P. Didkovskii, and S.M. Gurevich, "The Electroslag Welding of Titanium Using Electrode Wires", Avtom. Svarka, No.1, 1961, p48-51.

40. H.S. Gurev., et al., "Solidification in Gas Metal-Arc Welds", Welding Journal, Vol.39, No.7, 1963, p298s.

41. A. Mitchell, and J. Cameron, "The Electrical Conductivity of Some Liquids in the System CaF_2-CaO-Al_2O3_n, Met. Trans., Vol.2, 1971, p3361-3366.

42. A. Mitchell, and S. Joshi, "The Thermal characteristics of the Electroslag Process", Met. Trans., Vol.4, Mar., 1973, p631-642.

43. B.E. Paton, "Electrosalg Welding of Very Thick Material", Welding Journal, No.12, 1962, p1115-1123.

44. A.H. Dilawari, T.W. Eagar, and J. Szekely, "An Analysis of Heat and Fluid Flow Phenomena in Electroslag Welding", Welding Journal, Vol.57, No.1, 1978, p24s-29s.

45. T. Deb Roy, J. Szekely, and T.W. Eagar, " Heat Generation Patterns and Temperature Profiles in Electroslag Welding", Met. Trans. Vol.11B, No.4, 1973, p593.

46. H.C. Campbell, "Electroslag, Electrogas, and Related Welding Processes", WRC Bulletin, No.154, Sep., 1970.

47. C.E. Jackson, "Fluxes and Slags in Welding" WRC Bulletin, No.190, Dec., 1973.

48. C.L. Chai, J.J. Gullotti, and T.W. Eagar, "Submerged-Arc Welding of Titanium", Technical Report No.2, M.I.T., Massachusetts, Contract No. N00014-77-C-0569, Sep., 1978, p30-38.

49. H.E. Pattee, and H.W. Mishler, "Soviet Development and Use of Fluxes for Welding Titanium and Its Alloys", Report, Battelle, Ohio, Apr., 1982, p1-27.

50. S.M. Gurevich, and L.K. Bosak, " The Effects of Calcium Fluoride in Type AN-T Fluxes on Their Technical Properties", Avt. Svarka., No.11, 1964, p47-50.

51. S.M. Gurevich, V.N. Zamkov, S.D. Zagrebenyuk, and N.A. Kushnirenko, "The Effect of Fluxes Containing Rare Earth Elements on the Structure and Properties of Welds in VT15 Alloy", Avt. Svarka., No.4, 1964, p93-94.

52. "Molten Salt Chemistry", ed. by M. Blander, Interscience, 1964.

53. "Fluoride — Handbooks, Manuals, Etc.", ed. by Paul Hagenmuller, Academic Press, 1985.

54. "Electrosalg Processes Principles and Practice", by G. Hoyle, Applied Science Publisher, 1983, p8-26.

55. "Welding Power Handbook", by A.F. Manz, AWS, 1973, p29-46.

56. "Welding Processes and Power Sources", by E.R. Pierre, 2nd edition, 1974, p160-178.

57. M.R. Scholl, "Alloy Design for Electroslag Welded railroad Rail", M.S. Thesis, Oregon Graduate Center, 1983.

58. Y.Y. Kompan, and N.S. Perepechko, "Regulating the Electrical Parameters of Welding Conditions for Welding Titanium and Its Alloys", Avt. Svarka., No.10, 1978, p46-47, and p52.

59. A.H. Dilawari and J. Szekely, " A Mathematical Model of Slag and Metal Flow in the ESR Process", Met. Trans., Vol.8B, June, 1977, p227.

60. A. Mitchell, "Chapter 2. Electrochemical Reactions in the Electroslag Process", The Electroslag Melting Process, Bulletin 669, U.S. Department of Interior, Bureau of Mines, 1976.

61. A. Mitchell, and G. Beynon, "Electrode Polarization in the DC Electroslag Melting of Pure Iron", Met. Trans., Vol.2, Dec., 1971, p3333-3345.

62. V.F. Grabin, et. al., "Structure and Properties of the Heat Affected Zone in the Electroslag Welding of a High Strength Titanium Alloy" Avt. Svarka., No.9, 1973, p20-23.

63. Y.Y. Kompan, "Electroslag welding the VT10 Titanium Alloy", Avt. Svarka., No.4, 1965, P50-52.

64. V. Y. Malin, "Electroslag Welding of Titanium and Its Alloys", Welding Journal, Vol.64, No.2, 1985, p42s-49s.

65. J.D. Culp, "Fracture Toughness and Fatigue Properties of Steel Plate Butt Joints Welded by Submerged Arc and Electroslag Welding Procedures" Research Report No.R-1011, Michigan Department of State Highways and Transportion, 1976.

66. J.D. Culp, "Electroslag Weldments: Performance and Needed Research", Welding Journal, Vol.58, No.7, 1979, p27-41.

67. G. Terlinde, and G. Luetjering, "Influence of Grain Size and Age Hardening on Dislocation Pile-Ups and Tensile Fracture for a Ti-Al Alloy", Met. Trans., Vol.13A, July, 1982, p1283-1292.

68. D.M. Bowden, and E.A. Starke, "The Effect of Microstructure and Deformation Behavior on the Hot Ductility of Ti-6Al-2Nb-1Ta-0.8 Mo", Met. Trans., Vol.15A, 1984, p1687-1698.

69. M.A. Greenfield, and H. Margolin, "The Mechanism of Void Formation, Void Growth, and Tensile Fracture in an Alloy Consisting of Two Ductile Phases", Met. Trans., Vol.3A, 1972, p2649-2659.

70. H. Margolin, and Y. Mahajan, "Void Formation and Void Growth, and Tensile Fracture in Ti-6Al-4V", Met. Trans., Vol.9A, 1978, p781-791.

71. B.K. Damkroger, G.R. Edwards, and B.B. Rath, "Investigation of Subsolidus Weld Cracking in Alpha-Beta Titanium Alloys", Welding Journal, Vol.68, No.7, 1989, p290s-302s.

72. Y. Mahajan, and W.A. Baeslack III, "Transgranular Fracture of Heat-Treated Weldments in a High-Strength Alpha-Beta Titanium Alloy", Scripta Metallurgica, Vol.13, 1979, p1125-1129.

73. C. R., Brooks, Heat Treatment, Structure and Properties of Nonferrous Alloys. Published by ASM, 1982, Metals Park, Ohio, p331-339.

74. G. Welsch, and W. Bunk, "Deformation Modes of the Alpha Phase of Ti-6Al-4V as a Function of Oxygen Concentration and Aging Temperature", Met. Trans., Vol.13A, 1982, p889-899.

75. M.J. Harrigan, M.P. Kaplan, and A.W. Sommer, " Effect of Chemistry and Heat Treatment on the Fracture Properties of Ti-6Al-4V Alloy", Titanium and Titanium alloys, ASM, 1982, p50-79.

76. E.W. Yim, and M. Feinleib, "Electrical Conductivity of Molten Fluorides", J. Electrochem. Soc., Vol.104, No.10, 1957, p622-630.

77. V.N. Kolisnyk, "Measurement of the Electrical Conductivity of Fluxes at Between 1300 and 2300 °C", Avt. Svarka., No.4, 1964, p10-14.

78. B.E. Lopaev, A.A. Plyshevskii, and V.V. Stepanov, " The Electrical Conductivity of Fused Fluxes Used for Electroslag Remelting and Electroslag Heating of Ingot Feeder Heads", Avt. Svarka., No.1, 1966, p27-29.

79. L.F. Grantham, E.B. Harrelson, P.H. Shaw, and C.M. Larsen, "Cell Assembly to Measure the Electrical Conductivity of Molten Salts to Their Critical temperatures", The Review of Scientific Instruments, Vol.39, No.5, 1968, p699-702.

80. G.D. Robbins, "Measurement of Electrical Conductivity in Molten Fluorides — A Survey", J. Electrochem. Soc., Vol.116, No.6, 1969, p813-817.

81. "Fused Salt Mixtures: Specific Conductivity Tables", by P.V. Clack, Sandia Laboratories, NTIS Report No. SC-R-69-1386, 1969.

82. P.P. Evseev, and A.F. Fillipov, Izv. VUZou. Cher. Met., No.3, 1965, p74.

83. G.I. Zhmoidin, and Izv. Akad. Nauk USSR. Metally., No.3, 1970, p71.

84. H. Winterhager, R. Kammel, and A. Gad, Forschungsberichte der Nordrheim-Westfalen. No.2, 1971, p115.

85. T. El Gammal and M. Hajduk, Arch. Eisenhuttenw., Vol.49, 1978, p235.

86. D. Banerjee, "Identification of the Interface Phase in Titanium Alloys", Met. Trans. Vol.13A, Apr., 1982, p681-684.

87. D. Banerjee, and J.C. Williams, "The Effect of Foil Preparation Technique on Interface Phase Formation in Ti Alloys", Scripta Met., Vol.17, No.9, 1983, p1125-1128.

88. D. Banerjee, C.G. Rhodes, and J.C. Williams, "On the Nature of Alpha/Beta Interfaces in Titanium Alloys", Proc. 5th Int. Conf. Ti Alloys, Munich, W. Germany, 1984, p1597-1604.

89. J.C. Chesnutt, C.G. Rhodes, and J.C. Williams, "Relationship Between Mechanical Properties, Microstructures, and Fracture Topography in alpha + beta Titanium Alloys", Fractography-Microscopic Cracking Processes, ASTM STP 600, 1976, p99-138.

90. F.S. Lin, E.A. Starke, Jr., S.B. Chakrabortty, and A. Gysler, "The Effect of Microstructure on the Deformation Modes and Mechanical Properties of Ti-6211: Par 1. Widmanstatten Structures", Met. Trans., Vol.15A, No.6, 1984, p1229-1246.

91. C.H. Liu, K.E. Johnson, and H.A. Laitinen, "Electroanalytical Chemistry of Molten Salts", Molten Salt Chemistry, ed. by M. Blander, Interscience, 1964, P681-733.

92. E.M. Leven, and McMurdie, Phase Diagrams for Ceramists, Am. Cer. Soc., Columbus, Ohio, 1975 Supplement.

93. P.S. Myers, O.A. Uyehara, and G.L. Borman, "Fundamentals of Heat Flow in Welding", WRC Bulletin, No.123, July, 1967, p24-25.

94. J.L. Wilson, G.E. Claussen and C.E. Jackson, "The Effect of I^2R Heating on Electrode Melting Rate", Welding Journal, Vol.35, No.1, 1956, P1s-8s.

95. R. S. Chandel. "Mathematical Modeling of Melting Rates for Submerged Arc Welding", Welding Journal, Vol.66, No.5, 1987, P135s-140s.

96. Metals Handbook 9th Edition, Vol.6, "Welding, Brazing, and Soldering" ASM, 1983, p231.

97. G. Bacon, A. Mitchell, and R.M. Nishizaki, "Electroslag Remelting with All-Fluoride Low Conductivity Slags", Met. Trans., Vol.3, Mar., 1972, p631-635.

98. M.K. Mcquillan, "Phase Transformations in Titanium and Its Alloys" Metallurgical Reviews, Vol.8 No.29, 1963, P41-104.

99. J.C. Williams, M.J. Blackburn, "A Comparison of Phase Transformations in Three Commercial Titanium Alloys", Trans. ASM, Vol.60, 1967, p373-384.

100. I. Weiss, F. H. Froes, D. Eylon, and G.E. Welsch, "Modification of Alpha Morphology in Ti-6Al-4V by Thermomechanical Processing", Met. Trans., Vol.17A, No.11, 1986, p1935-1947.

101. G. Sridhar, R. Gopalan, and D.S. Sarma, "A Microstructural Characterization of Solution-Treated Titanium Alloy Ti-6Al-4V", Metallography, Vol.20, 1987, p291-310.

102. M. A. Greenfield, C.M. Pierce, and J.A. Hall, "The Effect of Microstructure on the Control of MechanicalProperties in AlphaBeta Titanium Alloys", Titanium Science and Technology, Vol. 3, eds. R-.I. Jaffee, and H.M. Burte, 1972, p.1731-1743.

104. D. Banerjee, D. Mukherjee, R.L. Saha, and K. Bose, "Microstructure and Tensile Ductility in a Beta Heat Treated Titanium Alloy", Met. Trans., Vol.14A, 1983, p413-420.

BIOGRAPHICAL NOTE

The author was born January 9, 1958 in Taichung, Taiwan, Republic of China. He received his Bachelor of Science degree in Materials Science and Engineering in 1980 from National Tsing Hua University, Hsinchu, Taiwan, and his Master of Science degree in Metallurgical and Materials Science Engineering in 1982 from National Cheng Kung University, Tainan, Taiwan. He served in the army as a supply officer from July, 1982 to May, 1984. He joined the Oregon Graduate Institute of Science and Technology in Fall 1984, and completed the requirements for his Ph.D degree in Materials Science and Engineering in January 1991.